Biomechanical Characterisation of Osteoporotic Bone

Caroline Frances Newe

A thesis submitted to Department of Bioengineering, University of Strathclyde in partial fulfilment of the requirements for the degree of Masters of Science

Department of Bioengineering
University of Strathclyde

August 2013

Copyright Statement

Signed: Date:

Summary

Osteoporosis and related fractures are among the most common health problems affecting contemporary society. Characterised by a fall in the bone mass of the sufferer and disruption to their bone microarchitecture, osteoporosis leads to heightened bone fragility and an increased risk of fracture. As osteoporosis frequently goes undiagnosed until a fracture occurs, an accurate and non-invasive method of assessing bone mechanical properties could be of great importance in the assessment of osteoporosis and fracture risk.

Although bone strength cannot be measured directly i*n vivo*, factors such as bone mineral density (BMD) and bone geometry, determined via imaging techniques such as peripheral quantitative computed tomography (pQCT), can be used to devise an estimate. In this study cadaveric human tibiae (n = 3) were analysed in an attempt to determine whether their mechanical properties were influenced by BMD and/or geometry. The tibiae were scanned using pQCT, following which they were mechanically tested in torsional loading, a mode of loading which frequently which causes fracture *in vivo*. BMD and geometric features of the tibiae were determined by image analysis of the pQCT scans. The results revealed the existence of a very strong relationship between bone strength and BMD (R^2 = 0.9989); and, a positive relationship between bone strength and geometric properties (J: R^2 = 0.3085, CSA: R^2 = 0.4607).

The results of the study suggest that both BMD and geometric features play an important role in bone strength and should be taken into account when assessing osteoporosis and fracture risk. Further work in this area could lead to the development of accurate, non-invasive techniques appropriate for the early diagnosis and subsequent monitoring of osteoporosis, thereby allowing the development of effective prevention and, where necessary, treatment and management strategies.

Acknowledgements

I would like to give my sincere thanks to Dr Sylvie Coupaud for providing me with the opportunity to carry out this project and for her help, guidance and encouragement throughout. I would also like to thank Dr. Phil Riches for his input and advice. Additional thanks go to John MacLean, Stephen Murray and John Wilson who were an incredible help throughout the duration of the project. I would also like to express my gratitude to the staff of the Laboratory of Human Anatomy at the University of Glasgow, in particular Dr Quentin Fogg for kindly supplying material, and Stuart McNally for all of his help and for very generously giving of his time and expertise.

Contents

List of Figures

List of Tables

1.0 Introduction

1.0 Introduction

1.1 Bone

There are approximately 206 distinct bones in the human body (Pack and Bassett, 2011) which, in combination with structures such as ligaments that connect and stabilise them, make up the skeletal system (Martini *et al*., 2012). Each bone is an individual organ, undergoing constant adaption in response to the loads generated by daily activity (Pack and Bassett, 2011). Individually and together, bones perform a number of important roles in the human body essential to daily existence.

1.1.1 Bone Composition and Structure

Bone is essentially a composite material, made up of a non-living matrix with living cells distributed in it. The fibrous, organic matrix is composed of proteins, primarily collagen, with inorganic mineral compounds interspersed throughout it (Jee, 2001). The presence of mineral salts, such as crystalline hydroxyapatite and amorphous calcium phosphate, contribute to the hardness, strength and weight bearing capabilities of bone (Gibson and Ashby, 1988), (Jee, 2001), (Bandyopadhyay-Ghosh, 2008). The organic matrix forms 30-35% of the dry weight of bone with the inorganic mineral salts constituting the remaining 65-70% (Jee, 2001). While bone is essentially brittle, the presence of collagen gives it a significant amount of elasticity, essential to endure the stresses generated by everyday activities such as walking and running (Bandyopadhyay-Ghosh, 2008).

Outwardly bones appear to be solid however the structure of bone is complex (Figure 1.1). Most bones are made up of two structures; a porous core of cancellous (spongy) bone surrounded by a dense outer shell of compact (cortical) bone (Gibson and Ashby, 1988). The smooth white appearance of bone can be attributed to the hard outer layer of compact bone. Accounting for

80% of the total bone mass of an adult skeleton, compact bone is found primarily in the shafts of long bones, such as those of the arms and legs, where strength is required (Jee, 2001).

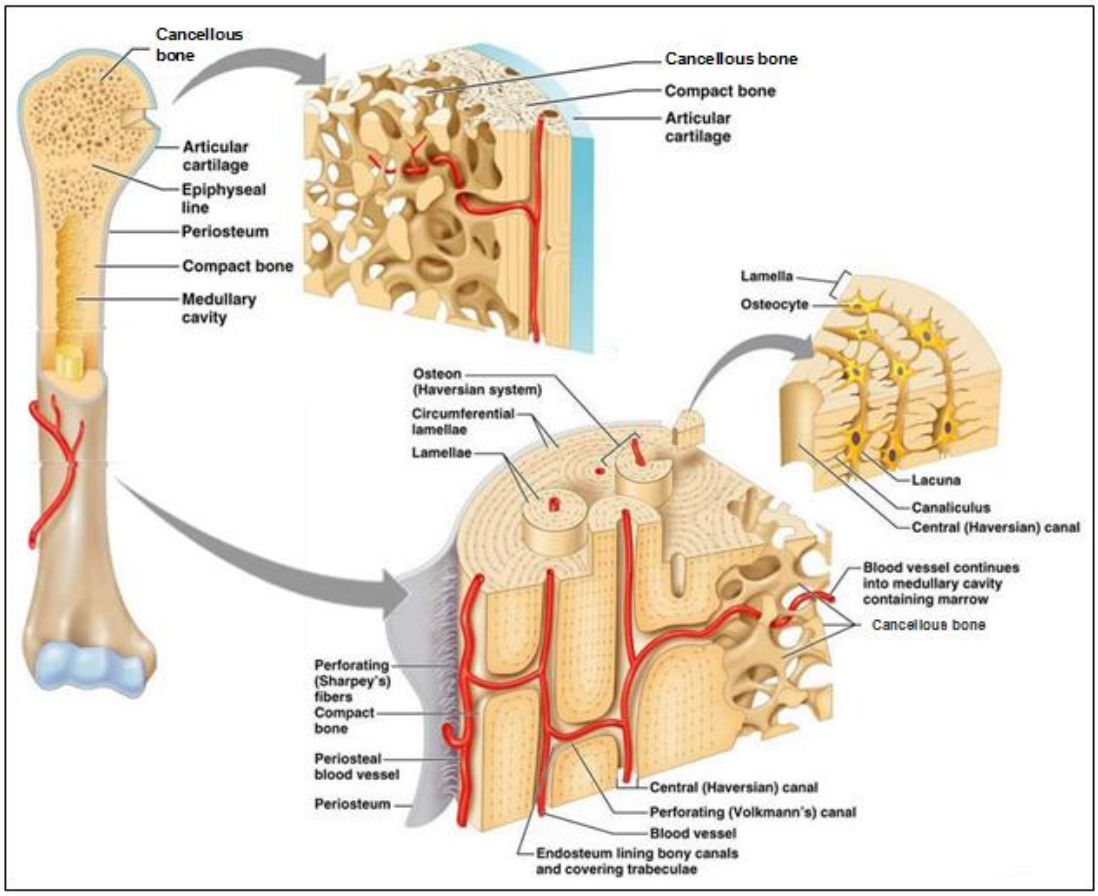

Figure 1.1: Internal structure of long bone detailing compact and cancellous bone structure – adapted from Marieb and Hoehn (2007)

Osteons, or Haversian systems, are the structural units of compact bone (Martini *et al*., 2012). They are elongated cylinders of calcified bone that act as weight-bearing pillars, able to withstand the mechanical stresses placed on the bone during everyday activities. At the centre of each osteon is a hollow canal, known as a Haversian canal, which contains blood, lymphatic vessels and nerves (Jee, 2001). This central blood vessel is very important as it ensures that every bone cell is close to a nutrient supply. The Haversian canal is surrounded by thin layers of bone in concentric rings called lamellae (Jee, 2001), (Martini,

2012). Cavities, or lacunae, are distributed throughout the lamellae. They are connected via canalicular channels which enable bone cells found resident within the lacunae to communicate with each other (Jee, 2001).

Cancellous bone accounts for the remaining 20% of total bone mass. It is found internal to compact bone in specific areas (Figure 1.2(a)), such as at the ends of the long bones of the legs, where lightness and strength are important. Cancellous bone is composed of an interconnected network of trabecular rods and plates in a honeycomb-like arrangement (Figure 1.2(b)) (Gibson and Ashby, 1988). The spaces between trabeculae in long bones, such as the femur, and other large bones, such as the ilium, are filled with red bone marrow. Yellow bone marrow may be found in intertrabecular spaces in other locations, and in the shaft of most long bones (Bartel *et al*., 2006), (Martini, 2012). The configuration of cancellous bone is advantageous as it supplies a large bearing area for joint articulation while minimising the weight of the bone, a design instrumental in reducing joint bearing stresses (Schwartz, 2007).

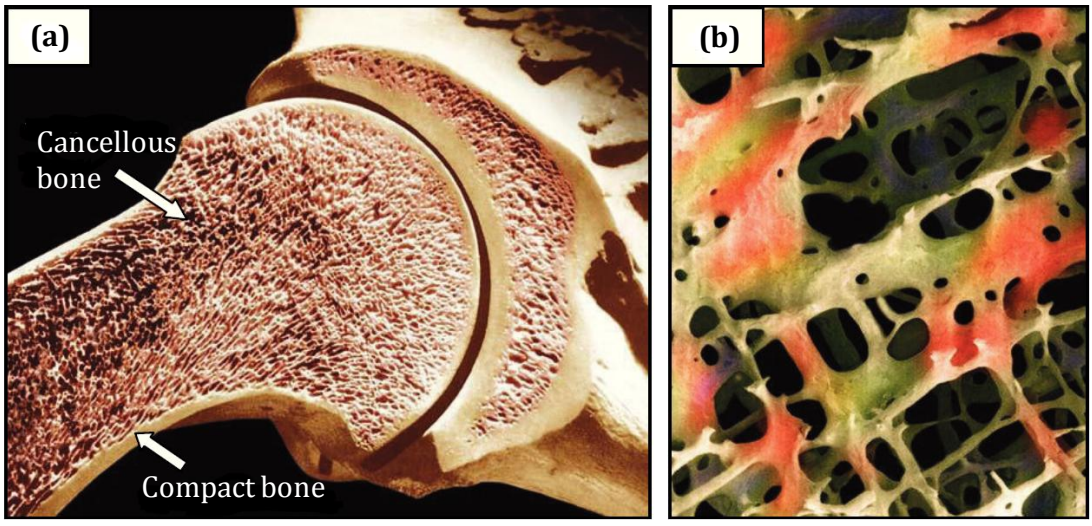

Figure 1.2(a): Section of humerus showing compact bone and cancellous bone (Dr D Fawcett, Encyclopædia Britannica Online) **(b):** Cancellous Bone (×30mag) (Dr F Hossler, Science Photo Library)

1.1.2 Bone Cells

A number of cells types are involved in the production and maintenance of bone (Figure 1.3). Osteoblasts are the cells responsible for forming the matrix which gives the structure resilience and flexibility (Lerner, 2012), (Van Wynsberghe *et al*., 1995). They are continually replenished and function by secreting collagen and producing mineral salts formed from calcium and phosphorous (Lerner, 2012), (Van Wynsberghe *et al*., 1995). When osteoblasts become trapped in the matrix they transform into osteocytes, mature bone cells that carry out cellular activities (Jee, 2001). Osteocytes keep the matrix in a stable and healthy state and play an active role in homeostasis by aiding the release of calcium from bone tissue into the blood (Van Wynsberghe *et al*., 1995). They play a role in regulating the activity of both osteoblasts and osteoclasts and in phosphate metabolism control (Lerner, 2012). Along with osteoblasts, osteoclasts are bone cells which play an important role in the remodelling of bone. They function by moving about on bone surfaces and resorbing bone matrix from areas where it is either unnecessary or deteriorating (Downey and Siegel, 2006), (Van Wynsberghe *et al*., 1995). The resorption of bone in both healthy and diseased states, such as osteoporotic bone, is as a result of osteoclastic activity (Downey and Siegel, 2006).

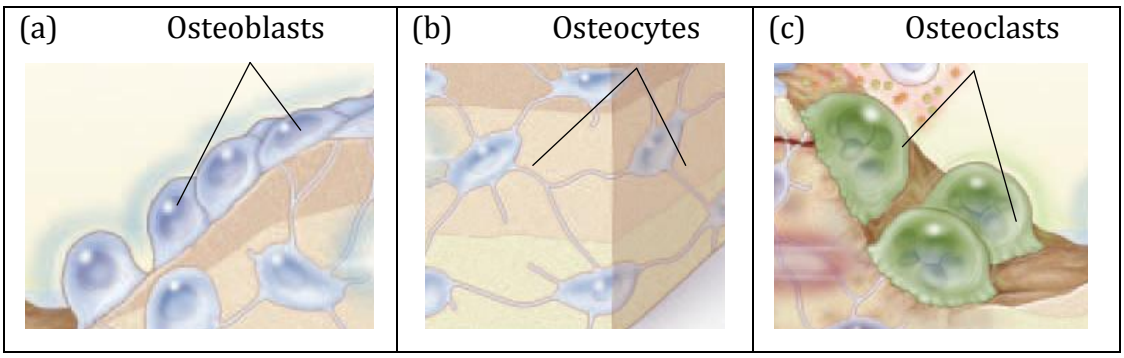

Figure 1.3: Cells involved in the production and maintenance of bone (adapted from Seeman and Delmas, 2006)

1.1.3 Bone Remodelling

Bone is a living tissue that continually remodels through its lifetime. The remodelling of bone is a dynamic process, in which old bone is removed and new bone is added to the skeleton. Typically the rates of bone removal and formation are balanced to ensure that the strength and integrity of the skeleton are maintained during the process. There are a number of reasons why bone remodels, including the regulation of calcium homeostasis, the repair of bone micro-damage caused by everyday stress, and the shaping of the skeleton during growth. The process of bone remodelling is shown in Figure 1.4.

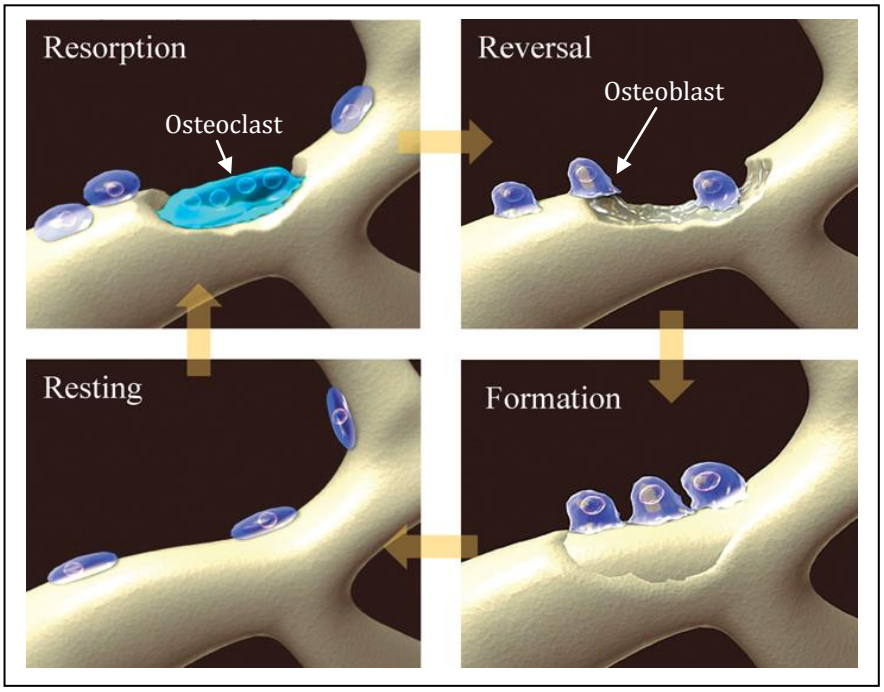

Figure 1.4: Bone remodelling process consisting of resorption, reversal, formation and resting (Coxon *et al.*, 2004)

In healthy bone resorption typically takes about 7-10 days and occurs when osteoclasts move along the bone surface, removing bone mineral and matrix and creating cavities on the surface (Coxon *et al.*, 2004). Resorption is followed in the bone remodelling cycle by reversal, where mononuclear cells prepare the surface of the bone for new osteoblasts to begin bone formation. The reversal

stage occurs over approximately 14 days (Sims and Baron, 2002). In the formation stage, lasting around 3 months, osteoblasts work to repair the cavities created via resorption by filling them with new bone. In the final resting stage, the restored bone surface is covered with protective lining cells and a resting period follows until a new remodelling cycle begins (Coxon *et al.*, 2004).

1.1.4 Functions of Bone

Bones carry out a number of functions, both mechanical and physiological in nature (Bartel *et al.*, 2006). As the principal component of the skeletal structure, bones serve an important structural function, enabling motion and providing protection for vital organs. Individual bones and collections of bones supply a frame to which soft tissues and organs are attached, giving structural support to the body (Martini *et al.*, 2012). Motion of the body is possible due to the action of bones and joints in conjunction with the muscles attached to them. The muscles generate forces which are transmitted to the bones causing them to move about the joint (Bartel *et al.*, 2006), (Martini *et al.*, 2012), (Pack and Bassett, 2011). A wide range of actions result, from precision motion of the fingertips, to movement of the whole body in activities such as walking (Martini *et al.*, 2012). Skeletal structures surround many internal organs and soft tissues, providing protection from injury, for example, the ribs which shield the heart and lungs, or the vertebrae which protect the spinal cord (Bartel *et al.*, 2006), (Martini *et al.*, 2012).

Bone acts as a reservoir of inorganic minerals such as calcium and phosphorus. A supply of such ions is maintained for use when needed by the body in various cellular activities and physiological processes (Martini *et al.*, 2012), (Pack and Bassett, 2011), (Schwartz, 2007). Calcium, for example, is essential to the body, playing an important role in cell membrane function, muscle contraction, and blood clotting (Martini *et al.*, 2012). If sufficient calcium is not obtained from

the diet, it is removed from the bones causing them to grow weaker over time and increasing their susceptibility to fracture (AAOS, 2012a). Consequently, bone tissue is instrumental in preserving the equilibrium of minerals in the body, a process known as homeostasis. In addition to stored minerals, bone contains energy reserves in the form of lipids stored in yellow bone marrow (Martini *et al*., 2012), (Pack and Bassett, 2011).

Bone also plays a role in haematopoiesis, which is the manufacture of red and white blood cells, via red bone marrow (Pack and Bassett, 2011). Red bone marrow, contained within cancellous bone located in the vertebrae, skull, sternum, pelvis, and at the ends of the long bones, provides sites for blood cell production (Bartel *et al*., 2006). Red blood cells are crucial due to their role in the transportation of oxygen to and removal of carbon dioxide from the cells and tissues of the body (Martini *et al*., 2012), (Pack and Bassett, 2011). White blood cells are a critical component of the immune system, protecting the body from attack by pathogens and removing toxic substances and abnormal or damaged cells (Martini *et al*., 2012). As the stem cells that produce white blood cells originate in red bone marrow (Martini *et al*., 2012), bone itself plays an important part in the immune system.

1.2 Bone Health

Due to the variability of bone structure between individuals, it is difficult to conclusively define healthy bone. Healthy bone may be, in part, regarded as having sufficient bone mass, structural, and mechanical properties to withstand the loading generated by everyday activities. The structural integrity of whole bones are influenced by a number of variables including the geometry of the bone, total bone mass and the properties of the individual tissues that make up the bone (Donnelly, 2011).

Peak bone mass corresponds to the point at which bone is at its maximum strength and size (AAOS, 2012a). Bone mass is typically expressed as bone mineral density (BMD) and it is one of the contributing elements to bone strength along with bone structure, quality and turnover (Ilich and Kerstetter, 2000). Peak bone mass is largely determined by genetics, but external factors including diet and physical activity can play a significant role in whether peak bone mass is attained (AAOS, 2012a), (U.S. Dept of Health and Human Services, 2004). Proportionally, 60 – 80% of peak bone mass is determined by genetic factors, for example the overall size and structure of the skeleton, with external factors governing the remaining 20 – 40% (Bartl and Frisch, 2009). Other factors may have a detrimental effect on bone mass, including poor diet, lack of exercise, smoking and excessive alcohol consumption (AAOS, 2012a).

The optimal time in which to build bone mass through diet and exercise is limited. Stages of rapid growth, during childhood, adolescence, and early adulthood provide the greatest opportunity in which to develop and build bone mass (AAOS, 2012a), (Bartl and Frisch, 2009), (U.S. Dept of Health and Human Services, 2004). The majority of people will achieve their peak bone mass at around 25 to 30 years old and it is difficult to build bone mass after this age (AAOS, 2012a), (Bartl and Frisch, 2009). After around 30 years of age, an average of 1% of bone is lost every year (Bartl and Frisch, 2009), consequently the stronger the bones are upon reaching this age, the more capable they are of coping with age related changes to bone. Men tend to have a higher peak bone mass than women of a comparable age due to the fact that they have larger bones and build greater mass during growth periods (AAOS, 2012a).

It is thought that approximately 60 to 85% of the world's population lead sedentary lifestyles (WHO, 2002). There are many negatives associated with such a lifestyle and it is potentially a serious public health problem. The issue of insufficient physical activity is particularly worrying in children, with it estimated that nearly two-thirds currently do not exercise enough (WHO, 2002).

The benefits of appropriate exercise in childhood are numerous, particularly in relation to building bone mass. More active children tend to possess a higher peak bone mass, which goes some way towards reducing the threat of excessive bone loss in later life (AAOS, 2012a), (Boreham and Riddoch, 2001).

Detailed mechanical and structural properties of bone are generally determined from biopsy samples or cadaveric specimens and therefore are not the most convenient method of establishing current bone health status. BMD measurement is typically used to determine bone health *in vivo* (NIH, 2012). BMD is defined as "*a measurement of bone mass, expressed as the amount of mineral in grams divided by the area scanned in* cm^2" (McGraw-Hill, 2002). In clinical settings bone mass, characterised by BMD, is used to indicate bone strength (Donnelly, 2011), (NIH, 2012) and bone strength and BMD are positively correlated (An, 2010). Due to the difficulties associated with precisely determining bone structure and mechanical properties *in vivo*, measurements of bone mass are instrumental in measuring overall bone strength and fragility (Ilich and Kerstetter, 2000).

1.2.1 The Importance of Bone Health

The maintenance of healthy bone is crucial at every stage of life (AAOS, 2012a). As detailed in Section 1.1.4, bone plays a key role in many tasks within the body and consequently poor bone health can have significant implications on overall health. The population of the United Kingdom (UK), and that of the world as a whole, is ageing. A combination of falling birth rates and increasing life expectancies has contributed to this population shift (Population Matters, 2011). In 2010 approximately 1.4 million people in the UK were aged 85 years or older and it is predicted that this figure will continue to increase (Office for National Statistics, 2012). By 2035 it is forecast that 3.5 million people will be aged over 85, accounting for 5% of the total population (Office for National Statistics, 2012). An ageing population has significant implications, including

placing greater burdens on health and social care services (House of Lords, 2013).

Particularly, there has been an increase in conditions typically associated with an aging population which impact greatly on healthcare costs and quality of life (AAOS, 2002), (Woolf and Pfleger, 2003). The increasingly elderly population, in combination with increasingly inactive lifestyles, suggest that issues associated with poor bone health will become a progressively larger problem. It is possible however to improve bone health at any age through sufficient calcium and vitamin D intake and appropriate levels of physical activity (U.S. Dept of Health and Human Services, 2004).

1.2.2 Bone Fractures

Despite the fact that bones are rigid, due to the presence of collagen they possess a degree of flexibility. As a result they will bend somewhat when a force is applied (AAOS, 2012b). A bone fracture will arise when the bone is subjected to a force greater than that which it can structurally tolerate, causing it to break or split (MedlinePlus, 2009). The severity of the fracture depends on the magnitude and type of force that caused the break (AAOS, 2012b). Bone fragility relates to how vulnerable a bone is to fracture (Turner, 2002) and an increase in fragility fractures due to a loss in bone mass is one of the most obvious outcomes of declining bone health.

In healthy bone, a fracture may result from traumatic loading or a sudden impact, such as a fall to the ground (AAOS, 2012b), (Turner, 2002). If the energy caused by impact is greater than the mechanical energy the bone is capable of absorbing, a fracture typically results (Turner, 2002). However in weakened bone, fractures may occur from non-traumatic loading during normal, everyday activities (Turner, 2002). Consequently preservation of bone strength is important to reduce incidences of fragility related fractures.

Fractures resulting from poor bone health are expensive and tend to become a burden on individuals and society as a whole (U.S. Dept of Health and Human Services, 2004). The effects of fractures can be significant for both the sufferer and their families. For example, during the first three months following a hip fracture, there is an associated increased risk of mortality of 2.8 to 4 times greater than that of individuals of a similar age with no fracture (U.S. Dept of Health and Human Services, 2004).

1.2.3 Bone Diseases

Bone is susceptible to a variety of injuries, diseases and disorders. They may originate from injury, infection, genetic conditions or abnormal growths and can manifest in a number of ways, including immune system deficiencies and alterations in movement and physique (U.S. Dept of Health and Human Services, 2004). Weak, poorly mineralised bone may result from nutritional deficiencies while genetic irregularities can lead to thin, weak bones or bones that are excessively dense (U.S. Dept of Health and Human Services, 2004). Bone mass and strength may also be negatively affected by factors including immobilisation, insufficient exercise, and smoking (Downey and Siegel, 2006). Conditions relating to bone health include:

Osteoarthritis: Joints are exposed to wear and tear throughout the course of daily life, frequently resulting in deterioration of joint function (Bartel *et al*., 2006), (Martini *et al*., 2012). Cumulative wear and tear, trauma or disease can lead to damage of the joint surfaces (Bartel *et al*., 2006) which in turn may restrict the normal smooth movement of the joint. Osteoarthritis, also known as degenerative joint disease, is a painful affliction affecting a large proportion of the population. It is characterised by joint inflammation, cartilage damage and the development of bony growths around the joint edges (NHS, 2012). The symptoms include joint stiffness, pain, swelling, and restricted motion.

Osteomalacia: The condition osteomalacia arises from poor bone mineralisation resulting in soft, weak, and flexible bones (Martini *et al*., 2012). If an individual suffers from osteomalacia there is insufficient mineral present to reinforce the collagen present in the bone matrix and consequently the bones become soft (U.S. Dept of Health and Human Services, 2004). Osteomalacia generally arises from a lack of vitamin D caused by an insufficient uptake of the vitamin from diet or inadequate exposure of the skin to sunlight (Duursma *et al*., 1997), (Martini *et al*., 2012). Rickets is a form of osteomalacia observed in children which is evident by the bowlegged appearance of sufferers. Bones become increasingly flexible due to their poor mineralisation and consequently cannot withstand the forces that arise as a result of the individual's weight, tending to bend laterally and bow as a result (Martini *et al*., 2012). The symptoms include muscle weakness, pain and partial fractures of the bones with the pelvis and ribs most frequently affected (Duursma *et al*., 1997).

Osteopetrosis: Osteopetrosis, also referred to as 'marble bone disease', is a rare inherited bone disease characterised by bones which have higher than normal density and are susceptible to fracture (Cassidy *et al*., 1948), (Stark and Savarirayan, 2009). There are a number of types of osteopetrosis which differ by the way in which they are inherited and how severe their symptoms are (Stark and Savarirayan, 2009). Osteoclastic abnormalities, for example irregularities in their function or differentiation, are responsible for increased bone density (Stark and Savarirayan, 2009). The outcomes of osteopetrosis can include a high risk of bone fractures, scoliosis of the spine, and arthritis in the hips.

Osteoporosis: The most common disease relating to bone health is osteoporosis (Calvo *et al.*, 1996). It is a chronic disease causing a loss of bone mass and decline in bone microarchitecture (Duursma *et al*., 1997). Osteoporosis can affect individuals of any age group however its incidence increases with age (SIGN, 2003). As an individual gets older, the rate of bone

breakdown increases while the degree bone formation has a tendency to decrease (U.S. Dept of Health and Human Services, 2004). The rate of bone formation is typically much less than that of bone resorption, with the resulting imbalance leading to loss of bone mass and increased skeletal fragility. Osteoporosis is typically the underlying cause of fractures in the elderly (U.S. Dept of Health and Human Services, 2004).

This list is by no means exhaustive and there are many other diseases and disorders associated with bone. Although some of the conditions detailed are rare, the more common disorders mentioned are widespread and bone health is a significant clinical concern. Osteoporosis and related fractures are among the most common problems affecting contemporary society and loss of bone as a consequence of disease or injury can lead to diminished quality of life at considerable socioeconomic cost (Planell and Navarro, 2009). Musculoskeletal problems have a significant impact on the individual concerned, their families, and health and social care systems, and are among the main causes of chronic pain, physical disability and work absenteeism worldwide (Planell and Navarro, 2009), (Woolf and Pfleger, 2003). Osteoporosis, one of the major concerns in this area affecting a large proportion of the population, will be the focus of this project.

1.3 Osteoporosis

1.3.1 Prevalence of Osteoporosis

Osteoporosis is a significant problem in the UK with an estimated 3 million individuals currently suffering from it (National Osteoporosis Society, 2008). It was estimated that in the time period 2000-2010, a total of 2.2 million osteoporotic fractures would occur in the UK at a direct cost of £20.3 billion to the UK healthcare economy (Burge *et al*., 2001). The indirect costs, to both the patient and their families or carers, should not be overlooked. Indirect costs may include loss of productivity due to sickness or early retirement and can

affect both the patient and their carers (NICE, 2012). It is predicted that by 2020, there will be 230,000 osteoporotic fractures per year with associated costs of over £2.1 billion per year (Burge *et al*., 2001).

Characterised by a fall in the bone mass of the sufferer and disruption to their bone microarchitecture, osteoporosis leads to increased bone fragility and a heightened threat of fracture (Wähnert *et al.*, 2012), (Wehrli, 2010), (Woolf and Pfleger, 2003). As structural changes typically include a decline in the apparent density and area, the decrease in mechanical properties, such as compression strength and elastic modulus, is to be expected. Osteoporotic bone is essentially bone that readily suffers from fracture (Boskey and Coleman, 2010).

The majority of osteoporotic fractures occur in regions with a high proportion of cancellous bone (Wehrli, 2010). A thinning of the trabecular network of cancellous bone is observed along with the conversion of trabecular plates to rods (Griffith and Genant, 2008), (Wehrli, 2010). The honeycomb-like structure of healthy cancellous bone can be observed in Figure 1.5(a). In Figure 1.5(b) the thinning of the trabecular struts, typical of osteoporotic bone, can be clearly seen. As osteoporosis progresses some of the trabeculae will disconnect from the bulk structure while others may be removed completely and as a result can no longer provide structural support (U.S. Dept of Health and Human Services, 2004). The outer shell of compact bone becomes thinner and an increase in porosity is observed (Griffith and Genant, 2008), (Wehrli, 2010).

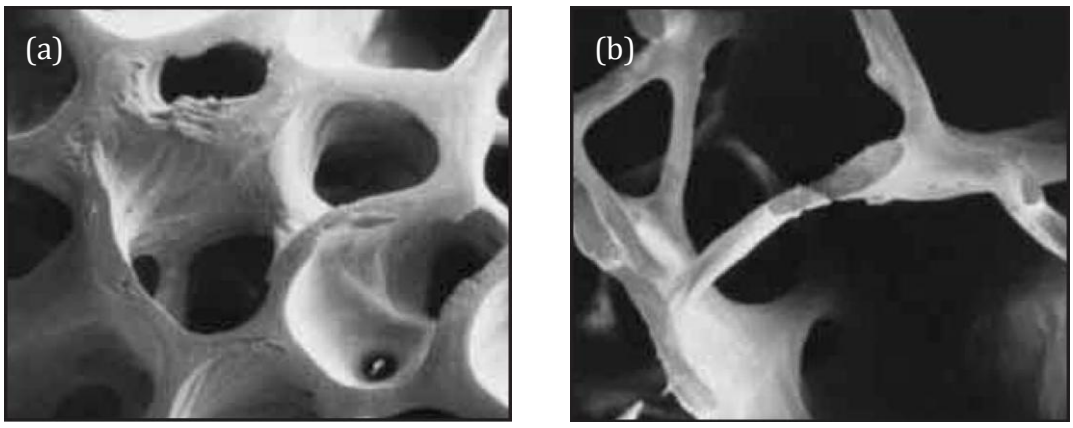

Normal Bone Osteoporotic Bone

Figure 1.5: Scanning electron micrographs of **(a):** normal bone and **(b):** osteoporotic bone (U.S. Dept of Health and Human Services, 2004)

1.3.2 Causes of Osteoporosis

Osteoporosis is typically associated with an ageing population and bone mass and strength generally fall as an individual grows older (Boskey and Coleman, 2010). However, it is not a disease strictly limited to older individuals and can result from a number of factors related to both the individual themselves, such as genetics, and external variables, for example their environment. The condition is primarily caused by poor development of bone mass during early life combined with accelerated bone loss as the individual ages (Downey and Siegel, 2006). A combination of genes, poor nutrition and lifestyle can result in relatively weak bone for many individuals, no matter what age they are (U.S. Dept of Health and Human Services, 2004). Environments and conditions where individuals experience reduced mechanical loading, such as in spinal cord injury and space flight, are known to result in bone loss (Poole *et al.*, 2005).

Osteoporosis usually goes undetected until a fracture occurs, consequently it is important to recognise at risk individuals and apply appropriate measurement and screening techniques (South-Paul, 2001), (NHS Choices, 2011b). A number of criteria can be applied to identify those who may be in danger of developing osteoporosis, some of which are detailed in Table 1.1. Despite the fact that both

men and women can be affected by osteoporosis, it is particularly prevalent in postmenopausal women, with one in three women compared to one in twelve men over the age of 50 experiencing an osteoporotic fracture (SIGN, 2003).

Table 1.1: Risk factors for developing osteoporosis – compiled from Downey and Siegel (2006) and South-Paul (2001)

Risk factors for developing osteoporosis	
Genetic factors	Female sex, a petite skeletal frame, hormone deficiency, and Caucasian or Asian ancestry
Nutritional factors	Low calcium or vitamin D intake, poor nutrition, alcohol abuse, tobacco abuse and high caffeine intake
Behavioural factors	Extended periods of inactivity or immobilisation, aging, smoking, particular medications or pharmacological agents, and low body weight

There are two types of osteoporosis, primary and secondary (Downey and Siegel, 2006). Primary osteoporosis is the most common form and is characterised by a decline in bone mass which is not caused by another chronic disorder (U.S. Dept of Health and Human Services, 2004), (South-Paul, 2001). It is associated with aging and/or a decrease in gonadal function (Downey and Siegel, 2006), (South-Paul, 2001). Early menopause or premenopausal oestrogen shortages in women can speed up the progression of primary osteoporosis (Downey and Siegel, 2006), (South-Paul, 2001). A number of the risk factors detailed in Table 1.1 can contribute to the development of primary osteoporosis, including prolonged periods of inactivity, insufficient calcium intake, and alcohol and tobacco misuse (South-Paul, 2001).

Secondary osteoporosis develops due to specific chronic conditions or medications which contribute considerably to increasing the rate of bone loss (U.S. Dept of Health and Human Services, 2004), (Downey and Siegel, 2006), (South-Paul, 2001). These conditions include gastrointestinal diseases, connective tissue diseases, renal failure, and medications, such as

glucocorticoids which are thought to be related to suppression of osteoblasts (Downey and Siegel, 2006), (South-Paul, 2001).

1.3.3 Clinical Diagnosis of Osteoporosis

Clinical measurement of BMD supplies a quantitative value of the bone mass per unit area in g/cm^2 and is the main factor used in diagnosis and subsequent monitoring of osteoporosis (NICE, 2012). It should be noted that clinical measurements of BMD do not return a true volumetric density, rather a two-dimensional (2D) areal density is provided. Consequently BMD measurements made in a clinical setting are referred to as projected areal BMD (aBMD), distinguishable from a true volumetric density (vBMD).

Diagnosis of osteoporosis consists of measuring the aBMD of the individual and comparing it to the mean aBMD of healthy, young adult women to give a T-score (Woolf and Pfleger, 2003). An individual is considered to have osteoporosis if they have a *"BMD that lies 2.5 standard deviations or more below the average value for young healthy women (a T-score of < -2.5 S.D.)"* as defined by the World Health Organisation (WHO) (WHO, 2004). A T-score of 0 indicates that the aBMD value is equivalent to that of a healthy, young adult and a score between +1 S.D. and -1 S.D. is considered normal (NIH, 2012).

Table 1.2 indicates how bone health varies with T-score. Measurements are most commonly taken at the lumbar spine and proximal femur, with the proximal femur the preferred location for prediction of fragility fracture risk (NICE, 2012). Osteoporosis may be tested for if the patient presents with characteristic fractures in sites such as the hip, vertebrae, and distal forearm following low-energy trauma (Woolf and Pfleger, 2003). The fractures that result are generally physically debilitating and in some cases can have a long-term detrimental effect on the patient's physical and mental health (U.S. Dept of Health and Human Services, 2004).

Table 1.2: World Health Organization Definitions Based on Bone Density Levels – reproduced from NIH (2012)

Level	Definition
Normal	Bone density is within 1 S.D. (+1 or −1) of the young adult mean
Low bone mass	Bone density is between 1 and 2.5 S.D. below the young adult mean (−1 to −2.5 S.D.)
Osteoporosis	Bone density is 2.5 S.D. or more below the young adult mean (−2.5 S.D. or lower)
Severe (established) osteoporosis	Bone density is more than 2.5 S.D. below the young adult mean, and there have been one or more osteoporotic fractures

2.0 Literature Review

2.0 Literature Review

2.1 Properties of Bone

The properties of bone depend on both the tissue material properties and the way in which the tissue is distributed, that is, the tissue geometry (Van der Meulen, *et al*., 2001). Although compact and cancellous bone possess the same basic composition, they vary greatly in terms of their respective architectures and material properties. Typical values of a number of healthy bone properties are detailed in Table 2.1. It should be noted that the properties of bone are also dependant on factors such as age, gender and anatomical site (Turner and Burr, 2001).

Table 2.1: Properties of healthy bone - compiled from An (2010), Bandyopadhyay-Ghosh (2008) and Jee (2001)

Property	Compact Bone	Cancellous Bone
Proportion of total bone mass (%)	80	20
Porosity (%)	5 – 10	50 – 90
Apparent density (g/cm^3)	1.8	0.1 – 0.9
Compressive strength (MPa)	100 – 230	2 – 12
Flexural tensile strength (MPa)	50 – 150	10 – 20
Young's modulus (GPa)	7 – 30	0.05 - 0.5

2.1.1 Bone Geometry

As detailed in Section 1.1.1, bone exists in two forms, compact and cancellous bone. Although both forms are composed of the same bone tissue (Schaffler and Burr, 1988), they vary greatly in their respective architectures. Bone geometry encompasses both the microscopic architecture of the cancellous bone trabeculae and the macroscopic structure of the whole bone (Donnelly, 2011). The macroscopic structure of the whole bone relates to the overall geometry of the bone including its shape and size (Griffith and Genant, 2008).

In the past there has been some debate over an exact quantitative definition of compact and cancellous bone (Zioupos *et al*., 2008). Many researchers have attempted to identify an appropriate quantitative range for compact and cancellous bone, typically based on their respective porosities or solid volume fractions. Zioupos *et al*. (2008) report an early qualitative definition made by Wolf in 1892 in which he described compact bone as being *"simply more dense cancellous bone"* (Zioupos *et al*., 2008).

More recently quantitative definitions have been attempted, with Gibson (1985) stating that a solid volume fraction of less than 70% was representative of cancellous bone, while compact bone was indicated by a volume fraction of greater than 70% (Gibson, 1985). In 1988, Shaffler and Burr described compact and cancellous bone with regards to their respective porosities, with compact bone possessing a porosity of less than approximately 15% and cancellous bone a porosity greater than approximately 70% (Schaffler and Burr, 1988). Bonucci (2000) supplied a range of porosity values for both compact, 5% to 30%, and cancellous bone, 30% to > 90% (Bonucci, 2000).

Despite the range of values proposed, it is clear that the main difference between compact and cancellous bone is in their respective porosities. A representation of the difference in porosities, or solid volume fractions, of compact and cancellous bone is shown in Figure 2.1. It is clear that although compact bone is very dense with a high solid volume fraction, it does contain a small degree of porosity. This low porosity value is attributed to the presence of osteon canals, Volkmann's canals, resorption lacunae, osteocytes and their caniliculi while the high porosity of cancellous bone is due to intertrabecular spaces (Bonucci, 2000).

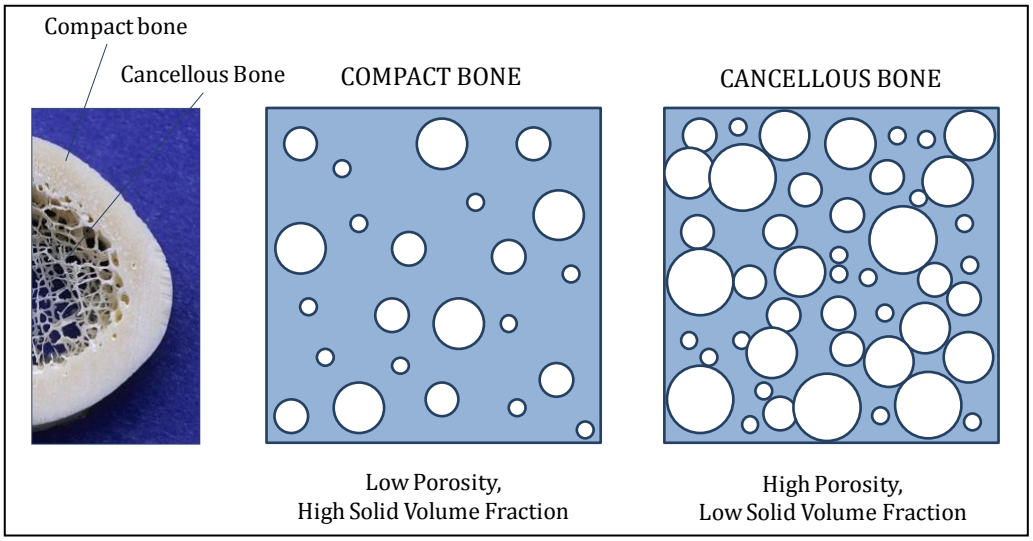

Figure 2.1: Schematic representation of relative solid volume fractions and porosities of compact and cancellous bone

The majority of bones in the body are composed of both compact and cancellous bone, with the compact bone forming the dense outer shell external to a porous cancellous core (Gibson, 1985). Consequently, the properties of the bone as a whole are influenced by the properties of the two forms of bone and their geometries. Porosity impacts greatly on the mechanical properties of a material such as bone. As the porosity of the structure increases, its strength and stiffness undergo a concurrent decrease. The opposite is also true, with an improvement in mechanical properties observed as the density of the structure increases (Schaffler and Burr, 1988). The solid, dense structure of compact bone makes it ideal for support and protection, while cancellous bone provides structural support and flexibility where lightness is important, and has a greater metabolic function than compact bone (Clarke, 2008), (Schwartz, 2007). However, both cancellous and compact bone contribute to overall bone strength (Wehrli, 2010).

The overall size and shape of the bone will also impact on its mechanical properties. It is unsurprising that large bones tend to be stronger than smaller bones (Bouxsein, 2005) however the distribution of material within the bone is also of importance. This is clear by the manner in which bones behave under

torsion and bending (Bouxsein, 2005), (Van der Meulen *et al*., 2001). The resistance of a bone to torsion and bending relates to the distribution of the bone material around the relevant neutral axis, as demonstrated for a tubular structure in Figure 2.2. The further the material is distributed from the neutral axis, the greater the resistance to bending or torsion (Bouxsein, 2005).

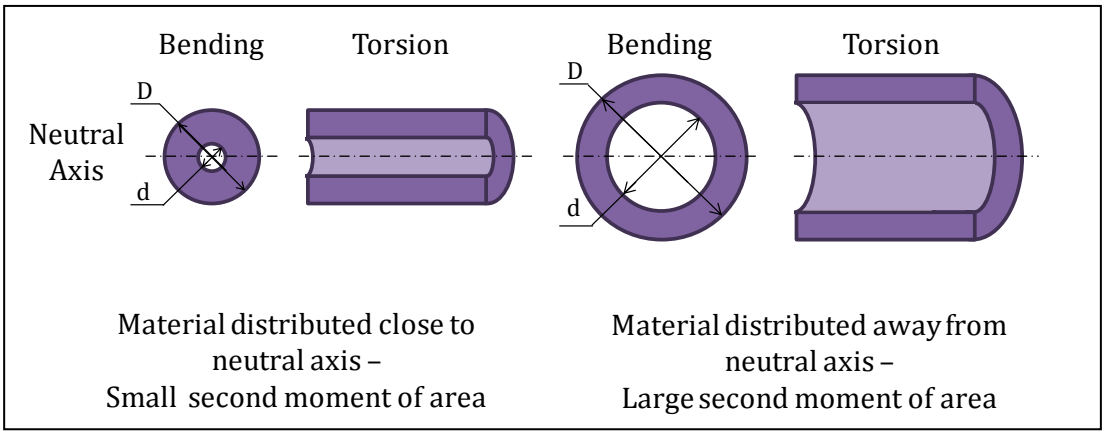

Figure 2.2: Schematic representation of influence of bone geometry on the second moment of area and polar second moment of area

The second moment of area, I, characterises the ability of the structure to resist bending. The polar second moment of area, J, is the equivalent to the second moment of area for a structure subjected to torsion and relates to the structure's resistance to twisting (Benham *et al.*, 1996). Dependent on the shape and area of the cross-section, for a hollow circular shaft such as those in Figure 2.2, I and J are calculated as follows:

$$I = \frac{\pi(D^4 - d^4)}{32}$$

$$J = \frac{\pi(D^4 - d^4)}{32}$$

Equation 2.1

where: I = second moment of area (m^4)

J = polar second moment of area (m^4)

D = shaft outer diameter (m)

d = shaft inner diameter (m)

Although the two hollow shafts shown in Figure 2.2 have the same wall thickness, and therefore would have the same mass, the second structure possesses a much larger value of I and J due to the fact that the material is distributed further from the neutral axis (i.e. it has greater outer and inner diameters). It is clear then that a bone with a larger outer diameter will demonstrate greater resistance to bending and torsion than one of a comparable mass but smaller outer diameter (Bouxsein, 2005), (Martin, 1991), (Van der Meulen *et al*., 2001).

2.1.2 Material Properties

When considering the properties of any material it is important to distinguish between structural properties and material properties. The structural properties of a material relate to the changes in shape and deformations of a specimen of the material due to the loads applied to it. Consequently structural properties, such as stiffness and ultimate force, are affected by the size and shape of the specimen and the properties of the material itself (Agnew and Bolte, 2011). The material properties however are the properties of the material independent of the specimen geometry (Bouxsein, 2005). Material properties include Young's modulus and ultimate stress.

Mechanical testing of materials is typically performed by applying load or torque to a specimen, and monitoring the resulting change in dimensions or angle (Walsh *et al*., 2002). The structural properties of the specimen, i.e. those influenced by specimen geometry, are determined from the collected force and displacement data (Figure 2.3(a)). The properties specific to the material are determined by normalising the data to take into account the geometry of the specimen, i.e. they are determined from the stress and strain generated in the sample due to the applied loads (Figure 2.3(b)).

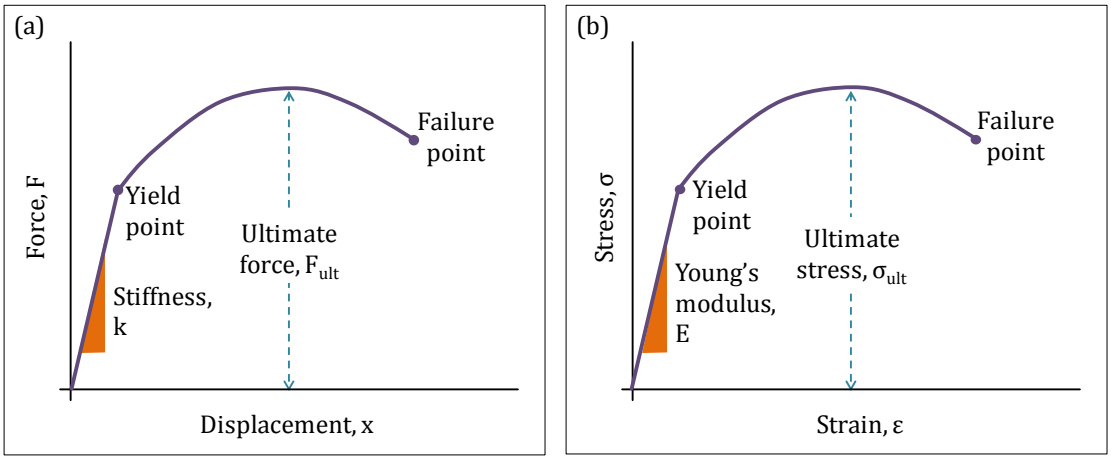

Figure 2.3(a): Typical force-displacement and **(b):** Stress–strain curve for a tensile test – adapted from Agnew and Bolte (2011)

The stress in the specimen at a particular load is determined by dividing the applied load by the original cross-sectional area (CSA) (Equation 2.2 (a)), while strain is calculated by dividing the change in specimen height/length by the original height/length (Equation 2.2 (b)). Structural properties can be found from the force-displacement curve while material properties can be determined from plotting stress–strain curves (An *et al.*, 2010).

$$\sigma = \frac{F}{CSA} \qquad \textbf{Equation 2.2 (a)}$$

$$\varepsilon = \frac{\Delta x}{x} \qquad \textbf{Equation 2.2 (b)}$$

where: σ = stress (Pa)

F = force (N)

CSA = cross-sectional area (m^2)

ε = strain

Δx = change in height/length (m)

x = original height/length (m)

In the case of bones, the material properties are influenced by the properties of the constituent tissues, such as the mineral and collagen content and aspects such as collagen fibre orientation and cross-linking (Donnelly, 2011), (Van der Meulen *et al*., 2001). As the bone tissue that forms both compact and cancellous bone is the same material, the variation in mechanical properties of the two forms of bone, such as strength, is due to their structural differences (Schaffler and Burr, 1988). It is clear that the properties of bone, such as its ability to bear load, are a function of both the material properties and the geometry (Van der Meulen *et al*., 2001).

2.2 Characterisation of Bone Strength

An awareness of bone properties is important in understanding bone strength and fracture risk. The strength of bone is essential to its ability to resist fracture and is dependent on the size and morphology of the bone and the intrinsic properties of the bone material (Figure 2.4) (Bouxsein, 2005), (Griffith and Genant, 2008).

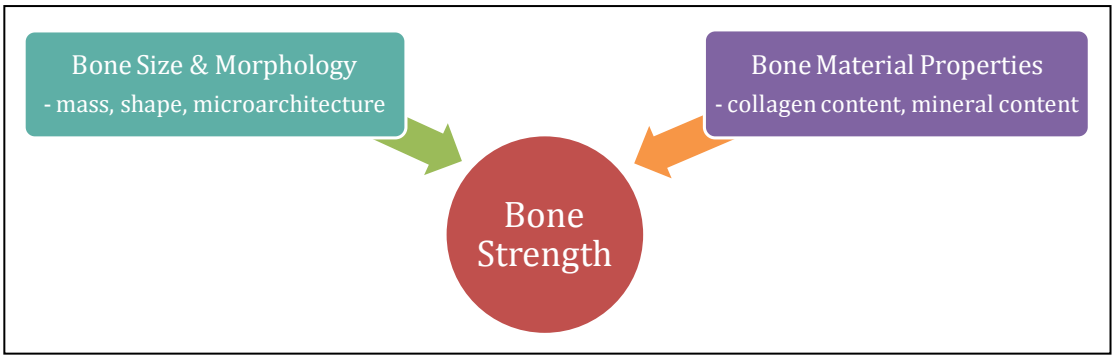

Figure 2.4: Determinants of bone strength – adapted from Bouxsein (2005)

A thorough characterisation using a range of techniques is necessary to identify the mechanical, structural and material properties of bone. *In vivo* and *in vitro* procedures are frequently utilised which can help to identify relationships between properties and bone health.

2.2.1 Bone Strength Estimation *In Vivo*

It is not currently possible to make direct measurements of bone strength *in vivo* (Griffith and Genant, 2008). Measurement of BMD is an accurate and reproducible method of determining bone mass *in vivo*, and is used widely as a predictor of bone strength (Donnelly, 2011), (Stepan, 2002). There are a number of methods available for measuring BMD, all of which are non-invasive, painless and typically involve exposure to low levels of radiation (Celenk and Celenk, 2012). A number of techniques are detailed in this section however others exist including radiogrammetry, radiographic absorptiometry (RA) and single x-ray absorptiometry (SXA) (Griffith and Genant, 2008).

2.2.1.1 Dual-Energy X-ray Absorptiometry (DXA or DEXA)

Dual-energy X-ray absorptiometry is the technique most commonly used in the clinical measurement of BMD (Bartl and Frisch, 2009), (Fewtrell, 2003). Its popularity results from the low radiation dose associated with it and the fact that scanners are widely available and relatively inexpensive (Bauer *et al*., 2010). BMD measurements obtained via DXA form the basis of the WHO criteria for diagnosis of osteoporosis in adults (Fewtrell, 2003). DXA is a 2D scanning method, and as such it does not report a true volumetric density in g/cm^3, rather it measures areal density, that is the amount of bone per unit of skeletal area, in g/cm^2 (Bartl and Frisch, 2009). It is a versatile technique and it is possible to measure the aBMD of the whole skeleton or of specific sites, such as those most vulnerable to fracture (Bartl and Frisch, 2009), (Dowthwaite *et al*., 2011), (Warming *et al*., 2002).

A DXA scan is essentially an x-ray that determines bone density (NHS Choices, 2011b). During the scan, two x-ray beams of different energies are passed through the body. A proportion of the radiation is absorbed by the bone and soft tissue with the remainder passing through the body (Bartl and Frisch,

2009), (Fewtrell, 2003). Detectors measure the proportion of radiation from the two beams that pass through the body, allowing the relative absorption by both the soft tissues and bone to be determined (Bartl and Frisch, 2009), (Fewtrell, 2003). The mineral content in a given region is then compared to the normal values for a healthy adult as identified by WHO (WHO, 2004).

The advantages of DXA include the fact that it is quick, taking only 5 to 10 minutes, and exposes the patient to a much lower radiation dose than a standard x-ray, typically 1 - 10 μSv (sievert) (Bartl and Frisch, 2009), (NHS Choices, 2011b). It is a completely painless, non-invasive procedure with the patient remaining fully clothed throughout (Bartl and Frisch, 2009). It is an accurate technique and has been shown to be useful in the prediction of fracture risk and in follow-up examinations to monitor disease progression and treatment effectiveness (Bartl and Frisch, 2009), (Dowthwaite *et al*., 2011).

Due to its low radiation dosage and rapid scanning time, DXA is the recommended technique for BMD measurement in children (Kröger *et al*., 1992). However, as T-scores relate to the average bone mass of a healthy adult, they do not have much significance in children (Fewtrell, 2003), (Griffith and Genant, 2008). Another disadvantage, not limited to children, is the fact that everything in the scan area is included in the measurement, for example aortic calcifications, which can cause inaccuracies in reported BMD values (Bartl and Frisch, 2009) (Bauer *et al*., 2010). The accuracy of measurements of the lumbar spine may be affected by scoliosis and vertebral deformity (Griffith and Genant, 2008), accordingly care must be taken when interpreting results. The fact that DXA reports aBMD as opposed to vBMD may be considered a limitation (Lochmüller *et al.*, 2002). A further drawback relates to the fact that DXA does not distinguish between compact and cancellous bone, rather it returns a total value or 'integral' BMD value (Griffith and Genant, 2008), (Lochmüller *et al.*, 2002).

2.2.1.2 Quantitative Computed Tomography (QCT)

Quantitative Computed Tomography (QCT) is a well established method of measuring BMD of the appendicular skeleton, that is the bones of the upper and lower limbs and the pectoral and pelvic girdles (Pack and Bassett, 2011), and the lumbar spine (Bartl and Frisch, 2009), (National Osteoporosis Society, 2008). Unlike DXA, it provides a true volumetric measurement of bone density in g/cm^3 (Bartl and Frisch, 2009), (Bauer *et al*., 2010), (Griffith and Genant, 2008), (National Osteoporosis Society, 2008). Of further benefit is that fact that separate measurements of cancellous and compact bone are possible, which is particularly advantageous in the diagnosis and monitoring of osteoporosis (Bartl and Frisch, 2009), (Bauer *et al*., 2010), (Lang *et al*., 1998).

Commercially available computed tomography (CT) scanners are used in a wide range of clinical situations. During a CT scan a large number of 2D x-ray image slices are taken through the body or region of interest (Medline, 2012). By scanning the patient alongside mineral-equivalent calibration phantoms, commercial CT scanners can be used to obtain QCT measurements (Griffith and Genant, 2008). The 2D x-rays can then be reconstructed to produce three-dimensional (3D) image datasets of the scanned area (Bauer *et al*., 2010). The analysis relies on the fact that x-rays are absorbed by structures within the body at different intensities due to their respective densities. Tissues with high material density appear brighter in CT images due to their higher x-ray attenuation (Bauer *et al*., 2010). It is this difference in attenuation values, expressed in Hounsfield Units (HU), that enables the distinction to be made between cancellous and compact bone (Bauer *et al*., 2010), (National Osteoporosis Society, 2008).

The use of calibration phantoms of known attenuation properties allows conversion of the Hounsfield numbers to vBMD values (Bartl and Frisch, 2009), (Bauer *et al*., 2010). The values obtained are not T-scores, but a measurement

of the mass of hydroxyapatite present per unit volume in mg/cm^3 (Bartl and Frisch, 2009).

The main disadvantage of QCT for BMD measurement is the relatively high radiation dosage of approximately 100 to 1000 mSv (Bartl and Frisch, 2009). QCT is unsuitable for use in pregnant women and healthy children as a result of the high radiation associated with it (Fewtrell, 2003). Although the radiation dosage is greater than that associated with DXA, it is dependent on the measurement procedure used and may be reduced in future with advances in scanner technology (Griffith and Genant, 2008).

The use of QCT has a number of advantages including a relatively short scan time of 20 minutes (Bartl and Frisch, 2009). As QCT provides a separate measurement of cancellous BMD, which is metabolically more active than compact bone, it is generally considered to be more sensitive and superior to other BMD measurement techniques in the assessment and monitoring of osteoporotic related bone loss (Griffith and Genant, 2008), (Lang *et al*., 1998). Additionally, the errors arising in DXA measurements associated with spinal deformities and aortic calcifications are not present in QCT (Bauer *et al*., 2010). QCT is a reliable and straightforward technique for the diagnosis and monitoring of osteoporosis and subsequent assessment of treatment effectiveness (Bauer *et al*., 2010).

2.2.1.3 Peripheral Quantitative Computed Tomography (pQCT)

Peripheral quantitative computed tomography is a specialised type of QCT capable of generating *in vivo* high resolution images and making vBMD measurements of peripheral whole bones, for example the femur and tibia (Griffith and Genant, 2008), (van Rietbergen *et al.*, 1998). Measurements are carried out using specially designed CT scanners which are much smaller and less expensive than standard CT scanners (Griffith and Genant, 2008). The

resolution of pQCT systems is sufficient for visualisation of the architecture of cancellous bone (van Rietbergen *et al.*, 1998). It has become an established technique in the evaluation of bone status and is routinely used in the assessment of osteoporosis (Braun *et al*., 1998).

The benefits of pQCT include the fact that, like traditional QCT, it returns a true volumetric density and separate readings of cancellous and compact bone (Dionyssiotis *et al*., 2007), (Lochmüller *et al.*, 2002). Unlike QCT however, the radiation dosage associated with pQCT is relatively low (1 μSv) (Bartl and Frisch, 2009), (Dionyssiotis *et al*., 2007), (Eser *et al*., 2004), (Fewtrell, 2003). The use of pQCT also permits a method of non-invasively assessing the 3D structure and geometry of the bones of the appendicular skeleton (Dionyssiotis *et al*., 2007), (Fewtrell, 2003). The technology has been shown to be capable of determining the strength and architecture of bone in a range of conditions, such as adaptations in structure as a result of physical activity and differences related to age and gender (Capozza *et al*., 2010).

Quantification of BMD *in vivo* is essential to establish an estimation of bone strength and predict fracture risk. The techniques detailed have both advantages and disadvantages associated with their use. As stated previously, DXA is widely used in clinical settings to measure BMD and diagnose osteoporosis (Fewtrell, 2003). The aBMD values returned from DXA scans present a good estimate of bone strength and fracture risk, and the technique itself has many benefits, such as the low level of radiation exposure (Ashe *et al*., 2006), (Dowthwaite *et al*., 2011). However, due to the fact that DXA only provides a 2D analysis of bone and does not distinguish between compact and cancellous bone, it cannot account for the geometric properties of bone or provide a measurement of true vBMD (Ashe *et al*., 2006), (Dowthwaite *et al*., 2011).

As bone strength is known to be influenced by both bone mass and bone architecture (Bouxsein, 2005), (Griffith and Genant, 2008), (Van der Meulen *et al*., 2001), a measurement technique that accounts for differences in geometry, such as QCT and pQCT, is potentially of more use in estimating bone strength *in vivo*. Although both QCT and pQCT allow separation of compact and cancellous bone in BMD measurements, the much lower radiation dosage associated with pQCT recommends its use over QCT, particularly in a research setting where an individual may be subjected to repeated scans in a short time period. Due to the advantages pQCT offers over other measurement methods (Table 2.2), pQCT has gained popularity in BMD measurement and much research is being conducted in this area using this technique (Ashe *et al*., 2006), (Capozza *et al*., 2010), (Dowthwaite *et al*., 2011), (Eser *et al*., 2004), (Kontulainen *et al*., 2007), (Rantalainen *et al*., 2011).

Table 2.2: Summary of techniques for measuring BMD

Method	DXA	QCT	pQCT
aBMD/vBMD	aBMD	vBMD	vBMD
Radiation exposure	1 - 10 µSv	100 - 1000 mSv	1 µSv
Separate reading of compact and cancellous bone	×	✓	✓
Time	5 - 10 min	≈ 20 min	2 min/2 mm slice

2.2.2 Mechanical Testing

An appreciation of the mechanical properties of bone is important, for instance, in gaining a better understanding of the biomechanics of normal, diseased or injured bone, and the effectiveness of rehabilitation programs (Tascau *et al.*, 2009). The mechanical properties of bone are influenced by the external and internal architecture along with the properties of the tissue itself (Van Rietbergen *et al.*, 1998). Bone is anisotropic in nature, that is, its mechanical properties are different in different loading directions (Özkaya *et al*., 2012a),

and bones are subject to compressive, tensile, bending and torsional loading *in vivo* (Beaupied *et al.*, 2007), (Mellon and Tanner, 2012), (Van der Meulen *et al.*, 2001). Consequently a range of loading regimes and directions are necessary to fully characterise bone.

Mechanical testing of bone permits the direct assessment of a range of mechanical properties, such as strength and elastic modulus, and a number of testing techniques exist. Bones may be sectioned into beams or rods for mechanical testing or can be assessed as a whole bone (An, 2010). Where possible, the mechanical characterisation of bone should be carried out in an environment similar to that which the bone experiences *in vivo*. Ideally bone specimens are assessed at 37°C in a hydrated condition (Turner and Burr, 2001). The use of appropriate environmental conditions is particularly important during long term tests such as fatigue experiments. However it is not as critical in short term tests due to the fact that there is less time available in which the bone can dehydrate.

2.2.2.1 Compressive or Tensile Loading

Compressive and tensile tests are common methods used to determine mechanical properties of bone (An *et al*., 2010), (Aspden, 2003), (Beaupied *et al*., 2007). Cancellous, compact and whole bone specimen may be assessed in such loading configurations (Beaupied *et al*., 2007). However tension is generally used for compact bone and compression is more common for cancellous bone, due to difficulties associated with preparing appropriate specimens for tensile testing (Aspden, 2003). In compressive or tensile loading, force is applied perpendicularly to the specimen surface and resultant changes in specimen dimensions are recorded at various loads (An *et al*., 2010).

In compression tests (Figure 2.4 (a)), a cylindrical or cuboidal specimen of known dimensions is placed between two parallel plates and compressive

loading is applied at an appropriate rate. A decrease in specimen height and increase in CSA are generally observed (An *et al.*, 2010). In a tensile test (Figure 2.4 (b)), the specimen is aligned along the loading axis, consequently tensile testing of whole bones with irregular shapes can be difficult (Beaupied *et al.*, 2007).

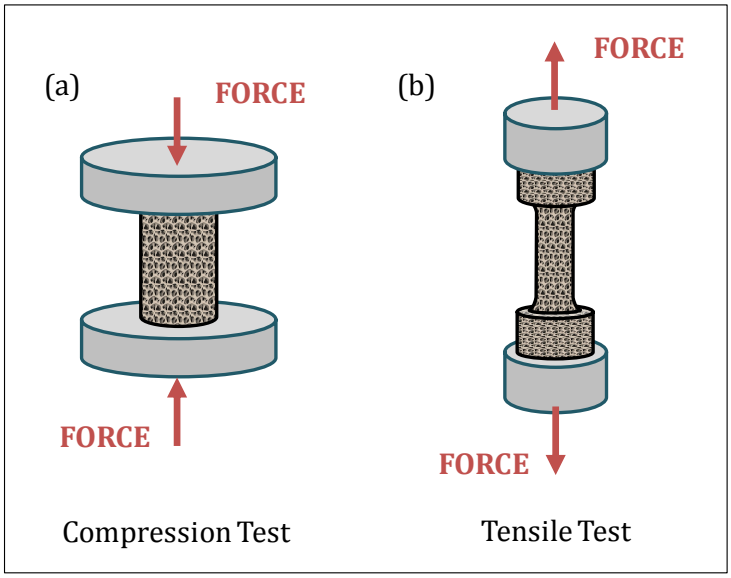

Figure 2.4: Representation of **(a):** compression and **(b):** tensile test of cancellous bone specimen

In assessing tensile properties, the specimen should be shaped so that the majority of the strain occurs in the central portion (Turner and Burr, 2001). Flat or rod shaped specimen are typically prepared with enlarged ends to permit gripping in the test machine, and a central portion with reduced CSA across which changes in length are measured (Benham *et al.*, 1996). Following careful alignment in the test machine, a tensile load is applied which stretches the specimen, typically resulting in a length increase and CSA decrease.

The collected force-displacement data allows determination of structural properties such as:

- Compressive/Tensile Stiffness (N/m): A measure of the specimen's resistance to deformation under the applied load, found by calculating

the gradient of the initial straight line portion of the force-displacement curve; and,

- Ultimate Force (N): The force necessary to cause the structure to fail, found by identifying the maximum force the structure can support.

Subsequent conversion of force and displacement to stress and strain (Equations 2.2(a) and (b)) permit the calculation of the equivalent material properties, i.e.:

- Young's Modulus (Pa) (also known as tensile modulus or elastic modulus): A measure of the ability of the material to resist deformation under the applied load, found by calculating the gradient of the initial straight line portion of the stress-strain curve; and,
- Ultimate Strength (Pa): The stress at which the material undergoes total failure, found by dividing the ultimate force by the specimen CSA.

2.2.2.2 Bending

Bending tests are frequently used to test whole bones and 3- and 4- point bending are popular test configurations (Sharir *et al*., 2008). The most frequently used test method is the 3-point bend test (Beaupied *et al*., 2007) as shown in Figure 2.5(a). In this test set-up, the whole bone is located symmetrically in the test rig, resting on two lower supports. A single central loading point applies an opposing force at the midpoint of the two supports. The force is applied in a downward direction, at right angles to the bone (Aspden, 2003), (Beaupied *et al*., 2007), (Sharir *et al*., 2008). The maximum load occurs at the point of application, i.e. the midpoint, and the bone under assessment will typically fracture at this site (Sharir *et al*., 2008). The reactions at the two supports are equal to half the force applied at the midpoint and act in the opposing direction (Figure 2.5(a)).

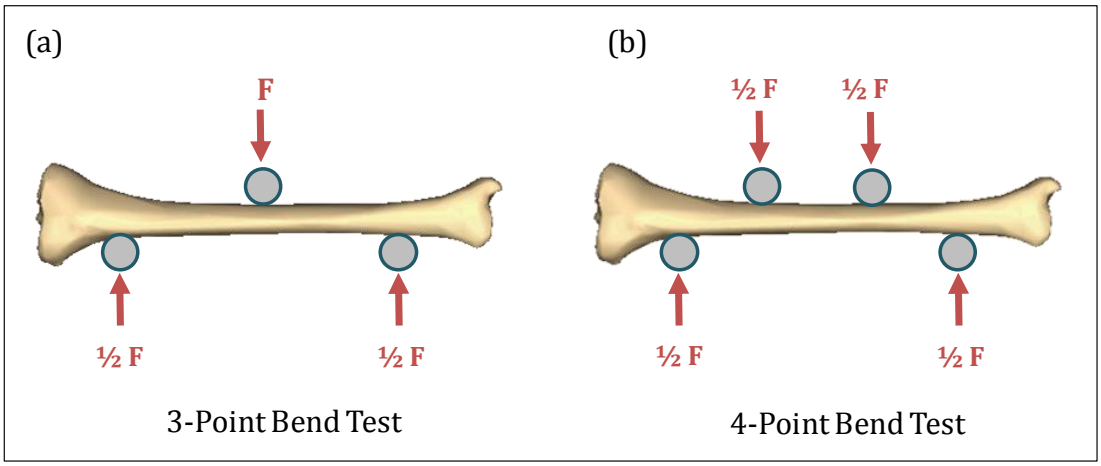

Figure 2.5: Representation of **(a):** 3-point bend and **(b):** 4-point bend test of a whole bone

The general set-up for 4-point bend tests (Figure 2.5(b)) is similar in that the specimen is supported by two lower points in the test rig. The compressive force however is applied in a downwards direction by two loading points located at equal distances from the midpoint (Beaupied *et al.*, 2007), (Sharir *et al.*, 2008). The region of bone located between the two loading points experiences a uniform moment (Sharir *et al.*, 2008). It is critical that the two loading points contact the bone at the same time to ensure the results obtained are accurate (Beaupied *et al.*, 2007). In both loading configurations, the force applied to the bone through the loading point is gradually increased and the resultant deflection recorded as a function of the applied force, allowing a force-displacement curve to be plotted. Generally the force is increased until the bone fractures.

Bending tests produce compressive forces and shortening of the top surface of the bone while the lower surface of the bone experiences tensile forces and lengthening (An *et al.*, 2010). The axis that lies midway between the two outer surfaces experiences zero loading and is known as the neutral axis (An *et al.*, 2010), (Sharir *et al.*, 2008). The tensile and compressive forces increase in magnitude linearly with distance from the neutral axis (Figure 2.6) (An *et al.*, 2010).

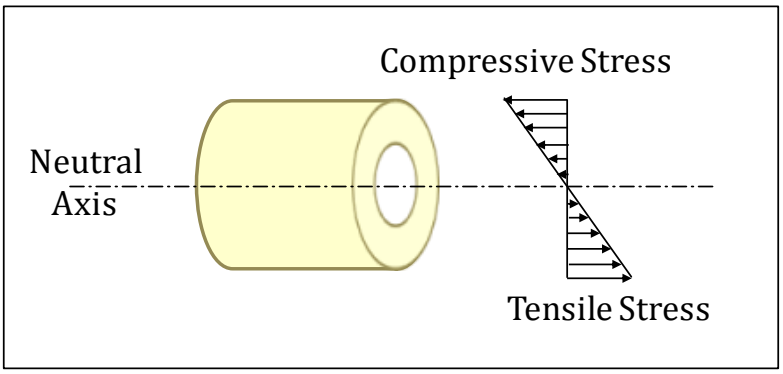

Figure 2.6: Distribution of stresses across the cross-section of a bone

The stress at any point in the bone can be calculated using Equation 2.3:

$$\sigma = \frac{My}{I} \qquad \textbf{Equation 2.3}$$

where: σ = bending stress (Pa)

M = bending moment (Nm)

y = perpendicular distance from point of interest to the neutral axis (m)

I = second moment of area (m^4) – calculated using Equation 2.1

Significant shear stress may be generated at the midpoint during 3-point bending and consequently 4-point bending is often the preferred loading configuration due to the absence of shear (Aspden, 2003). As the results of a 4-point bend tests are not influenced by applying the maximum bending moment at a specific point, this test set-up is particularly useful if the location at which the bone is most fragile is unclear (Beaupied et al., 2007). However due to the irregular surface geometry of most whole bones, it is often difficult to ensure both loading points in a 4-point bend test rig contact the surface simultaneously, leading to the more frequent use of 3-point bend tests (Aspden, 2003), (Sharir *et al.*, 2008).

2.2.2.3 Torsional Loading

Torsion tests are carried out to determine shear properties of the material, such as modulus of elasticity in shear, yield shear strength and ultimate shear strength. The properties determined during a torsion test are analogous to properties determined via a tensile test. Torsional testing is frequently used in assessing the strength of long bones and the shear stresses applied to the bones during movement (Beaupied *et al.*, 2007), (Belkoff and Haut, 2008), (Jämsä and Jalovaara, 1996). Additionally, torsional loading has been used to better understand spiral fractures which result only from loading in torsion (Psihogios, 1995), (Edwards and Troy, 2012).

In a torsion test (Figure 2.7), a whole bone or cylindrical specimen of bone is loaded in the test machine and torque applied, developing shear stress in the specimen (An *et al.*, 2010). Typically the ends of the specimen are embedded in polymer to allow the specimen to be gripped in the testing machine without damaging it (Beaupied *et al.*, 2007), (Sharir *et al.*, 2008). During the test one grip remains stationary while a torque, or twisting moment, is applied to the other and the angular deformation of the specimen as a function of the applied torque is measured.

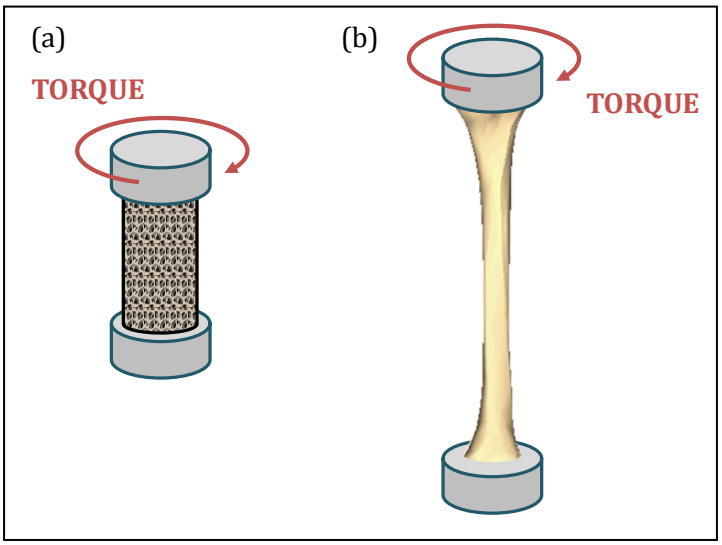

Figure 2.7: Representation of torsion test of a **(a):** cancellous bone specimen **(b):** whole bone

The applied torque causes the specimen to twist as the free end rotates relative to the fixed end, causing shear stress to development on all cross sections through the specimen. In Figure 2.8(a), the line AB lies parallel to the axis of rotation of the specimen. When the torsional moment, *T*, is applied to the free end of the specimen, the specimen deforms causing the straight line AB to twist, forming a helix AB' (Özkaya *et al.*, 2012b). The fixed end of the specimen remains stationary; consequently there is no deformation at point A. The deformation increases in magnitude moving away from the fixed end towards the free end of the specimen, where the angle γ, representing the shear strain, is a measure of the specimen deformation. The amount by which the specimen rotates is measured as the angle of twist, θ, in Figure 2.8(b). The stress magnitude increases with increasing distance from the axis of rotation as shown in Figure 2.8(c) (Bankoff, 2012).

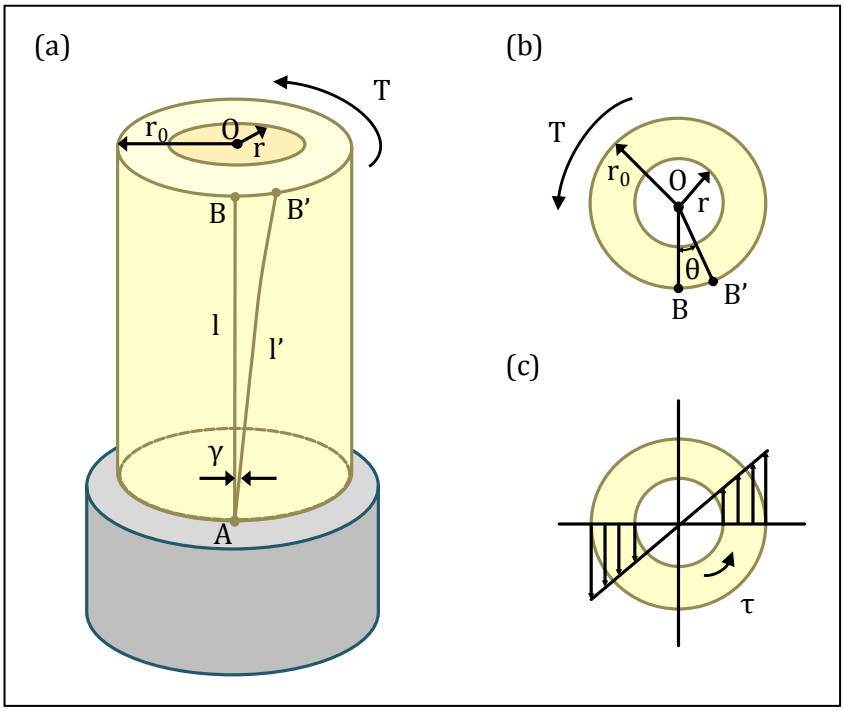

Figure 2.8(a): A circular shaft subjected to torsion, **(b):** a plane perpendicular to the centreline, **(c):** shear stress distribution as a result of torsion – adapted from Özkaya *et al.*, (2012b)

Shear stresses cause the elements of the specimen to slide relative to each other, while shear strain relates to the change in angle between two lines in specimen

which were perpendicular to each other prior to the application of torque (Morgan *et al*., 2009). The shear stress and shear strain caused as a result of torsion are calculated using Equations 2.4(a) and (b) respectively (An *et al*., 2010), (Özkaya *et al*., 2012b):

$$\tau = \frac{Tr}{J} \qquad \textbf{Equation 2.4(a)}$$

$$\gamma = \frac{\theta\, r_0}{l} \qquad \textbf{Equation 2.4(b)}$$

where: τ = shear stress (Pa)

T = torsional moment (Nm)

r = radial distance from point of interest to the axis of rotation (m)

J = polar second moment of area (m^4) – calculated using Equation 2.1

γ = shear strain

θ = angle of twist (radians)

r_o = outer radius of specimen (m)

l= length of specimen (m)

The shear modulus, G, of the specimen can then be calculated by relating the shear stress to the shear strain according to Equation 2.5.

$$G = \frac{\tau}{\gamma} \qquad \textbf{Equation 2.5}$$

where: G = shear modulus (Pa)

During routine daily activities and abnormal situations, such as trauma, a combination of compression and tension forces with bending and torsional moments are applied to the skeleton (Bouxsein, 2005), (Morgan *et al*., 2009). The accurate measurement of bone mechanical properties is an important task,

particularly in studies investigating osteoporosis and related conditions (Jämsä and Jalovaara, 1996). In an effort to assess and compare the properties of bone at different stages and conditions, researchers apply a range of mechanical tests representing compression, tension, bending and torsional loading (Agnew and Bolte, 2011), (Morgan *et al*., 2009). The behaviour of bone in bending and torsion is of particular concern as these loading modes generate the largest stresses in the bones of the appendicular skeleton (Bouxsein, 2005).

The fact that bone continually adapts to the forces it is subjected to results in the alignment of the trabeculae along the main loading axis where the greatest stresses, typically compressive or tensile, act (Beaupied *et al.*, 2007). *In vivo* bones are normally subject to compressive loading and bone is known to be strongest in compression (Belkoff and Haut, 2008). Compression and tensile tests are routinely used in the characterisation of bone, however, compression tests are generally less accurate than tensile tests as a result of specimen end effects generated during testing (Turner and Burr, 2001).

Although bones are normally loaded mainly in compression, failure may result from loading in any direction, especially if the failure is due to a traumatic event (Currey, 2012). The loads generated during traumatic events are typically not in line with the main loading axis, causing shear stresses to develop (Beaupied *et al.*, 2007). The use of torsion tests can provide useful information on the shear properties of bone (Beaupied *et al.*, 2007), (Belkoff and Haut, 2008) and torsional loading is more analogous to the type of loading experienced during traumatic events. Consequently the application of mechanical tests to determine bone properties are highly useful and clinically relevant, as long as the loading utilised during the tests are a good approximation of the relevant *in vivo* loading condition (Morgan *et al*., 2009).

2.3 Relating Bone Strength to BMD and Bone Geometry

As detailed in Section 1.2.1, osteoporosis results in a loss of mineral content and changes in bone architecture, such as a thinning of trabeculae and increase in porosity. It is clear then that osteoporotic bone will not be able to withstand the same loading as healthy bone, and a concurrent decrease in mechanical properties will be observed. As disorders such as osteoporosis increase the likelihood of bone fracture, it is important to consider the mechanical properties of bone in such conditions.

BMD measurement is widely used as an indicator of *in vivo* bone strength and as a predictor of fracture risk (Bonjour *et al*., 1994), (Griffith and Genant, 2008), (Haba *et al*., 2012), (Wachter *et al*., 2002). A correlation between BMD and bone strength has been recognised (Ilich and Kerstetter, 2000) and the relationship between BMD and fracture risk is well established and strong (Figure 2.9), with a 10% drop in bone density doubling the risk of fracture in vertebrae and tripling the risk for the hip joint (Bartl and Frisch, 2009). The difficulty associated with precisely assessing bone properties *in vivo* has led to the dependence on BMD measurements to gauge overall bone strength and fragility (Ilich and Kerstetter, 2000).

Despite the fact that BMD is commonly used clinically as a predictor of fracture risk, it is not a direct measurement of bone strength (Lloyd *et al*., 2004). Of further note is the fact that clinical measurements of BMD are a 2D areal measurement rather than a 3D volumetric measurement. Due to the limitations associated with relating fracture risk to BMD, clinical and scientific interest in more complete measures of bone quality have increased, with an aim to further improve the prediction of fracture risk (Donnelly, 2011). It is important to remember that bone strength is not influenced by BMD alone and the effect of bone geometry should not be overlooked (Griffith and Genant, 2008). In fact some researchers consider the geometry of the whole bone to be a more

important contributing factor to bone strength than aBMD or vBMD (Eser *et al.*, 2004).

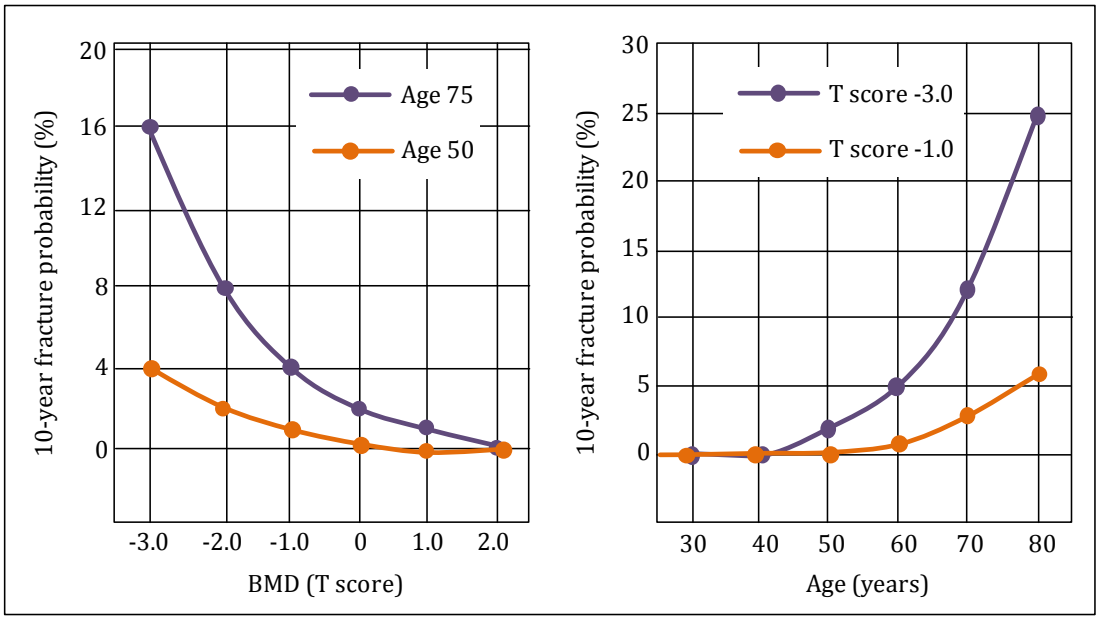

Figure 2.9: Relative risk of fracture according to BMD and age – redrawn from Bartl and Frisch (2009)

One of the reasons bone strength cannot be explained by BMD alone relates to the fact that changes in BMD do not necessarily echo the concurrent alterations in bone architecture (Griffith and Genant, 2008). For instance, for a particular bone a fall in BMD may result in the comparable thinning of a number of trabecular struts in one location, while the same fall in BMD could result in the total removal of trabecular struts in a different location. It is clear that complete removal of trabeculae will have a greater impact on bone strength than a uniform trabeculae thinning, consequently the same decrease in BMD will have a very different effect on bone strength. However as the majority of osteoporotic fractures are initiated in locations with a high degree of cancellous bone, the properties of such regions are of particular importance (Van Rietbergen *et al.*, 1998), (Wehrli, 2010).

Although osteoporosis related alterations in bone microarchitecture and diminished BMD are typically associated with increased fragility and fracture

risk, as bone ages, natural adjustments in geometry occur which attempt to preserve the strength of the whole bone (Bouxsein, 2005). Aging bone in the appendicular skeleton undergoes a remodelling process by which bone is resorbed, or removed, from the internal surface of the bone, along with formation of new bone on the outer surface (Bouxsein, 2005), (Griffith and Genant, 2008), (Morgan *et al*., 2009). This results in an increase in both the inner and outer diameters of long bones, leading to a decrease in cortical thickness but a parallel increase in, or at least maintenance of, second and polar second moments of area (Bouxsein, 2005), (Morgan *et al*., 2009). As material located further away from the neutral axis of the bone contributes to improved resistance to bending and torsional loading, such age related changes may work to lessen the fall in bone strength due to decreases in bone mass associated with aging (Morgan *et al*., 2009). It is important to realise that although such changes in geometry may improve bone strength, there may be little or no change in the bone BMD value (Bouxsein, 2005).

It is clear that BMD and geometry both contribute to bone strength and consequently measurement of both will allow improved prediction of bone mechanical properties *in vivo* and fracture risk (Griffith and Genant, 2008), (Van Rietbergen *et al.*, 1998). Imaging techniques, such as pQCT, allow measurement of BMD, overall bone geometry and relative fractions of compact and cancellous bone and accordingly may be used to obtain a more complete appreciation of bone strength (Augat *et al*., 1998), (Dambacher *et al*., 1998), (MacNeil and Boyd, 2007).

3.0 Project Aims and Objectives

3.0 Project Aims and Objectives

The overall aim of the project was to investigate the relationships between bone mechanical properties, BMD and geometric features. To achieve this, cadaveric human tibiae were analysed in an attempt to ascertain whether their mechanical integrity was influenced by BMD and/or geometry. The following specific objectives were identified:

- Mechanical testing of tibiae in a mode of loading analogous to that which causes fracture *in vivo*; and,
- Image analysis of pQCT scans of the same tibia to determine BMD and geometric features such as polar second moment of area.

An understanding of the connections between bone strength, BMD and geometric parameters could allow more informed predictions of a patient's fracture risk to be made from their BMD scan data. An accurate and non-invasive assessment of bone mechanical properties could be of great importance in the diagnosis of osteoporosis and bone fracture risk so that preventive measures could be taken in time.

4.0 Materials and Methods

4.0 Materials and Methods

As identified in Section 2, a relationship exists between bone strength, BMD, and bone geometry. While BMD is routinely used in the diagnosis of osteoporosis; as a marker of bone strength; and, in the prediction of fracture risk, the additional use of geometric analysis may provide a more complete description of bone strength *in vivo.* In this study, a combination of mechanical tests and image analysis were used in an attempt to establish a relationship between bone strength, BMD and geometric parameters of cadaveric tibiae.

The use of BMD measurement in combination with geometric analysis could allow improved estimations to be made of the bone mechanical properties of patients undergoing *in vivo* BMD measurement, and consequently a more refined prediction of fracture risk could be obtained. An accurate and non-invasive assessment of bone mechanical properties could be of great importance in the diagnosis of osteoporosis and bone fracture risk so that preventive measures, such as pharmacological and/or physical intervention, could be taken in time.

4.1 Cadaveric Material

Human cadaveric tibiae (n = 3) from individuals exhibiting different levels of bone health were provided by the Laboratory of Human Anatomy at the University of Glasgow, Scotland. The specimens were initially supplied as intact lower-limbs, inclusive of all bones and soft tissue distal to the mid-femur. Following scanning, the specimens were returned to the Laboratory of Human Anatomy where all soft tissue was removed by Mr Stuart McNally. The tibiae were cleaned and cut to an appropriate length using a band saw prior to transportation to the Bioengineering Department at the University of Strathclyde. The specimens were frozen and stored in an appropriate manner prior to mechanical testing. Relevant consents relating to the use of the cadaveric lower-limbs for research and teaching purposes were obtained by the

HMIA (Her Majesty's Inspector of Anatomy) licence holder at the University of Glasgow. Ethical approval was sought from the University of Strathclyde University Ethics Committee for both the scanning (UEC13/08 Coupaud/Gislason) and mechanical testing (UEC13/23 Coupaud/Newe/Riches/Gislason/Fogg) (Appendix A) of the cadaveric tibiae.

4.2 pQCT Scans

The intact lower limbs were scanned using peripheral quantitative computed tomography (pQCT). This technique is particularly useful for use in a study such as this as it permits distinctions to be made between compact and cancellous BMD and measurement of geometric properties (Capozza *et al.*, 2010), (Dionyssiotis *et al.*, 2007), (Eser *et al.*, 2004). The scans were carried out by Dr Sylvie Coupaud using a Stratec XCT 3000 (Stratec Medizintechnik, Pforzheim, Germany) scanner (Figure 4.1) based in the Queen Elizabeth National Spinal Injuries Unit (QENSIU) at the Southern General Hospital, Glasgow.

Figure 4.1: pQCT scanner with subject undergoing scan (image courtesy of Dr S Coupaud)

In Figure 4.1 the scanning procedure for a patient can be seen, with the individual positioned on the scanner chair with their extended lower limb

resting inside the central gantry of the scanner. During scanning of the cadaveric specimens, each specimen was located in a similar manner within the central gantry. Specimens were double bagged during scanning and the scanning area thoroughly cleaned afterwards to prevent any risk of contamination.

Prior to scanning, the length of the tibia was estimated by locating the knee and ankle joints. Cross-sectional images, or slices through the tibia, were obtained at regular intervals, equivalent to 1% of the tibia length, resulting in 100 images for each specimen with a voxel edge size of 0.5 mm. The images were obtained in two sets; the first image set (Slices 1-50) detailed the proximal region of the bone and the second (Slices 51-100), the distal region (Figure 4.2). Due to the nature of the scanning technique, it was possible to have a level of overlap between the two image sets. Any overlap present was accounted for during analysis. The cross-sectional image slices were exported as jpegs and corresponding csv (comma separated values) files for subsequent image analysis.

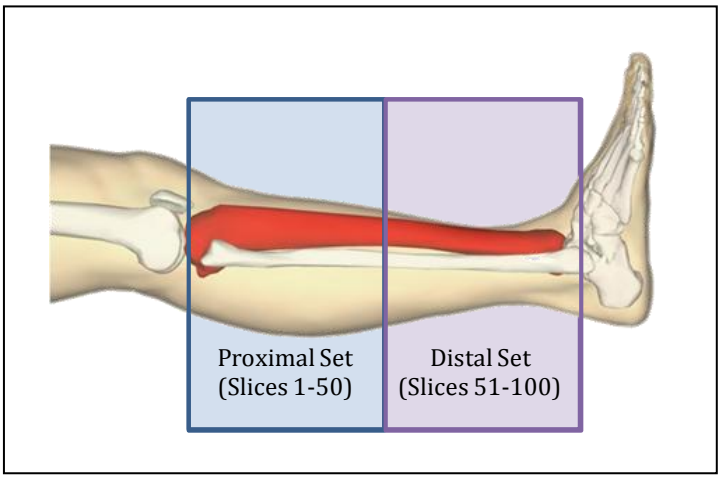

Figure 4.2: Diagram detailing proximal and distal image sets (tibia in red)

4.3 Mechanical Testing

Torsional tests were performed on the stripped tibiae by Caroline Newe using an Instron ElectroPuls E10000 Test System (Instron, UK) fitted with a 10kN

load cell located in the Bioengineering Department at the University of Strathclyde. The tibiae were allowed to thaw at room temperature prior to mechanical testing. To permit gripping of the specimen in the testing machine, the proximal and distal ends of the tibia were placed in purpose-built steel specimen holders (Figure 4.3). The specimen holders were then filled to a depth of 20 mm using polyester filler (David's Isopon P38, W. David & Sons Ltd, Northants, UK) so that the bone ends were firmly fixed in place. The section of the tibia located between the holders, the gauge length, was measured and recorded. The long axis of the bone was aligned as accurately as possible along the loading axis of the testing machine.

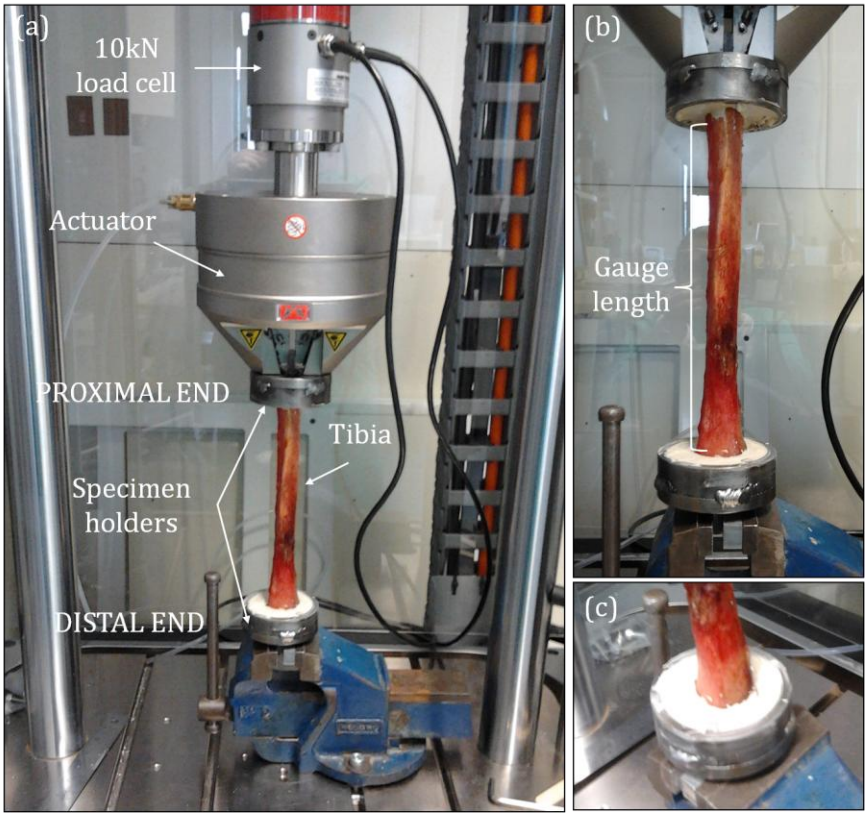

Figure 4.3(a): Specimen mounted in Instron test machine **(b):** Close up view of specimen gauge length and **(c):** specimen holder with polyester filler (images obtained with permission from the Laboratory of Human Anatomy at the University of Glasgow)

The tibiae were orientated in the test machine with the distal end attached to the base and the proximal end attached to the actuator. Rotational torque was

applied in an appropriate direction so as to load the proximal end of the tibiae in external rotation, i.e. a clockwise torque was applied to right limbs while an anticlockwise torque was applied to left limbs (Figure 4.4). The actuator rotated at a fixed rate of 1.0°/s until the bone fractured or an angle of 60° was reached. Torque and rotation data were collected at 1000 Hz during the test from which torque–rotation curves were plotted. Parameters including rotational stiffness, K, and torque at ultimate failure, T_{ult}, were calculated from the curves where possible.

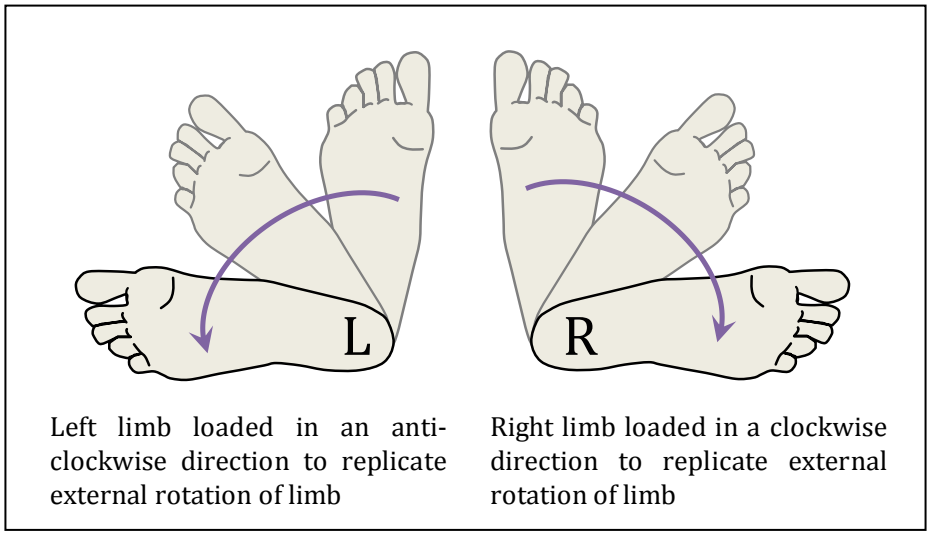

Figure 4.4: Schematic representation of direction of loading to cause external rotation of the limb

4.4 Image Analysis

Although it is not feasible to obtain direct measurements of bone strength *in vivo* (Griffith and Genant, 2008), the use of image analysis allows informed estimates of bone strength to be made. Parameters which impact on bone strength, such as BMD and geometric properties of bone cross-sections, can be readily obtained from image analysis. The cross-sectional image slices obtained from the pQCT scans of the tibiae were analysed by Caroline Newe using ImageJ software, version 1.48a, an open source image processing program (Schneider *et al.*, 2012).

As stated previous, the pQCT image slices were exported as jpegs and csv files. The image slices through the specimen are composed of volumetric elements arranged in rows and columns known as voxels. The individual voxels build up a representation of the original image and the greater the number of voxels, the closer the resemblance to the original image. The jpeg files obtained were 8-bit images consisting of voxels with 256 (2^8) possible grey levels (Figure 4.5). Voxels with low greyscale values represent low density regions of the scanned area whereas high greyscale values represent areas with greater density. In Figure 3.4 the large peak around zero corresponds to the air around the specimen, the mid-height peak represents the soft tissue surrounding the bone, and the smallest peak closest to the end of the scale signifies the bone.

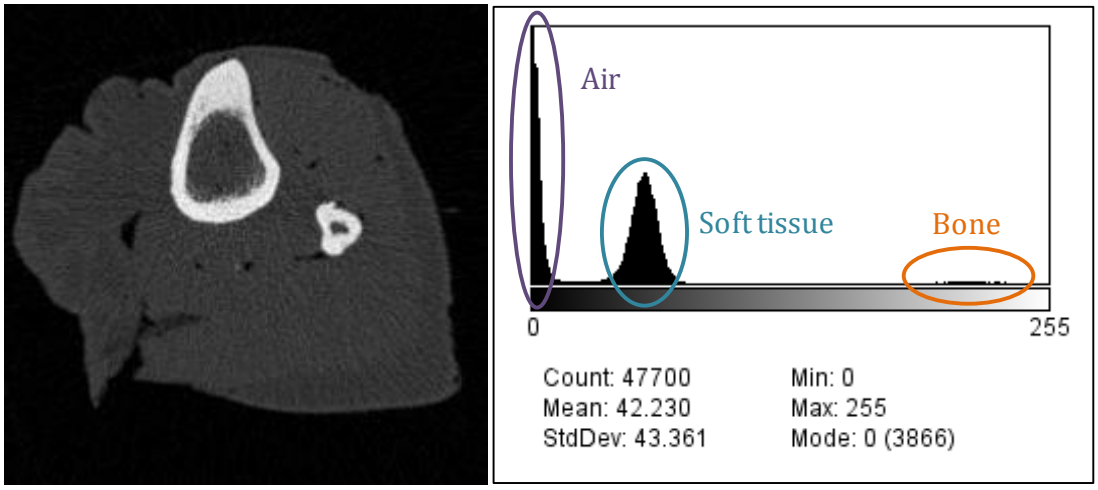

Figure 4.5: Jpeg image of **s**pecimen with histogram displaying corresponding greyscale values (image courtesy of Dr S Coupaud)

pQCT scans collect data in the form of Hounsfield (HU) units which provide a scale for determining tissue density. The HU scale was defined according to the x-ray attenuation of certain materials. The scale is set so that air has a value of -1000 HU, water is 0 HU and fully calcified bone has a value of +1000 HU (Horwood *et al.*, 2001). The scale extends further in the positive direction, reaching approximately +4000 HU for very dense metals. The HU values collected during pQCT scans permit calculation of BMD for the bone. As the jpeg images consisted of only 256 greyscale values, they could not be used directly to

determine BMD without appropriate calibration. However, the csv files contained the raw HU data collected during the scan. Each image slice had a csv associated with it which contained n rows × m columns, corresponding to the overall size of the representative image in voxels (n×m). Each cell in the spreadsheet represented a voxel, containing the voxel HU number (Figure 4.6).

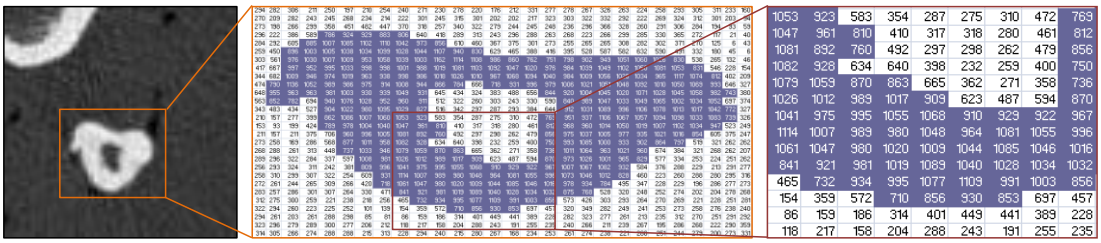

1053	923	583	354	287	275	310	472	769
1047	961	810	410	317	318	280	461	812
1081	892	760	492	297	298	262	479	856
1082	928	634	640	398	232	259	400	750
1079	1059	870	863	665	362	271	358	736
1026	1012	989	1017	909	623	487	594	870
1041	975	995	1055	1068	910	929	922	967
1114	1007	989	980	1048	964	1081	1055	996
1061	1047	980	1020	1009	1044	1085	1046	1016
841	921	981	1019	1089	1040	1028	1034	1032
465	732	934	995	1077	1109	991	1003	856
154	359	572	710	856	930	853	697	457
86	159	186	314	401	449	441	389	228
118	217	158	204	288	243	191	255	235

Figure 4.6: Section of csv file depicting bone and surrounding soft tissue

In order to create images that maintain the HU data, the csv files for each specimen were individually imported into ImageJ, scaled (1 voxel : 0.5 mm × 0.5 mm × 0.5 mm), and exported as a TIFF file (Tagged Image File Format). The TIFF files were 32-bit images, capable of contain up to $\approx 4.3\times10^{9}$ (2^{32}) possible greyscale levels, consequently the HU numbers obtained during the scan were maintained, allowing BMD values and geometric data to be determined from the raw data obtained during the scan. Note that BMD calculations were carried out for every slice within the image set whereas geometric analysis was performed on the images within the set corresponding to the specimen shaft.

4.4.1 BMD Calculation

As BMD measured by pQCT is reported in units of mg/cm^3, it was necessary to convert the HU numbers to density values. The calibration equation applicable to the scanner used in this study is given in Equation 4.1 (Findlay, 2012):

$$BMDIm = (HUIm \times 1.495) - 341 \qquad \textbf{Equation 4.1}$$

where: BMDIm = BMD (mg/cm^3)

HUIm = Voxel greyscale value (HU)

It should be noted that the calibration equation was not applied directly to the image, rather analysis was performed on the TIFF files and the resulting HU values were converted to mg/cm^3 using Equation 3.1. In order to isolate the bone from the surrounding air and soft tissue, and compact bone from cancellous bone, it was necessary to apply thresholding to the images (Figure 4.7). The threshold values identified by the manufacturer of the pQCT scanner used in this study are as follows: Muscle/soft-tissue – 34 mg/cm^3, Bone – 200 mg/cm^3; and, Compact bone – 710 mg/cm^3 (Findlay, 2012). Equation 3.1 was used to convert the BMD values in mg/cm^3 to HU units (Table 4.1), allowing the TIFF files to be thresholded with respect to HU.

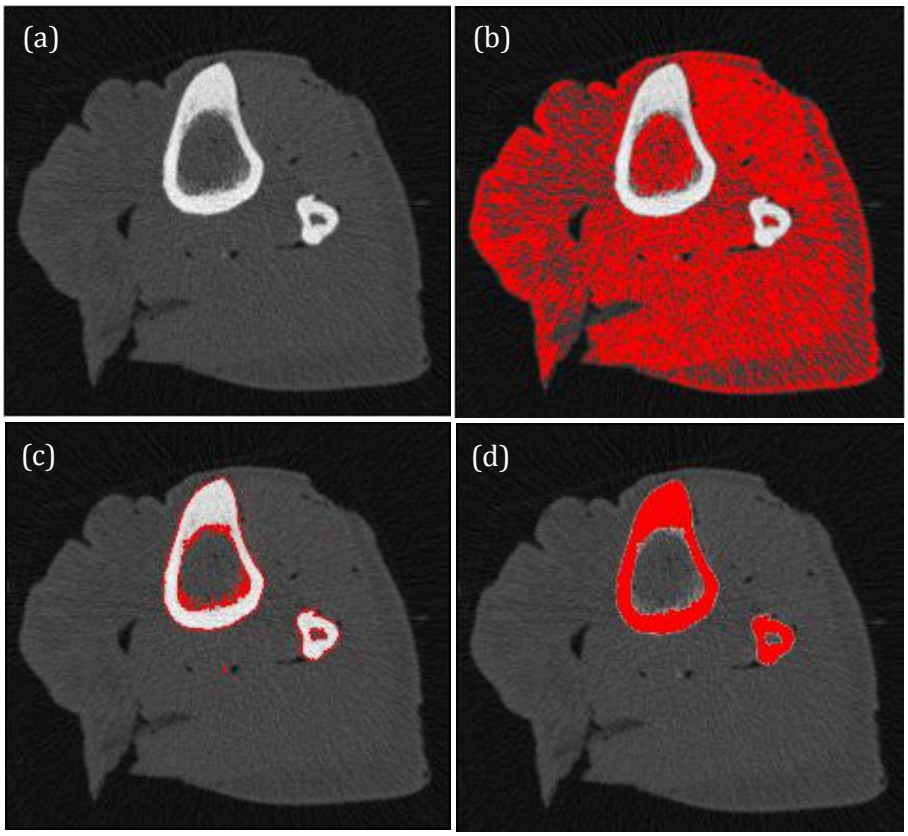

Figure 4.7(a): TIFF image of bone and soft tissue **(b):** Isolated muscle/soft tissue (threshold: 205.8-361.9) **(c):** Bone isolated from muscle/soft tissue less compact bone (threshold: 361.9-703.0) **(d):** Isolated compact bone (threshold: 703.0-max HU number)

Table 4.1: Conversion of BMD values in mg/cm^3 to HU units

Structure	Density (mg/cm^3)	HU
Muscle/soft-tissue	34	250.836
Bone	200	361.873
Compact bone	710	703.010

Further threshold limits enabled division of the bone into areas of:

- Low-BMD (threshold: 200 - 400 mg/cm^3, 361.873 - 495.652 HU), corresponding mainly to cancellous bone;
- Medium-BMD (threshold: 400 - 800 mg/cm^3, 495.652 - 763.211 HU), corresponding mainly to porous compact bone; and,
- High-BMD (threshold: > 800 mg/cm^3, > 763.211 HU), corresponding to dense compact bone (Roldán *et al*., 2001).

Following application of the relevant threshold images, voxels which fell inside the applied threshold range retained their greyscale value, while those that fell outside the threshold range were designated as empty space, appearing as solid black in the image (greyscale value of 0) (Figure 4.8(b)). Following thresholding, the image was cropped to remove the fibula and some of the soft tissue present. For each slice the mean greyscale value was determined using a function built-in to the ImageJ software and input into Equation 4.1 to calculate the corresponding BMD in mg/cm^3 (Vijay *et al*., 2011).

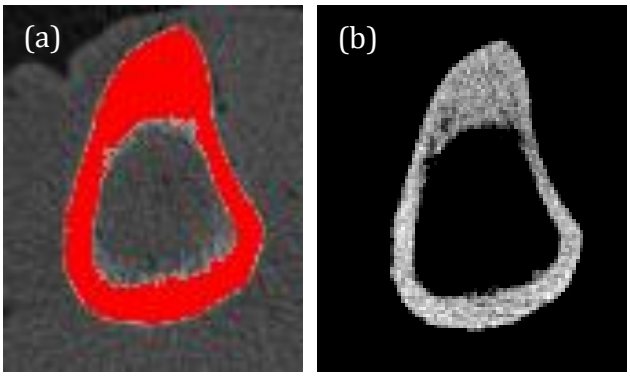

Figure 4.8(a): Threshold applied to isolate compact bone **(b):** Thresholded image where grey voxels represent bone and black voxels represent empty space

To establish the state of the specimens in relation to osteoporosis, further analysis was carried out on Regions 1 and 3 of each specimen. These regions correspond to areas with a high proportion of cancellous bone, where manifestations of osteoporosis are most evident. The specimens were screened for osteoporosis by identifying a region of interest (ROI) which encompassed the entire bone cross-section (Figure 4.9(a)). The area of the ROI was determined using the software, following which a new ROI with an area 45% of the original ROI was defined, corresponding to the central core of the specimen cross-section (Figure 4.9(b)). The mean HU value of the new ROI was found allowing the BMD to be calculated as before.

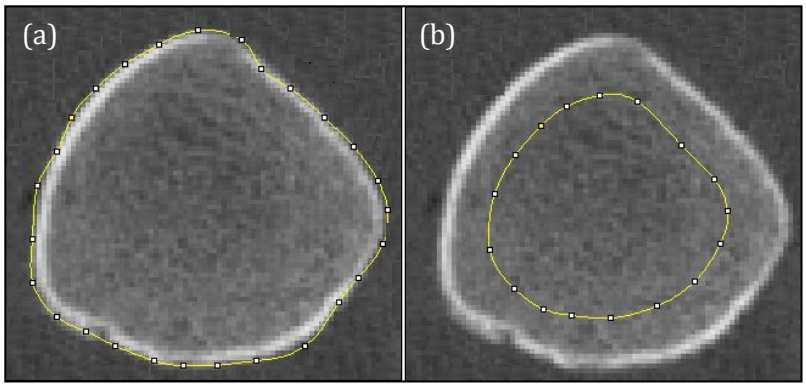

Figure 4.9(a): ROI of entire bone cross-section **(b):** ROI of central core (45% by area of entire bone cross-section)

4.4.2 Geometric Analysis

Geometric measurements of the bone cross-sections provide information relating to the bone mechanical properties based on the distribution of bone mass (Nelson *et al.*, 2000). Following the application of the relevant threshold as detailed in Section 4.4.1, the images were binarised, that is the images were converted to 1-bit, displaying only two colours, black or white. In the analysis carried out in this section black represented solid material (compact bone) and white represented the open space (pores and surrounding air) (Figure 4.10(a)).

The geometric parameters determined for the isolated compact bone were:

- Compact cross-sectional area, CSA_{Comp}: cross-sectional area of isolated compact bone with all soft tissue and voids eliminated (mm^2) (Figure 4.10(a));
- Tibia cross-sectional area, CSA_{Tib}: cross-sectional area of tibial shaft inclusive of compact bone, central cavity, soft tissue and voids (mm^2) (Figure 4.10(b));
- Cavity cross-sectional area, CSA_{Cav}: cross-sectional area of central cavity of shaft (mm^2) (Figure 4.10(c));
- Compact bone outer perimeter, P_{Outer}: external perimeter of compact bone, or, external perimeter of the tibia cross-section (mm) (Figure 4.10(d));
- Compact bone inner perimeter, P_{Inner}: internal perimeter of compact bone, or, external perimeter of central cavity (mm) (Figure 4.10(e));
- Average compact bone thickness, T_{Comp}: CSA_{Tib} and CSA_{Cav} were replaced by ellipses of equivalent area and their respective major and minor axes used to calculate an estimate of the compact bone thickness along the major and minor axes (mm) (Figure 4.10(f));
- Circularity: a measure of the structural efficiency of the specimen, calculated using Equation 4.2:

$$Circularity = \frac{4\pi CSA_{Tib}}{P_{Outer}^{\ 2}} \qquad \textbf{Equation 4.2}$$

  A value of 1.0 indicates a perfect circle. As the value approaches 0.0, it indicates an increasingly elongated shape; and,
- Polar second moment of area, J: a property of the cross-sectional area that characterises the ability of the structure to resist twisting (mm^4).

It should be noted that the investigator was blind to the history of the donors, i.e. sex, age and health status, at the time of mechanical testing and image analysis.

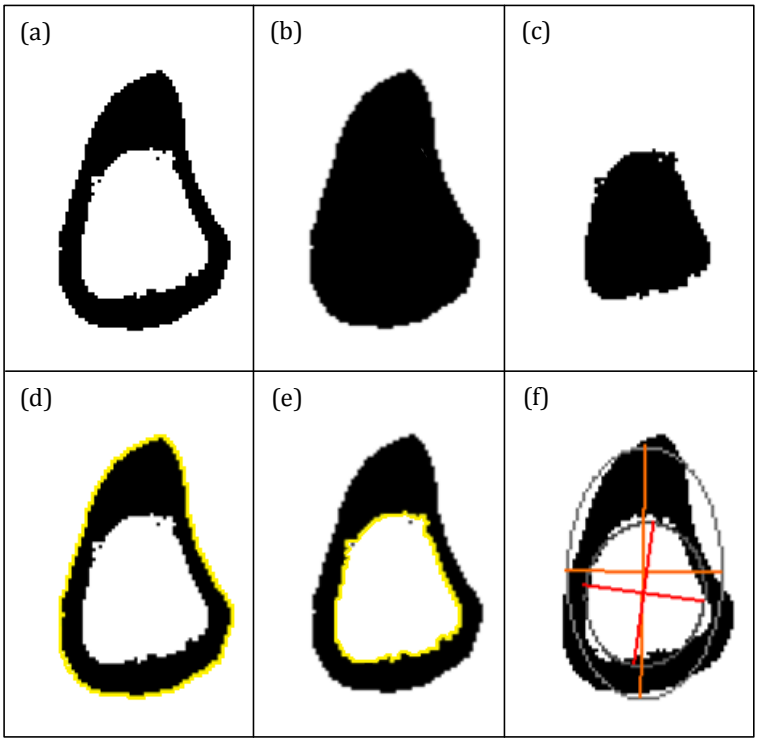

Figure 4.10(a): Compact cross-sectional area, **(b):** Tibia cross-sectional area, **(c):** Cavity cross-sectional area, **(d):** Periosteal perimeter, **(e):** Endocortical perimeter, **(f):** Average compact bone thickness

4.5 Statistical Analysis

A simple correlation analysis was performed between BMD and the geometric properties of the tibiae shafts. The data for the three specimens were combined and analysed to determine overall relationships between BMD and compact bone cross-sectional area and between BMD and polar second moment of area. The R^2 values, also known as the coefficient of determination, were found for the combined datasets. The R^2 value gives an indication of the correlation between two variables (Rowntree, 2000). If a perfect relationship existed between the two variables, the R^2 value would be 1. Counter to this, if no relationship was present between the two variables, the R^2 value would be 0. A positive value of R^2 indicates a positive correlation, i.e. as the value of one variable increases the value of the second variable also increases, while a negative value signifies a negative correlation. Generally a R^2 value of $> \pm 0.7$ is considered a strong correlation while a R^2 value of $< \pm 0.3$ is considered a weak correlation.

5.0 Results

5.0 Results

5.1 Specimen Considerations

Three tibia specimens were examined during the course of the study (Table 5.1). The specimens were labelled A, B and C with specimen B and C obtained from the same individual. Prior to mechanical testing the tibiae were cut to size using a bandsaw. A portion of the proximal (≈ 62 mm) and distal (≈ 18 mm) regions of specimen A were removed to facilitate mounting in the specimen holder (Figure 5.1). Consequently the gauge length of the specimen contained both compact and cancellous bone.

Table 5.1: Specimen details

Specimen Label	Right/Left	Specimen Length (mm)	Gauge Length (mm)
A	Right	357	242
B	Right	433	167
C	Left	441	153

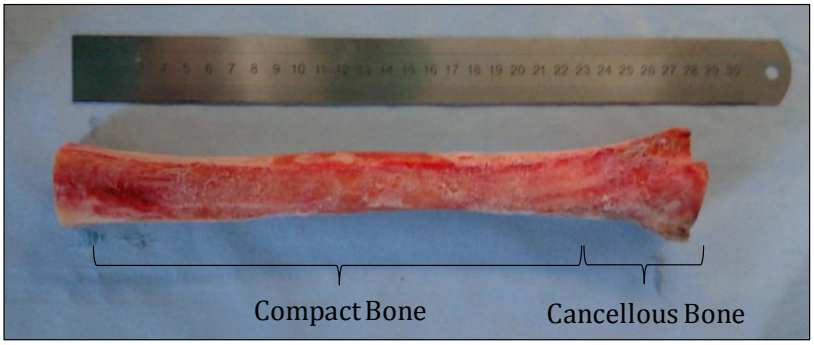

Figure 5.1: Image of specimen A indicating compact and cancellous regions (image with permission from the Laboratory of Human Anatomy at the University of Glasgow)

The pQCT scans of specimens B and C revealed the presence of structural defects, in the form of screw holes, at both the proximal and distal ends (Figure 5.2). As a result it was necessary to cut both bones to a smaller gauge length than that of specimen A. This mode of sectioning resulted in the removal of the largely cancellous regions. Consequently solely the shaft, containing predominantly compact bone, was tested in torsion (Figure 5.3).

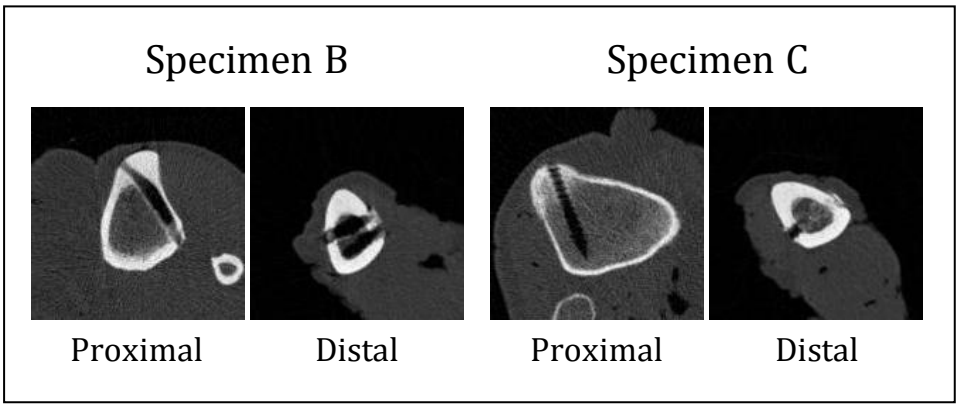

Figure 5.2: Image slices through specimens B and C highlighting defects (images courtesy of Dr S Coupaud)

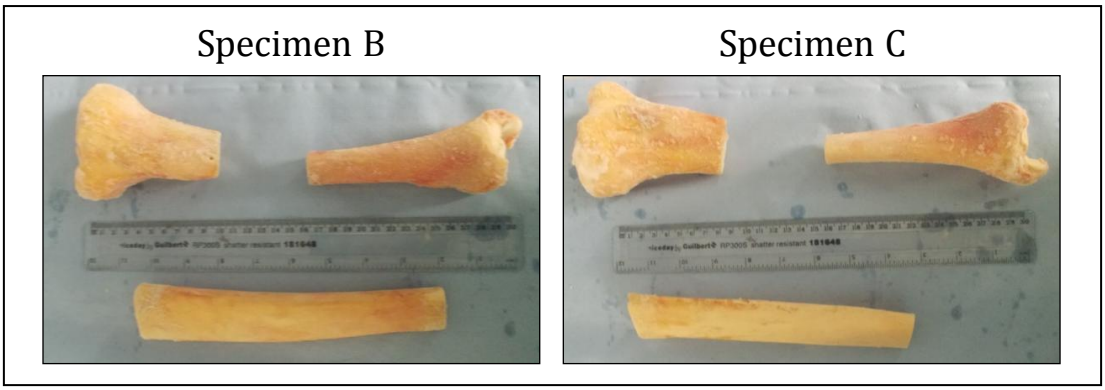

Figure 5.3: Sectioning of specimens B and C (images obtained with permission from the Laboratory of Human Anatomy at the University of Glasgow)

In the geometric analysis, the specimen image stacks were divided into three regions consisting of the proximal, shaft and distal regions (Regions 1, 2 and 3 respectively) to facilitate analysis. During the scanning of specimen B it was not possible to capture the most proximal region of the specimen (Region 1), consequently the image analysis of specimen B consisted of Regions 2 and 3.

5.2 Mechanical Testing

Torque-rotation and shear stress-shear strain curves were plotted for each specimen, allowing calculation of rotational stiffness and shear modulus. The individual curves for each specimen are shown in Figure 5.4. For each curve a straight line was drawn from the origin (0, 0) through as much of the initial straight portion of the curve as possible. The gradient of the straight line was calculated by dividing the change in y co-ordinate by the change in the x co-

ordinate. The torsional stiffness of the specimens was determined by calculating the gradient of the initial straight line portion of the rotation-torque curves (Figure 5.4(a)) while the shear modulus was calculated from the initial straight line portion of the stress-strain curve (Figure 5.4(b)). The Table 5.2 details the torsional stiffness and shear modulus of the three specimens.

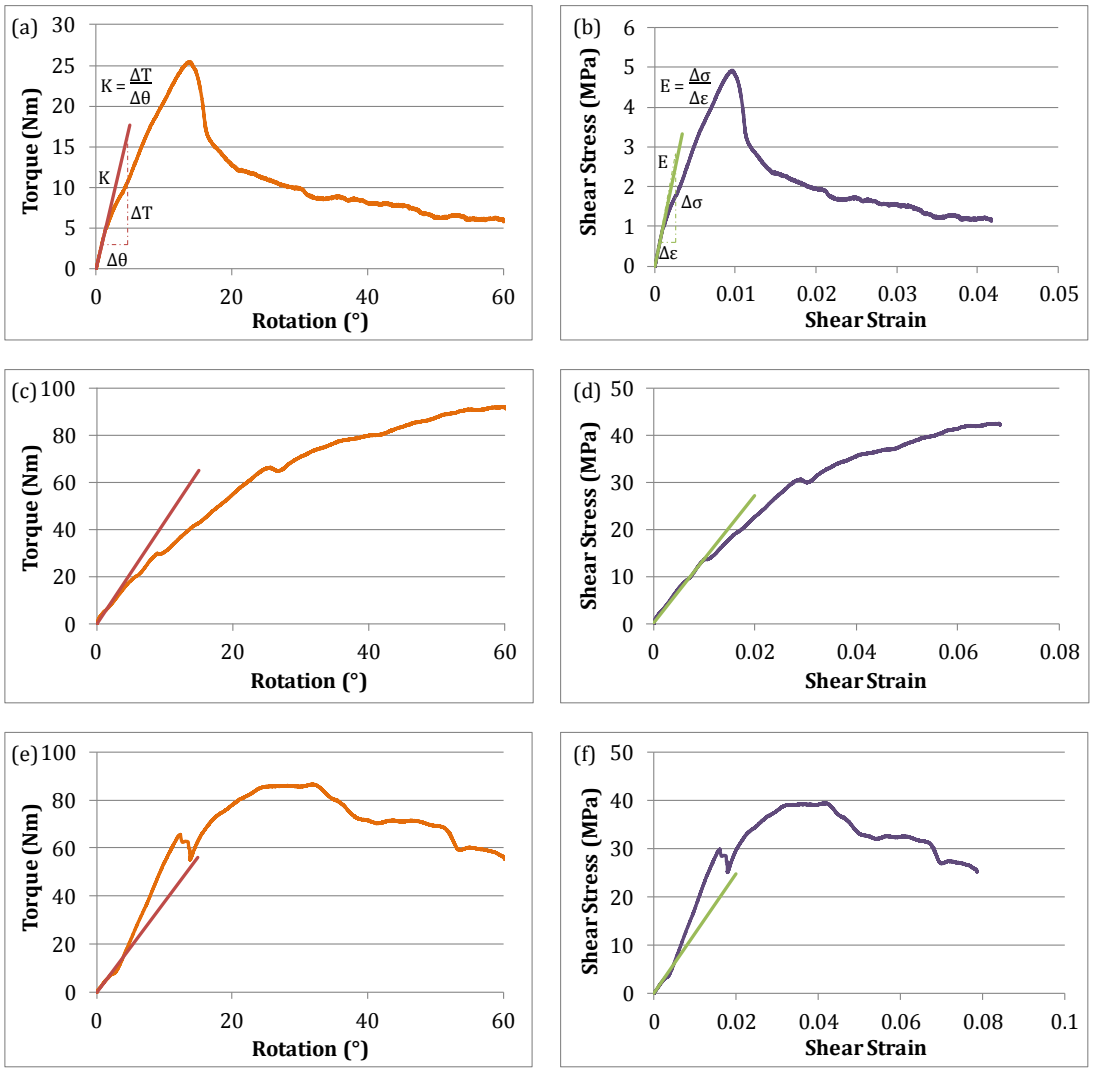

Figure 5.4: Specimen A **(a):** torque-rotation and **(b):** stress-strain curves; Specimen B **(c):** torque-rotation and **(d):** stress-strain curves; and, Specimen C **(e):** torque-rotation and **(f):** stress-strain curves

Table 5.2: Rotational stiffness and shear modulus of specimens

Specimen	Rotational Stiffness, K (Nm/°)	Shear Modulus, G (MPa)
A	3.540	953.963
B	4.354	1362.352
C	3.743	1232.204

Specimen B was found to possess the greatest rotational stiffness and shear modulus (K = 4.354 Nm/°, G = 1362.352 MPa), followed by specimen C (K = 3.743 Nm/°, G = 1232.204 MPa), with specimen A demonstrating the lowest values (K = 3.540 Nm/°, G = 953.963 MPa). The values of rotational stiffness and shear modului followed the same pattern between specimens, with specimen B > specimen C > specimen A. The three tibiae displayed comparable values of rotational stiffness (average: 3.879 ± 0.424 Nm/°) while a greater variation existed between shear modulus values (average: 1182.840 ± 208.622 MPa). As shear modulus is a material property, the variation between specimens could be due to the fact that specimen A contained regions of cancellous and compact bone while B and C contained predominately compact bone. The comparable values of G for specimens B and C are due to that fact that they were obtained from the same individual and possessed a similar cross-section.

Specimen A was the only specimen that fractured during the torsional test. The tibia fractured at the distal end where there was a relatively high proportion of cancellous bone (Figure 5.5). The tibia fractured at an approximate 45° angle (Figure 5.5(c)) and a short spiral fracture pattern was evident. As specimen A fractured, it was possible to determine the ultimate torque, T_{ult}, of the specimen by identifying the maximum torque value of 25.450 Nm, corresponding to the peak in Figure 5.4(a). The corresponding ultimate shear stress, τ_{ult}, was 4.930 MPa, τ_{ult}, also known as the torsional strength of the material (Figure 5.4(b)), is a measure of its ability to withstand the application of torque.

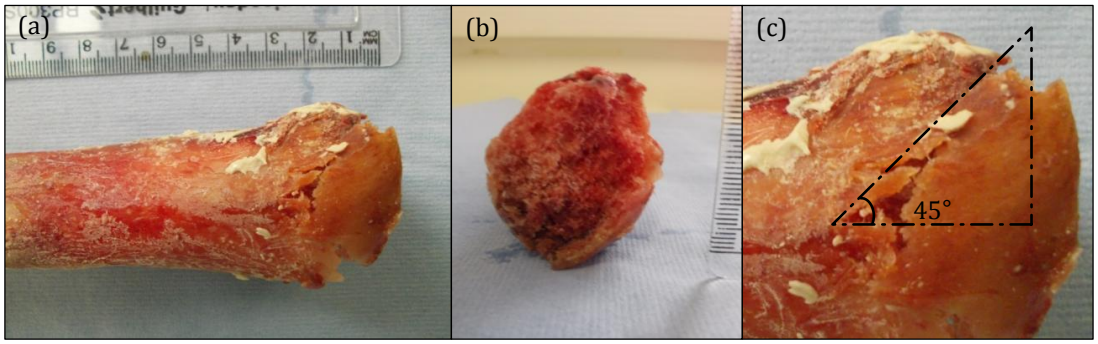

Figure 5.5(a): Specimen A following fracture, **(b):** end view of fracture site, **(c):** close up of fracture showing 45° spiral fracture (images obtained with permission from the Laboratory of Human Anatomy at the University of Glasgow)

As specimens B and C consisted of the tibial shaft, which is predominantly compact bone, they were much stronger in torsion than specimen A. As a result specimens B and C did not fracture, in fact, they twisted out of the polyester filler as the test progressed. For that reason only the initial portion of the curve at small rotation angles was deemed relevant to the bone itself (rotation angle < ≈7°). It should be noted that the lack of peak torque and shear stress values in Figures 5.4(c) and (d) are due to the gradual twisting of specimen B out of the filler material, whereas the peaks present in Figures 5.4(e) and (f) represent the fracturing of the filler material as specimen C twisted and broke free.

5.3 Image Analysis

In order to perform image analysis on the pQCT scans of the tibia, the image set for each scan was divided into three sections corresponding to the three regions illustrated in Figure 5.6. Within Regions 1 and 3, every second image slice was analysed, while within Region 2, every third slice was examined. BMD measurement was performed over all three regions while geometric analysis was carried out on Region 2, corresponding to the main tibial shaft, alone. The analysed slices were numbered sequentially with 1 corresponding to the most proximal end of the specimen.

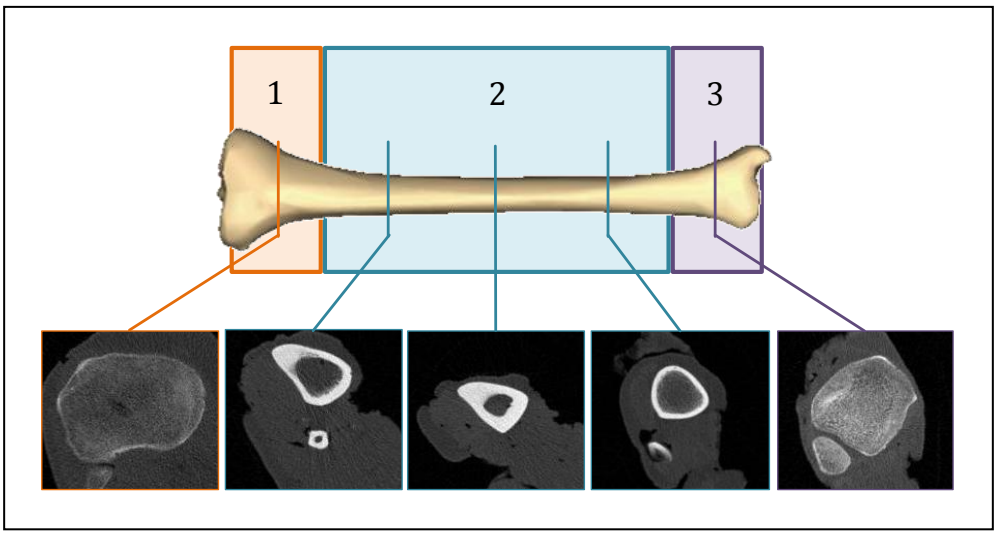

Figure 5.6: Division of scan set into regions for image analysis

5.3.1 BMD Calculation

Figure 5.7 demonstrates the percentage of compact bone (Threshold 2: 703.010 HU – MAX HU) relative to the total bone volume (Threshold 1: 361.873 HU – MAX HU) for specimen A along its length. The higher % of compact bone in the shaft can be clearly seen. The progression of the change in composition from the proximal region (mainly cancellous bone), through the shaft (predominantly compact) to the distal region (cancellous) can be readily visualised. In moving from the proximal end, the proportion of compact bone increased, reaching a maximum at the approximate mid-point of the tibia, before decreasing again towards the distal end.

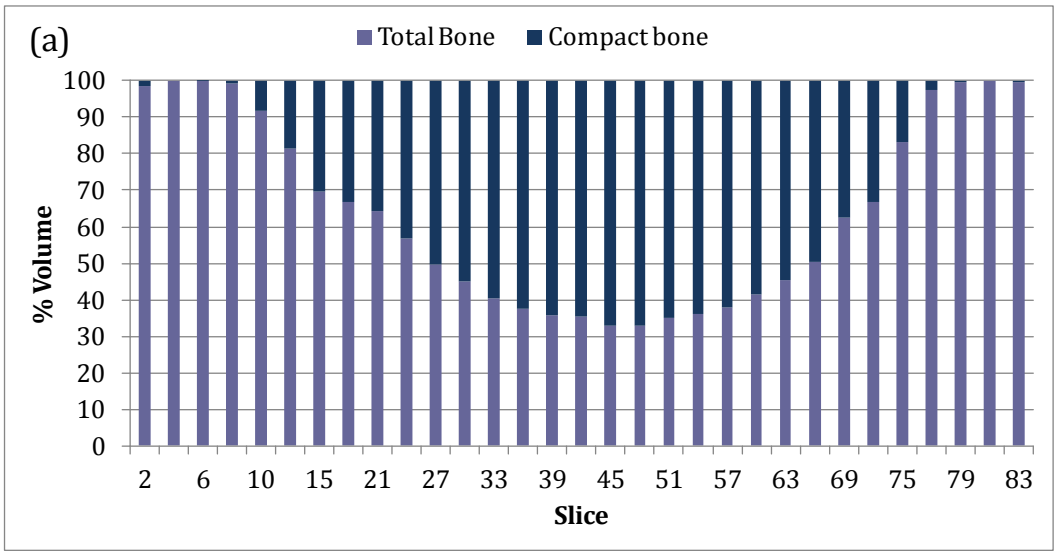

Figure 5.7: % volume of compact bone present in specimen A

Specimens B and C demonstrated a similar pattern, with the greatest proportion of compact bone found at the mid-point of the specimens. Specimens B and C contained a greater proportion by volume of compact bone than specimen A. This is likely to be due to inter-person variation as B and C were obtained from the same individual. Specimen A contained a greater proportion of cancellous bone at its midpoint (32.62 %) compared to specimens B (13.57 %) and C (13.36%).

The threshold ranges 3 (361.873 HU – 495.652 HU), 4 (495.652 – 763.211 HU) and 5 (763.211 HU – MAX HU) were then applied to separate each slice into regions of low-, medium- and high-BMD bone. In general, each slice contained areas of low-, medium- and high-BMD bone (Figures 5.8(a), 5.9(a) and 5.10(a)). To establish the amount of each bone type within a slice, the BMD value for each threshold range was multiplied by its respective volume, yielding a value for the bone mineral content (BMC) in mg. Figures 5.8, 5.9, and 5.10 display the BMD and BMC content of each BMD bone type for specimens A, B and C respectively. Tables 5.3, 5.4 and 5.5 detail the breakdown of BMC by volume, allowing average BMD values to be calculated for each threshold range within each region, as well as an overall BMD value for the whole bone.

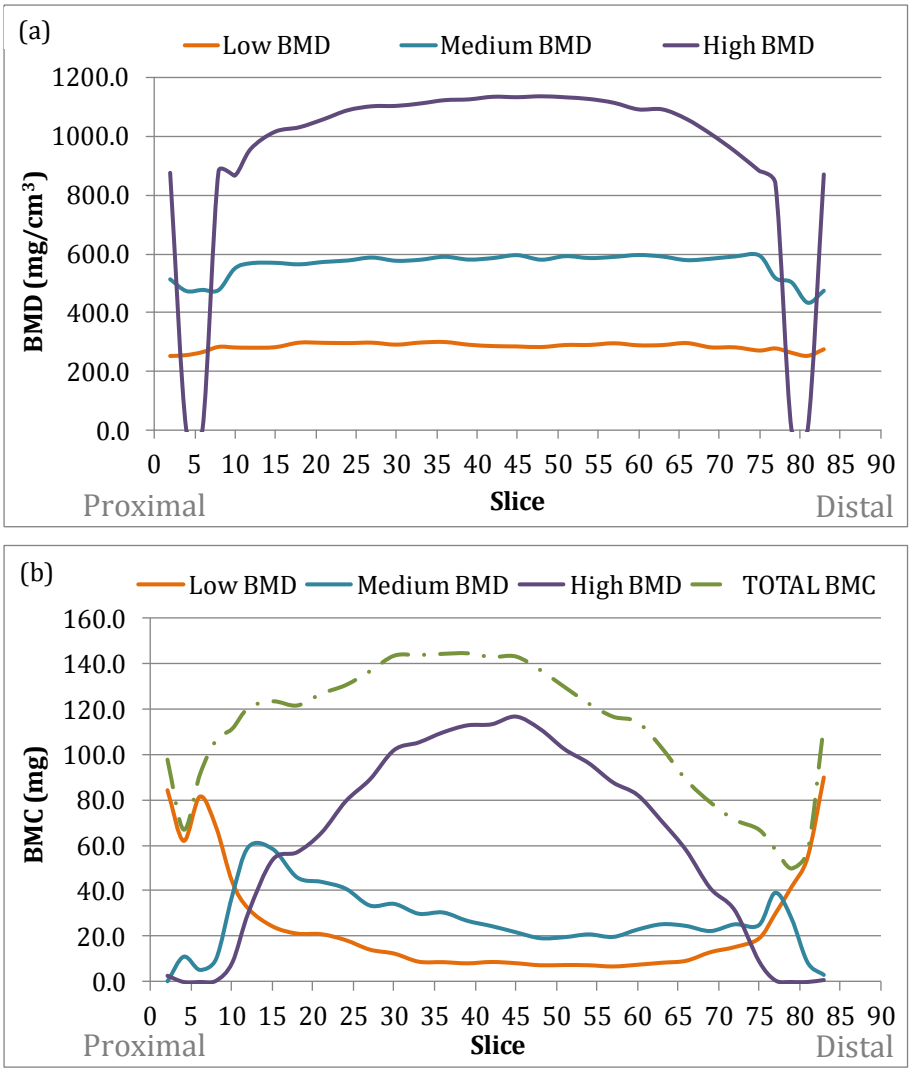

Figure 5.8(a): BMD and **(b):** BMC content for specimen A

Table 5.3: BMC by volume for specimen A

	Region 1			Region 2			Region 3		
	Low-BMD	Med-BMD	High-BMD	Low-BMD	Med-BMD	High-BMD	Low-BMD	Med-BMD	High-BMD
BMC (mg)	339.1	122.8	11.8	261.7	611.7	1713.3	234.3	100.1	10.7
Vol (cm³)	1.3	0.2	0.01	0.9	1.1	1.6	0.9	0.2	0.01
BMD (mg/cm³)	266.0	512.0	867.1	290.8	580.3	1094.3	268.2	529.0	876.5

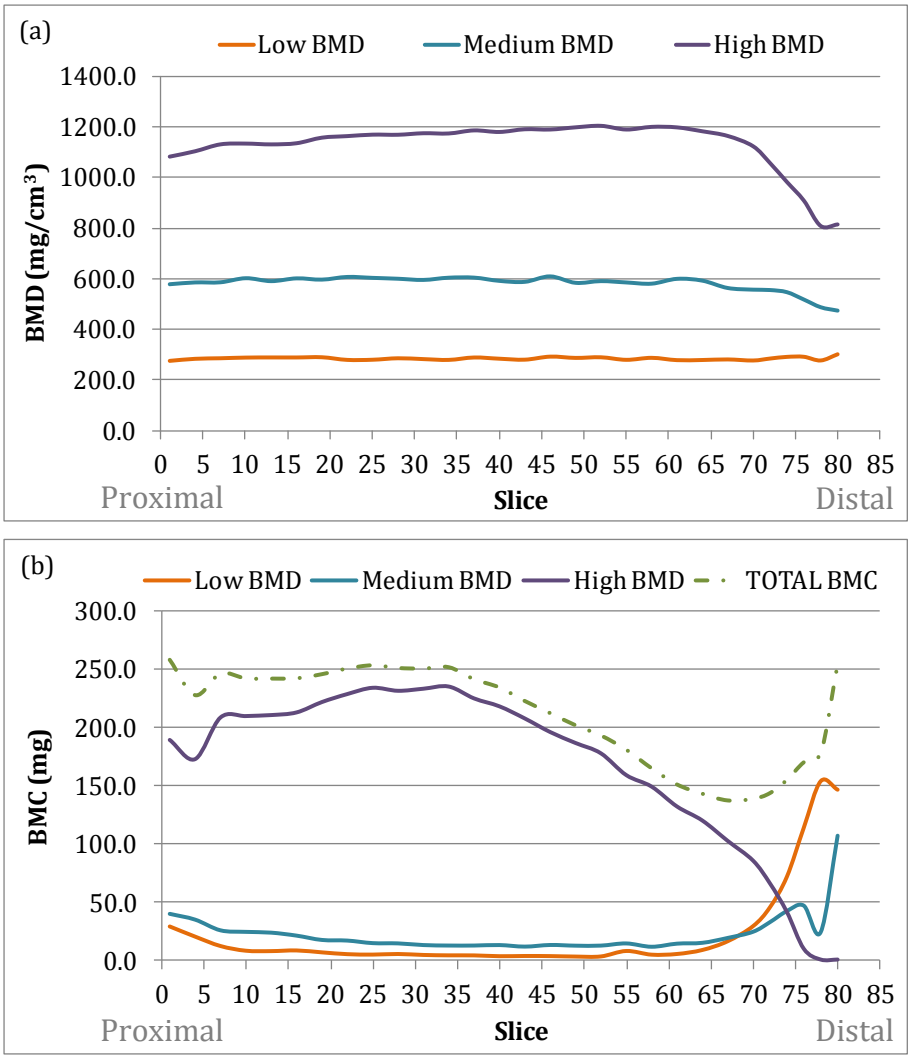

Figure 5.9(a): BMD and **(b):** BMC content for specimen B

Table 5.4: BMC by volume for specimen B

	Region 1			Region 2			Region 3		
	Low-BMD	Med-BMD	High-BMD	Low-BMD	Med-BMD	High-BMD	Low-BMD	Med-BMD	High-BMD
BMC (mg)	0.0	0.0	0.0	188.9	400.3	4448.8	561.5	276.6	201.0
Vol (cm³)	0.0	0.0	0.0	0.7	0.7	3.8	1.9	0.5	0.2
BMD (mg/cm³)	0.0	0.0	0.0	283.2	590.8	1166.7	289.6	509.0	1061.5

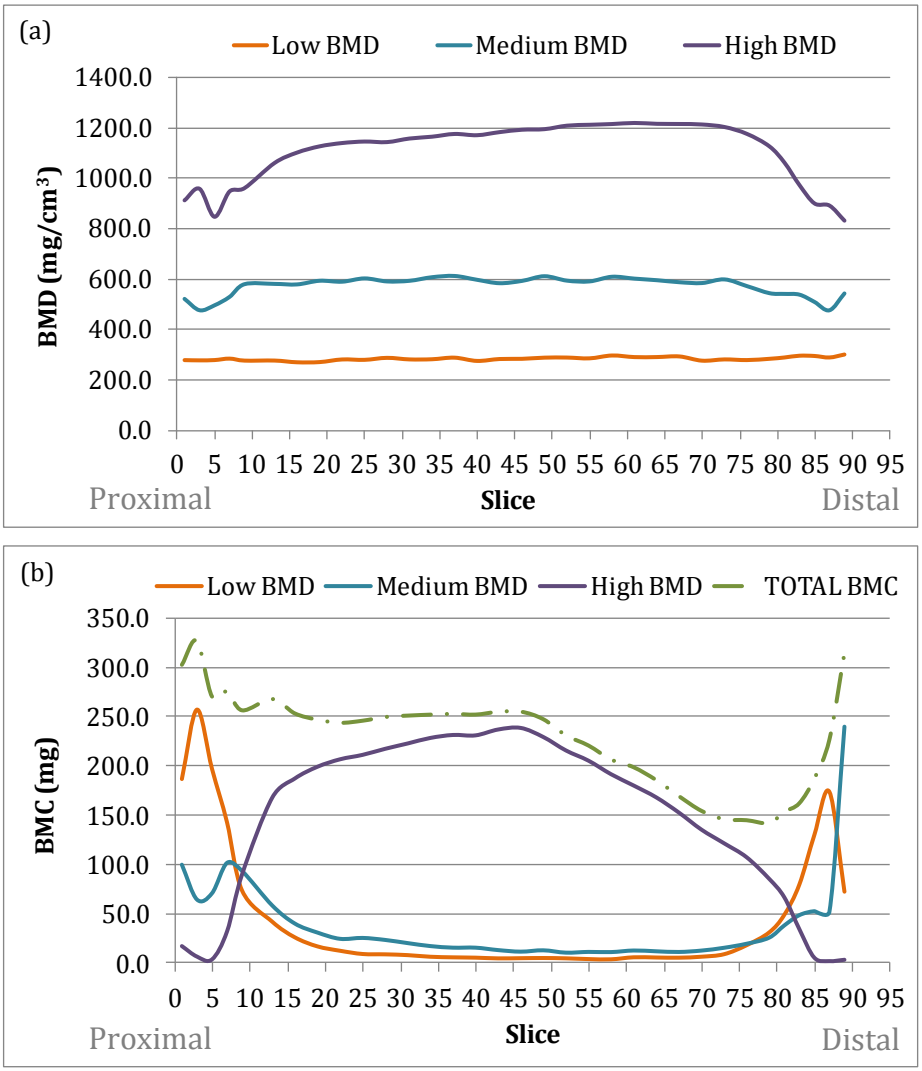

Figure 5.10(a): BMD and **(b):** BMC content for specimen C

Table 5.5: BMC by volume for specimen C

	Region 1			Region 2			Region 3		
	Low-BMD	Med-BMD	High-BMD	Low-BMD	Med-BMD	High-BMD	Low-BMD	Med-BMD	High-BMD
BMC (mg)	855.3	431.1	146.9	240.3	451.6	4379.0	502.4	432.0	109.1
Vol (cm³)	3.2	0.8	0.2	0.9	0.8	3.7	1.7	0.8	0.1
BMD (mg/cm³)	263.5	523.1	951.6	280.8	588.0	1173.6	293.4	529.3	1018.3

From Figures 5.8(b), 5.9(b) and 5.10(b), it is clear that the shafts of the tibiae contained a greater proportion of high-BMD bone than the ends of the tibiae. Despite the fact that the tibial shaft has a smaller CSA than the bone ends, the high proportion of dense compact bone results in the higher total BMC content of the shaft. The ends of the bones contained the highest proportion of low-BMD bone, corresponding to cancellous bone. The quantity of medium-BMD bone followed a similar pattern to that of low-BMD bone with the highest proportion at the ends and the lowest in the shaft. The average BMD values for specimens A, B and C were 556.167 mg/cm^3, 776.180 mg/cm^3 and 617.899 mg/cm^3 respectively.

Table 5.6 details the average BMD values determined for the central core of regions 1 and 3 of each specimen. This step in analysis was performed to establish whether the tibiae under investigation were osteoporotic. Osteoporotic bone is identified as having a BMD value 2.5 standard deviations or more below the young adult mean (NIH, 2012). In a study by Eser *et al*. (2004), a cancellous bone BMD value of 245.8 ± 45.0 mg/cm^3 was determined for a healthy reference group. According to this reference value, cancellous bone with a BMD value of < 133.3 mg/cm^3 is deemed osteoporotic. The analysis indicated that specimen A exhibited osteoporosis at both the proximal and distal ends, while specimen B and C did not display any signs of osteoporosis.

Table 5.6: BMD of central core (45% by area of entire bone cross-section)

	BMD (mg/cm^3)	
Specimen	Region 1 (Proximal)	Region 3 (Distal)
A	109.589	133.582
B	-	216.695
C	204.249	255.053

5.3.2 Geometric Analysis

In the geometric analysis of the tibiae, Region 2 was analysed to characterise features including compact bone cross-sectional area (CSA_{Comp}), compact bone outer perimeter (P_{Outer}), compact bone inner perimeter (P_{Inner}), compact bone thickness (T_{Comp}), circularity, and polar second moment of area (J). As only Region 2 was analysed, the slices were renumbered sequentially, where slice 1 was the most proximal slice within the shaft. In this section the results of CSA_{Comp}, T_{Comp}, and J will be discussed.

Figure 5.11 shows how CSA_{Comp} varied over the length of the shaft for each tibia. The CSA_{Comp} of specimen A was lower than that of B and C. As specimen B and C were obtained from the same individual, it is understandable that they demonstrated similar CSA_{Comp} over their lengths. For all three specimens, CSA_{Comp} initially increased from the proximal end towards the mid-length of the shaft where it reached a maximum, and subsequently decreased towards the proximal end.

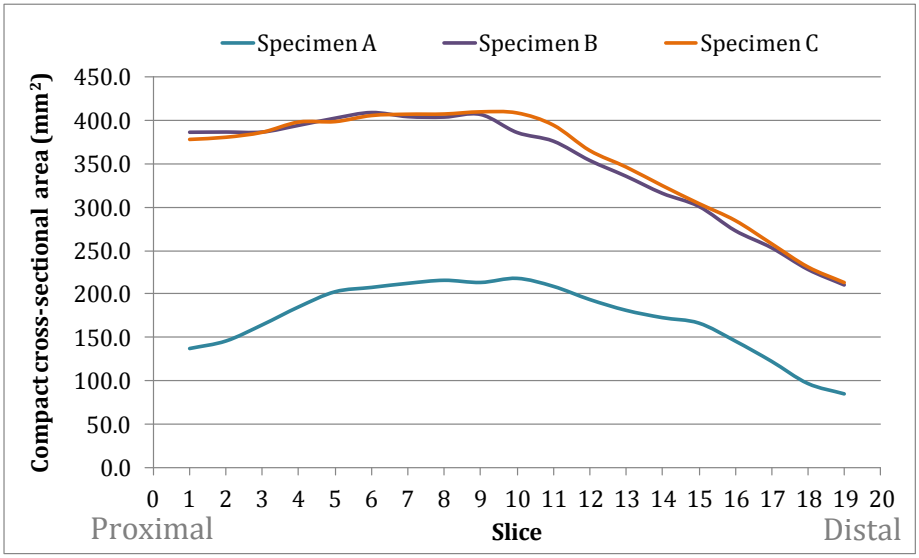

Figure 5.11: Cross-sectional area of compact bone present within tibiae

The variation in compact bone thickness (along the major and minor axes) is displayed in Figure 5.12. It can be seen that for all specimens compact bone

thickness increased towards the mid-point of the tibiae reaching a maximum value, following which it decreased towards the distal end. Figure 5.13 details the differentiation made between the major and minor compact thickness. In specimen A, major and minor T_{Comps} were quite comparable, with an average difference of 1.366 ± 0.560 mm between the two measurements. The average thicknesses in the major and minor directions were 3.643 ± 1.222 mm and 2.277 ± 0.761 mm respectively. For specimens B and C there was a comparatively much larger average difference between the major and minor T_{Comp} (4.99 ± 1.393 mm and 4.056 ± 1.508 mm respectively). The major T_{Comp} was approximately twice that of the minor T_{Comp} for both specimen (B: Major – 7.904 ± 1.792 mm, Minor – 3.706 ± 0.728 mm, C: Major – 7.606 ± 1.801 mm, Minor – 3.651 ± 0.774 mm).

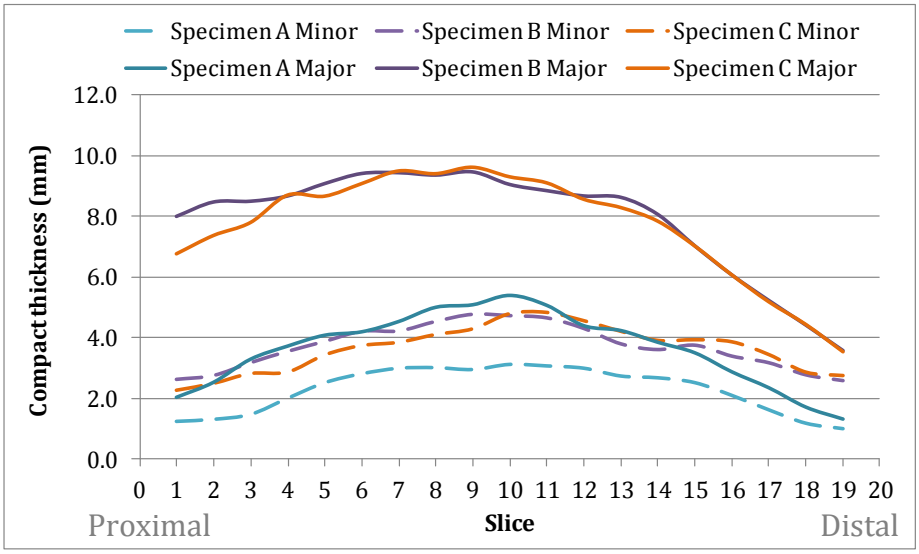

Figure 5.12: Inner and outer perimeters of compact bone over length of tibiae

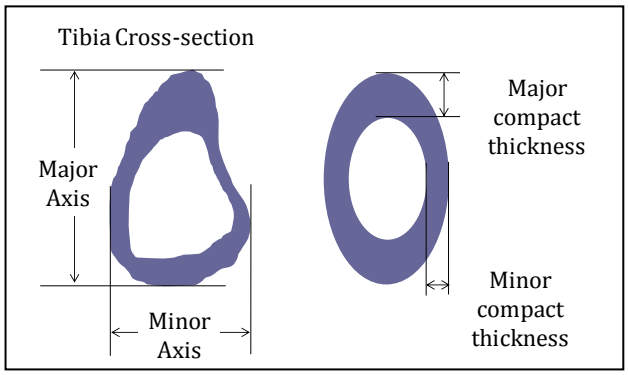

Figure 5.13: Measurement of major and minor compact thickness

While CSA_{Comp} and T_{Comp} give an indication of the amount of compact bone present within the specimen, the second polar moment of area is a measure of how the compact bone is distributed around the central axis of the bone and its resistance to twisting. In Figure 5.14 it is clear that J decreases along the length of the bone, from a maximum at the proximal end to a minimum at the distal end. This suggested that tibiae are more susceptible to torsional loads at the distal end compared to the proximal end. Although specimen A failed in torsion at a point outside the analysed region, it did fail at the distal end of the bone. As mentioned previously, in the course of testing, specimens B and C twisted out of the polyester filler material supporting them in the specimen holder. The specimen broke free from the holder located at the distal end of the specimen which could indicate that had the whole bones been available for testing, they too may have fractured at the distal end. Figures 5.12, 5.13 and 5.14 highlight the fact that the geometric properties of the tibia vary greatly over its length.

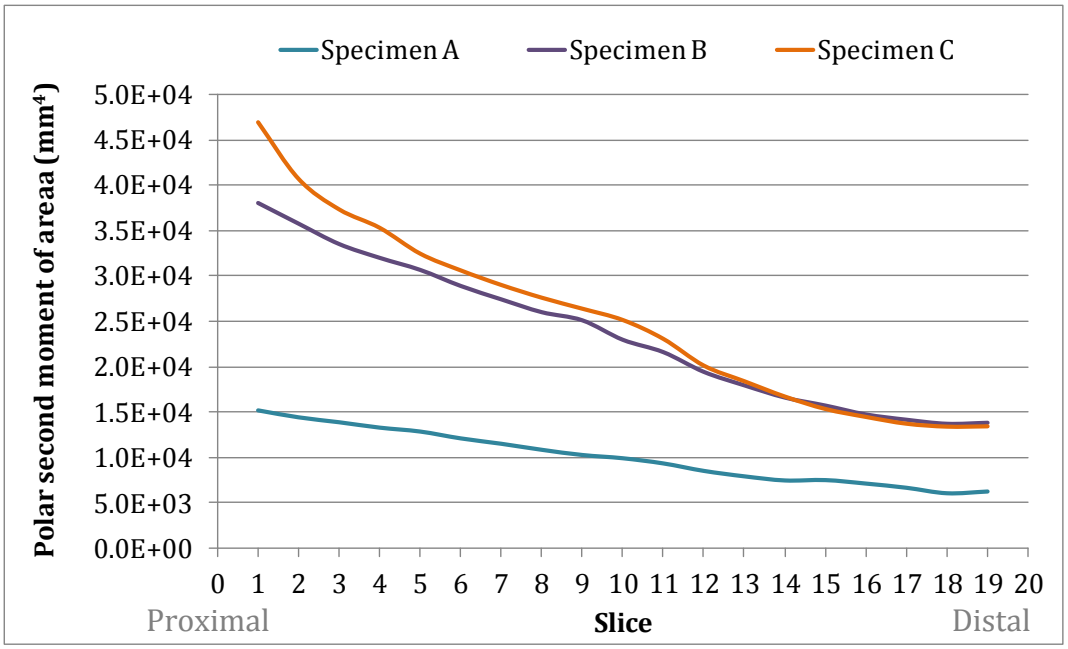

Figure 5.14: Variation in polar second moment of area over length of tibiae

5.4 Correlation between BMD and Geometric Properties

In Figure 5.15(a), the correlation between BMD and the compact bone cross-sectional area of the tibiae shafts can be seen, while Figure 5.15(b) details the relationship between BMD and second polar moment of area. While Figure 5.15(a) demonstrates that the BMD content increases reasonably linearly with increasing CSA (R^2 = 0.6123), Figure 5.15(b) suggests that the relationship between J and BMD is much weaker (R^2 = 0.1632). This is due to the fact that J is an indication of how the material is distributed, not the amount of material present. For example, the two slices through the tibia in Figure 5.16 contain the same compact bone CSA and similar BMD values, however they possess very different J values due to the manner in which the material is distributed around the axis of rotation.

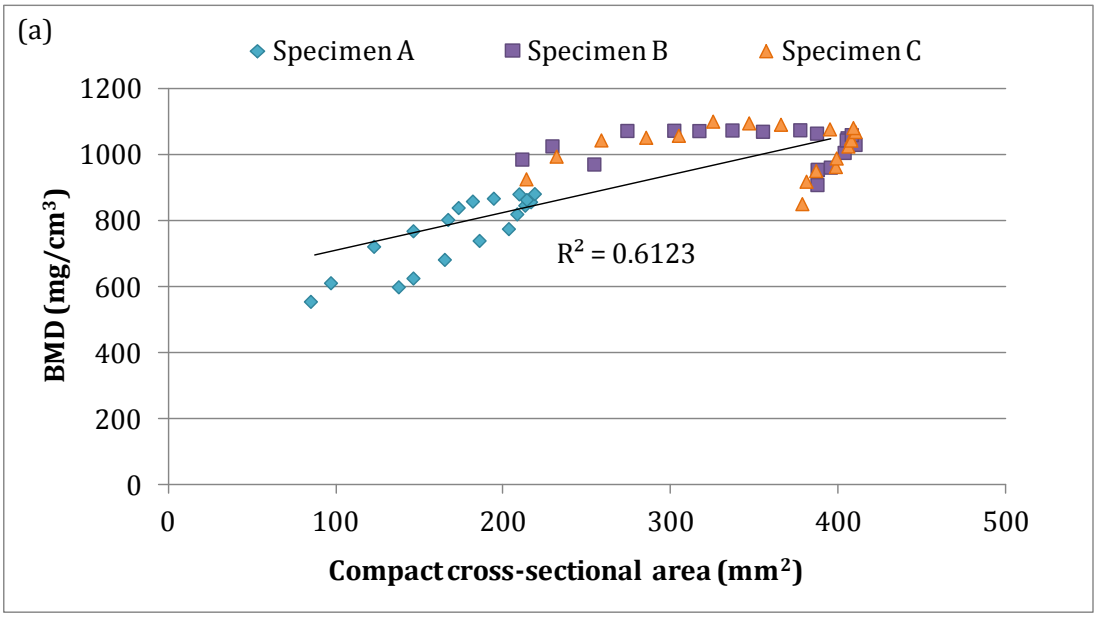

Figure 5.15(a): Correlation between BMD and compact bone cross-sectional area

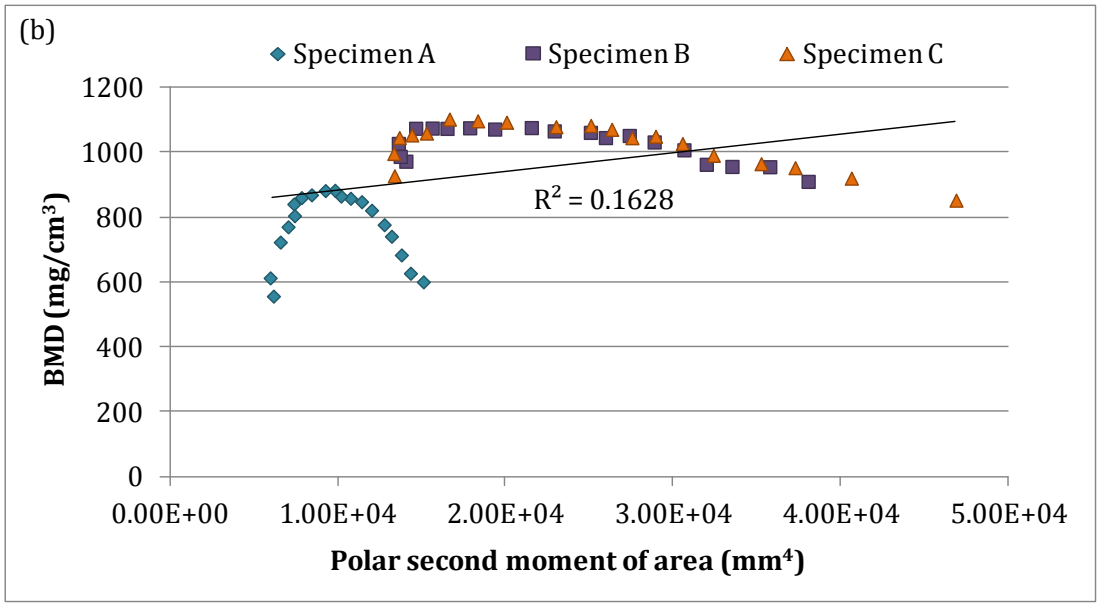

Figure 5.15(b): Correlation between BMD and second polar moment of area

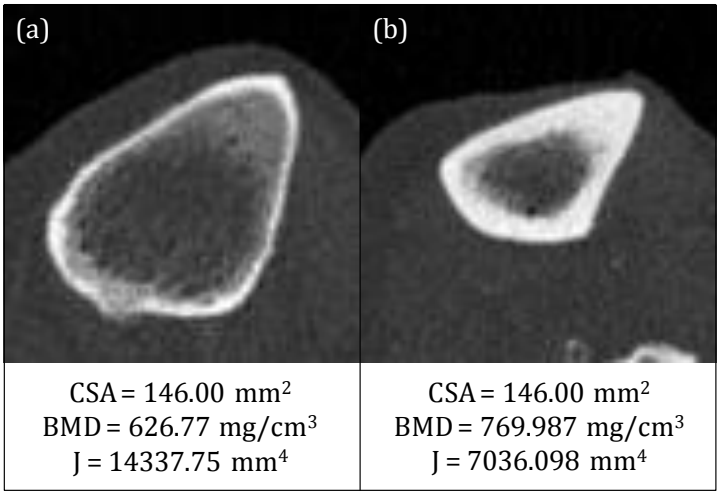

Figure 5.16: Variation of J over two slices with the same CSA of compact bone

Despite the fact that the slice in Figure 5.16(a) possesses a greater proportion of cancellous bone than that of Figure 5.16(b), theoretically it would demonstrate a greater resistance to torsional loading due to its higher value of J.

5.5 Correlation between Mechanical Tests, BMD and Geometric Properties

Due to the fact that two out of the three specimens tested failed to fracture during the test, resulting in an inability to determine their torsional strength, comparisons were made between torsional stiffness, average BMD of the whole bone and geometric properties. In Figure 5.17, the correlation between specimen torsional stiffness and average whole bone BMD can be seen while Figure 5.18 shows the relationship between torsional stiffness and average second polar moment of area. Figure 5.17 indicates that a strong positive correlation existed between the torsional stiffness of the specimen and its average BMD (R^2 = 0.9989). A positive correlation also existed between rotational stiffness and polar second moment of area in Figure 5.18, albeit a relatively weak one (R^2 = 0.3085), and a similar relationship was observed between K and compact bone CSA (R^2 = 0.4607).

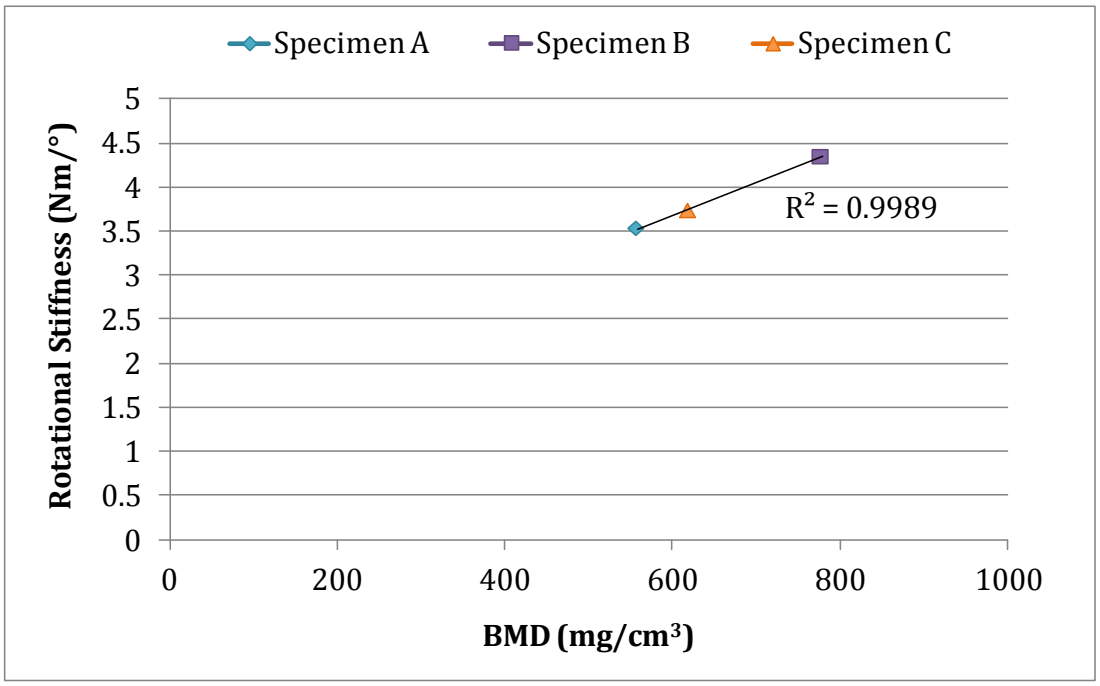

Figure 5.17: Correlation between K and average BMD

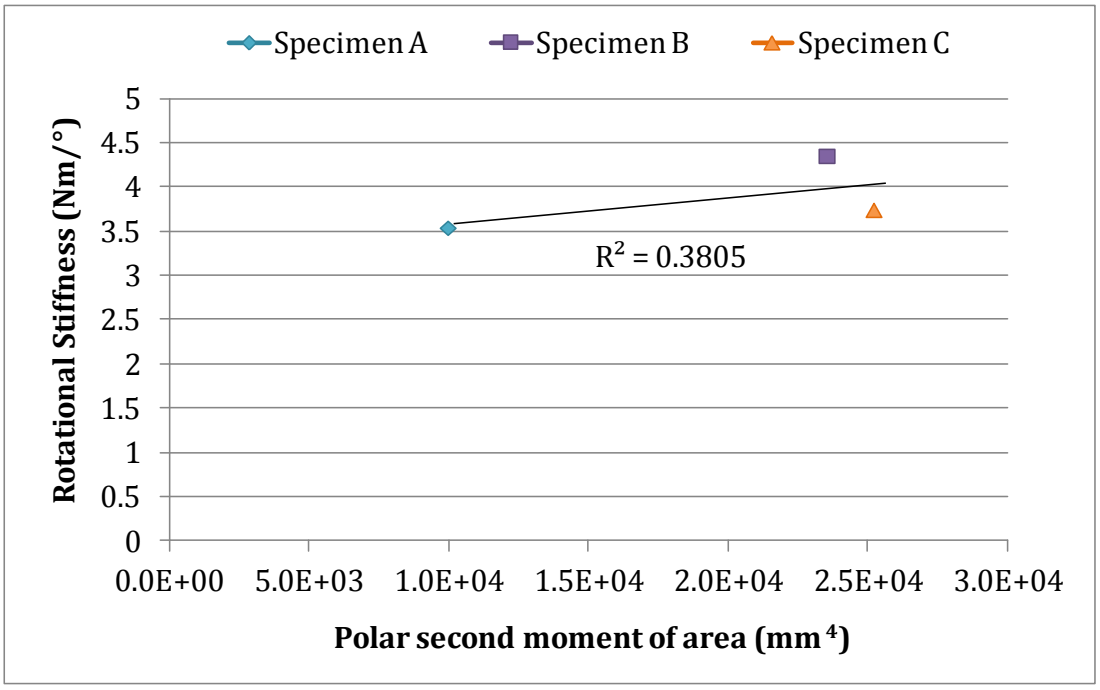

Figure 5.18: Correlation between K and average J

6.0 Discussion

6.0 Discussion

Fractures of the tibia in the older population most frequently result from simple falls, with the complexity of the fracture increasing with increasing levels of osteoporosis (Schmidt *et al*., 2003). As torsional and bending actions produce the largest stresses in the bones of the appendicular skeleton (Bouxsein, 2005), (Cristofolini and Viceconti, 2000), for example the tibia, such loading configurations are of particular interest when studying properties of such bones. Torsion tests were performed on the tibiae in an attempt to quantify their shear properties.

During testing specimen A fractured at the distal end in a region with a relatively high proportion of cancellous bone. The location of the fracture was not unexpected due to the much greater porosity of cancellous bone compared to compact bone. As the porosity of a structure increases, the amount of material present to support the load decreases, and fracture susceptibility increases as a result (Schaffler and Burr, 1988). It stands to reason that if a load is applied to a structure of variable mechanical properties, such as a whole bone, the structure will tend to facture at a point close to where the properties transition (Benham *et al.*, 1996).

When a load is applied to such a structure (Figure 6.1), the region with greater mechanical properties will support and distribute the load, while the region of inferior mechanical properties cannot. As a result the structure will typically fail at a point close to where the two regions meet, such as the transition between compact bone and cancellous bone. The tibia fractured at an approximate 45° angle (Figure 5.5(c)) and a short spiral fracture pattern was evident, typical of long bones tested to destruction via torsional loading (Beaupied *et al.*, 2007), (Edwards *et al*., 2013), (Lind *et al*., 2001), (Salminen, 2005).

The failure of specimens B and C to fracture is potentially due to the lack of cancellous bone at the ends of the specimen. As a result there was no transition of mechanical properties from high (compact bone) to low (cancellous bone), and consequently there was no weaker point at which the bone could readily fail.

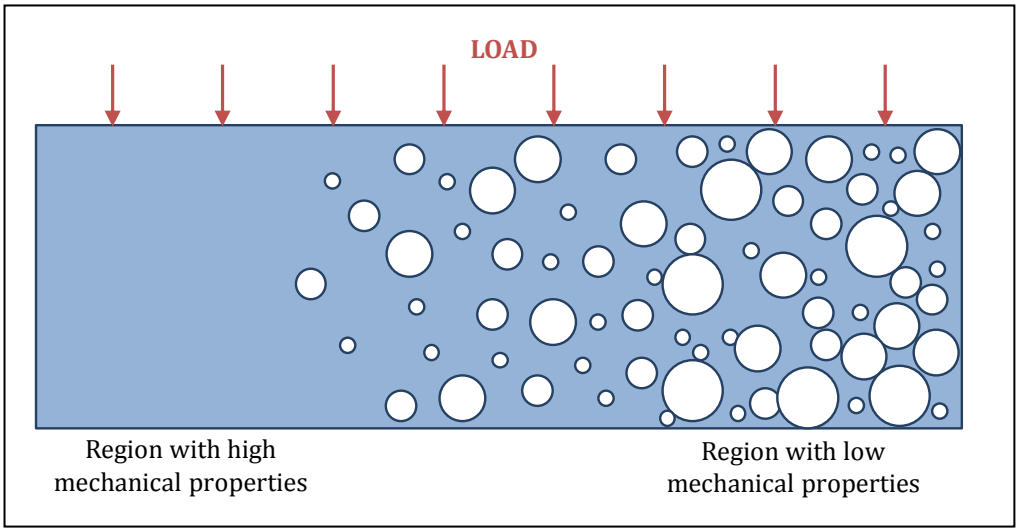

Figure 6.1: Schematic demonstrating the transition of mechanical properties

The scanning, mechanical tests and image analysis were performed blind, i.e. the investigator was not aware of the sex, age or health status of the donors. Following the investigation, it was revealed that specimen A was obtained from a 96 year old female while specimens B and C were obtained from a 55 year old male. The fact that specimen A was identified as osteoporotic while specimens B and C were not, which is expected due to the age and sex of the donors, suggests that the analysis procedure has merit in the diagnosis of osteoporosis.

In the screening of the specimens for osteoporosis, the comparable BMD values for Regions 1 and 3 within specimens A and C (A: Region 1 – 109.589 mg/cm^3, Region 3 – 133.582 mg/cm^3, C: Region 1 – 204.249 mg/cm^3, Region 3 – 255.053 mg/cm^3) suggest a reasonable level of intra-subject reliability. Further to this, the comparable values found for Region 3 of specimens B and C (Region 3: B –

216.695 mg/cm^3, C – 255.053 mg/cm^3), which were obtained from the same individual, suggests that a scan of one leg gives a good indication of overall bone health. The variation between specimen A and specimens B and C implies that the technique is capable of detecting inter-subject variations and consequently highlights the fact that it is possible to identify an individual with osteoporosis from a bone scan. The use of such techniques could allow the diagnosis of an individual with osteoporosis at a stage before a bone fracture occurs.

It is clear that the human tibia possesses a complex geometry which is specialised for its function. The high variability in architecture and structural strength of the tibia along its length was investigated by Capozza *et al*. (2010). The decrease in polar moment of area moving from the proximal to the distal end, as noted in this investigation, was observed via pQCT scan analysis. The change in second moment of area was attributed to the structural adaptation of the tibia in response to a high proportion of uniaxial compression in the distal region. It is thought that the relatively high occurrences of torsional and bending fractures in this region are due to the decrease in second moment of area moving distally (Capozza *et al*., 2010). A recent study suggested that the shape of the tibia is optimised to resist bending in the sagittal plane (Cristofolini *et al*., 2013). It was proposed that the reductions in cross-section and moments of area moving from the proximal to the distal end of the tibia are a result of the optimisation of tibiae geometry to support a moment which varies linearly along the its length (Cristofolini *et al*., 2013).

There was a very strong positive correlation between specimen torsional stiffness and average BMD of the whole bone ($R^2 = 0.9989$). As K is a measure of the ability of the specimen to resist deformation under the application of torsional loading, this relationship indicates that the greater the average BMD of a particular bone, the higher its resistance to twisting under torque. The positive correlation between rotational stiffness and polar second moment of ($R^2 = 0.3085$) suggests that as the value of J increases, so too should the

resistance to deformation. There appeared to be a much stronger correlation between bone strength and BMD measurement (R^2 = 0.9989) than that of bone strength and geometric properties (J: R^2 = 0.3085, CSA: R^2 = 0.4607). However it should be noted that due to the limited number of specimen available for use in this study, definitive conclusions should be approached with caution.

The relationship between bone strength and BMD has been widely investigated. A positive link between BMD and bone strength, as identified in this investigation, has been reported for a number of different bones, BMD measurement techniques, and loading configurations. Reasonably strong correlations have been established between vertebral (R^2 = 0.64) and femoral strength (R^2 = 0.54), measured via compression tests, and aBMD, determined via DXA (Cheng *et al.*, 1998). Similar findings were reported in a study by Link *et al.* (2001), in which high resolution magnetic resonance imaging (HR-MRI) was used to predict femoral bone strength *in vivo*. The BMD of the femoral specimens were measured using DXA, following which bone strength was determined via compression tests. A strong correlation between BMD and compressive strength was identified (R^2 = 0.74).

The contributions of density and geometry to the load at which femoral bone failed were studied by Bousson *et al*. (2006). The BMD and geometric features of proximal femurs were measured using QCT, following which the femurs were mechanically tested to failure in a stance configuration. It was established that 43% of the variance in femoral failure load could be explained by geometric parameters, compared to 72% for density related variables. They further concluded that QCT determined BMD measurements could potentially better explain the variance in failure load than BMD determined via DXA.

Contrary to the findings in this investigation, a study by Varghese (2011) determined that geometry-based indicators of bone strength outperformed density-based indicators. QCT scans were used to investigate the relationship

between geometry and bone strength of human cadaveric long bones in a variety of loading conditions. The author observed a higher correlation between geometric factors, such as cross-sectional area, and bone strength (R^2 > 0.72) in comparison with density measurements (R^2 > 0.58). A similar conclusion was reached by Gutekunst *et al*., (2012) in a study in which the effectiveness of BMD and geometric factors as indicators of human metatarsal bone resistance to destructive loading. BMD and geometric strength indices, determined from volumetric QCT (vQCT), were shown to be strongly correlated to the ultimate force measured by 3-point bending. The authors suggested that the correlation between geometric indices and ultimate force were stronger than that of BMD and ultimate force.

The greater contribution of geometric factors to bone strength over BMD was again suggested by Augat *et al*. (1996). The influence of geometric properties and BMD (determined via pQCT) on the fracture loads of the radius and femur were studied, with it reported that geometric properties were highly correlated with fracture load (distal radius: R^2 = 0.89, femur: R^2 = 0.84) while the relationship between BMD and load at facture was less strong (distal radius: R^2 = 0.56, femur: R^2 = 0.45). The conclusion that both geometry and density contribute substantially to the skeletal strength was drawn.

Although the conclusion that bone strength is more strongly influenced by geometric features than BMD reached in the investigations by Augat *et al*. (1996), Gutekunst *et al*. (2012) and Varghese (2011) was contrary to the overall conclusion reached in this project, it should be noted that in all three investigations, a positive correlation was found between BMD and bone strength, albeit not as strong as that between bone strength and geometric properties.

Despite the wide range of bones under investigation, coupled with a variety of loading configurations and scanning techniques assessed in the literature, the

fact that BMD and geometric properties are highly correlated with bone strength is very clear. Consequently the consideration of both BMD and geometric properties should be taken into account when diagnosing osteoporosis and assessing an individual's fracture risk.

One of the major limitations of the study was the small sample size. Due to the time available and difficulties associated with obtaining appropriate cadaveric material, the testing and analysis of further specimens was outside the scope of this investigation. It is possible to determine what sample size would be necessary to achieve a specified correlation coefficient. For example, to detect a simple correlation coefficient of $R^2 = 0.7$ from a sample of n specimens, using a two sided test at a 5% significance level ($\alpha = 0.05$) with 80% power ($\beta = 0.2$), the required sample size would be 14 ($n = 14$) (BioSS, 2006). With a larger sample size, a greater range of tests could be performed allowing a more complex and thorough analysis of the results to be undertaken, such as a multivariate regression analysis.

A further limitation was the tendency of the specimens which were solely the shaft (B and C) to break free from the specimen holders during the test. This could have been overcome through adaptation of the sample holder, for example, placing a bolt through the bone to restrict its relative motion within the polyester filler material. Such an arrangement should ensure that the bone would move with the test machine allowing a more accurate test to be performed. The fact that comparisons were made using the rotational stiffness rather than the ultimate strength of the specimen could be considered a limitation. However due to the inability to obtain ultimate strength values for specimens B and C, the use of rational stiffness was an appropriate substitution.

7.0 Conclusions and Future Work

7.0 Conclusions and Future Work

The overall aim of the project was to identity whether a conclusive relationship exists between bone mechanical properties, BMD and geometric features. This was fulfilled by the characterisation of cadaveric human tibiae via mechanical testing and image analysis. The overall outcomes of the project were the identification of:

- a very strong relationship between bone strength and BMD (R^2 = 0.9989); and,
- relatively weak positive relationships between bone strength and geometric properties (J: R^2 = 0.3085, CSA: R^2 = 0.4607).

The results of the study indicate that both BMD and geometric features should be taken into account when assessing osteoporosis and fracture risk. Due to the small sample size used in the study, the results should be interpreted with care. Further work in this area, to include a larger sample size along with the investigation of a variety of loading configurations, would work to alleviate any concerns relating to the validity of the results.

The use of a greater sample size with greater inter-bone variability, along with more extensive loading conditions, such as compressive and 3-point bending, would greatly improve the accuracy and reliability of the results. The application of strain gauges to the tibiae during mechanical testing, along with modification of the specimen holders to limit the possibility of the specimens coming free from the holder during the test, would further enhance the study.

The use of pQCT alongside image analysis software, such as ImageJ, is advocated for use in investigations into BMD and structural properties. The ability of pQCT to separate compact and cancellous bone is particularly useful as the manifestation of osteoporosis is more apparent in cancellous bone than in compact. The successful BMD and geometric analysis of the pQCT scans using

ImageJ, a freely available open source image processing program, indicates that the determination of structural properties alongside BMD from scan images is readily achievable. Further work in this area would include the automation of the analysis process by the creation of an appropriate macro for use within ImageJ, allowing rapid and reliable analysis of the scan data.

The application of imaging techniques, such as pQCT, to assess the determinants of bone strength has great use in the analysis of osteoporosis and assessment of fracture risk. The combination of such imaging techniques alongside mechanical testing of representative specimens could allow the development of robust techniques appropriate for the early diagnosis of osteoporosis, the assessment of individuals at high risk of fracture, and, the monitoring of the efficacy of applied treatments. This project marks a starting point in this process and it is envisaged that further work in this area could lead to the development of an accurate and non-invasive method of reliably predicting bone mechanical properties and fracture risk *in vivo*.

8.0 References

8.0 References

AGNEW, A. M., BOLTE, J. H. (2011) 'Bone Fracture'. In: *Bone Histology: An Anthropological Perspective.* Eds: CROWDER, C. M., STOUT, S. D. CRC Press LLC, Boca Raton., pp 221-240.

American Academy of Orthopaedic Surgeons (AAOS) - Fractures (Broken Bones) (2012b, October – last update). [Online] Available: orthoinfo.aaos.org/topic.cfm? topic=A00139 [2013, June 10]

American Academy of Orthopaedic Surgeons (AAOS) - Healthy Bones at Every Age (2012a, July – last update). [Online] Available: orthoinfo.aaos.org/topic.cfm?topic=a00127 [2013, June 26]

American Academy of Orthopaedic Surgeons (AAOS) - The Bone and Joint Decade (2002 – last update). [Online] Available: orthoinfo.aaos.org/topic.cfm?topic=A00282 [2011, April 4]

AN, Y. H. (2010) 'Mechanical Properties of Bone' In: *Mechanical testing of bone and the bone-implant interface*. Eds: AN, Y. H., DRAUGHN, R. A. CRC press, Boca Raton, Florida, pp. 41-64.

AN, Y. H., BARFIELD, W. R., DRAUGHN, R. A. (2010) 'Basic Concepts of Mechanical Property Measurement and Bone Biomechanics' In: *Mechanical testing of bone and the bone-implant interface*. Eds: AN, Y. H., DRAUGHN, R. A. CRC press, Boca Raton, Florida, pp. 23-40.

ASHE, M. C., KHAN, K. M., KONTULAINEN, S. A., GUY, P., LIU, D., BECK, T. J., MCKAY, H. A. (2006) Accuracy of pQCT for evaluating the aged human radius: an ashing, histomorphometry and failure load investigation. *Osteoporosis International*, **17** (8), pp. 1241-1251.

ASPDEN, R. M. (2003) 'Mechanical Testing of Bone Ex Vivo' In: *Bone research protocols* (Vol. 80). Eds: HELFRICH, M. H., RALSTON, S. H. Humana Press Inc., Totowa, NJ.

AUGAT, P., REEB, H., CLAES, L. E. (1996) Prediction of fracture load at different skeletal sites by geometric properties of the cortical shell. *Journal of Bone and Mineral Research*, **11** (9), pp. 1356-1363.

AUGAT, P., GORDON, C. L., LANG, T. F., IIDA, H., GENANT, H. K. (1998) Accuracy of cortical and trabecular bone measurements with peripheral quantitative computed tomography (pQCT). *Physics in Medicine and Biology*, **43**(10), pp. 2873 – 2883.

BANDYOPADHYAY-GHOSH, S. (2008) Bone as a Collagen-hydroxyapatite Composite and its Repair. *Trends in Biomaterials & Artificial Organ*, **22** (2), pp. 112-120.

BANKOFF, A. D. P. (2012) Biomechanical Characteristics of the Bone, [Online] Available: cdn.intechweb.org/pdfs/21043.pdf [2012, July 7]

BARTEL, D. L., DAVY, D. T., KEAVENY, T. M. (2006). *Orthopaedic biomechanics*. Pearson/Prentice Hall.

BARTL, R., FRISCH, B. (2009) *Osteoporosis [electronic Book]: Diagnosis, Prevention, Therapy*. Springer.

BAUER, J. S., VIRMANI, S., MUELLER, D. K. (2010) Quantitative CT to assess bone mineral density as a diagnostic tool for osteoporosis and related fractures – White Paper. *Philips CT Clinical Science.* Available: clinical.netforum.healthcare.philips.com/us_en/Explore/White-Papers/CT/Quantitative-CT-to-assess-bone-mineral-density-as-a-diagnostic-tool-for-osteoporosis-and-related-fractures

BEAUPIED, H., LESPESSAILLES, E., BENHAMOU, C. L. (2007) Evaluation of macrostructural bone biomechanics. *Joint Bone Spine*, **74** (3), pp. 233-239.

BELKOFF, S. M., HAUT, R. C. (2008) 'Experimental Methods in Biological Tissue Testing'. In: *Springer Handbook of Experimental Solid Mechanics Part D 31*. Ed: SHARPE, W. N. Springer US, pp. 871-890.

BENHAM, P.P., CRAWFORD, R. J. ARMSTRONG, C.G., (1996) *Mechanics of Engineering Materials*, Second Edition, Pearson Education Limited, England.

Biomathematics and Statistics Scotland (BioSS): Sample size table for detecting a correlation. (2006 – last update). [Online] Available: www.rowett.ac.uk/~gwh/corr.html [2013, August 27]

BONJOUR, J. P., THEINTZ, G., LAW, F., SLOSMAN, D., RIZZOLI, R. (1994) Peak bone mass. *Osteoporosis international*, 4 (1), pp. S7-S13.

BONUCCI, E. (2000) 'Mechanical testing of the bone and the bone–implant interface'. In: *Basic Composition and Structure of Bone*. Eds: AN, Y. H., DRAUGHN, R. A. CRC Press LLC, Boca Raton.

BOREHAM, C., RIDDOCH, C. (2001) The physical activity, fitness and health of children. *Journal of sports sciences*, **19** (12), pp. 915-929.

BOSKEY, A. L., COLEMAN, R. (2010) Aging and bone. *Journal of Dental Research*, **89** (12), pp. 1333-1348.

BOUXSEIN, M. L. (2005) Determinants of skeletal fragility. *Best Practice & Research Clinical Rheumatology*, **19** (6), pp. 897-911.

BRAUN, M. J., META, M. D., SCHNEIDER, P., REINERS, C. (1998) Clinical evaluation of a high-resolution new peripheral quantitative computerized tomography (pQCT) scanner for the bone densitometry at the lower limbs. *Physics in medicine and biology*, **43** (8), pp. 2279 - 2294.

BURGE, R. T., WORLEY, D., JOHANSEN, A., BHATTACHARYYA, S., BOSE, U. (2001) The cost of osteoporotic fractures in the UK: projections for 2000-2020. *Journal of Medical Economics*, **4** (1-4), pp. 51-62.

CALVO, M. S., EYRE, D. R., GUNDBERG, C. M. (1996). Molecular basis and clinical application of biological markers of bone turnover. *Endocrine Reviews*, **17** (4), pp. 333-368.

CAPOZZA, R. F., FELDMAN, S., MORTARINO, P., REINA, P. S., SCHIESSL, H., RITTWEGER, J., COINTRY, G. R. (2010) Structural analysis of the human tibia by tomographic (pQCT) serial scans. *Journal of Anatomy*, **216** (4), pp. 470-481.

CASSIDY, W. J., ALLMAN, F. C., KEEFE, G. J. (1948) Osteopetrosis. *Archives of Internal Medicine*, **82** (2), pp. 140.

CELENK, C., CELENK, P. (2012) Bone Density Measurement Using Computed Tomography. *Computed Tomography-Clinical Applications*, pp. 123-136.

CHENG, X. G., LOWET, G., BOONEN, S., NICHOLSON, P. H., VAN DER PERRE, G., DEQUEKER, J. (1998) Prediction of vertebral and femoral strength in vitro by bone mineral density measured at different skeletal sites. *Journal of Bone and Mineral Research*, **13** (9), pp. 1439-1443.

CLARKE, B. (2008) Normal bone anatomy and physiology. *Clinical journal of the American Society of Nephrology*, **3** (Supplement 3), pp. S131-S139.

COXON, J. P., OADES, G. M., COLSTON, K. W., KIRBY, R. S. (2004) Advances in the use of bisphosphonates in the prostate cancer setting. *Prostate Cancer and Prostatic Diseases*, **7**, pp. 99–104.

CRISTOFOLINI, L., ANGELI, E., JUSZCZYK, J. M., JUSZCZYK, M. M. (2013) Shape and function of the diaphysis of the human tibia. *Journal of Biomechanics*, **46** (11), pp. 1882–1892.

CRISTOFOLINI, L., VICECONTI, M. (2000) Mechanical validation of whole bone composite tibia models, *Journal of Biomechanics*, **33**, pp. 279-288.

CURREY, J. D. (2012) The structure and mechanics of bone, *Journal of Materials Science*, **47**, pp. 41–54.

DAMBACHER, M. A., NEFF, M., KISSLING, R., & QIN, L. (1998) Highly precise peripheral quantitative computed tomography for the evaluation of bone density, loss of bone density and structures. *Drugs & Aging*, **12** (1), pp. 15-24.

DIONYSSIOTIS, Y., TROVAS, G., GALANOS, A., RAPTOU, P., PAPAIOANNOU, N., PAPAGELOPOULOS, P., LYRITIS, G. (2007) Bone loss and mechanical properties of tibia in spinal cord injured men. *Journal of Musculoskeletal and Neuronal Interactions*, **7** (1), pp. 62.

DONNELLY, E. (2011) Methods for assessing bone quality: a review. *Clinical orthopaedics and related research*, **469** (8), pp. 2128-2138.

DOWNEY, P. A., SIEGEL, M. I. (2006) Bone biology and the clinical implications for osteoporosis. *Physical therapy*, **86** (1), pp. 77-91.

DOWTHWAITE, J. N., FLOWERS, P. P., SCERPELLA, T. A. (2011) Agreement between pQCT-and DXA-derived indices of bone geometry, density, and theoretical strength in females of varying age, maturity, and physical activity. *Journal of Bone and Mineral Research*, **26** (6), pp. 1349-1357.

DUURSMA, S. A., RAYMAKERS, J. A., VERHAAR, H. J. J. (1997) Osteoporosis, osteomalacia and Paget's disease of bone. *Reviews in Clinical Gerontology*, **7**, pp. 127-136.

EDWARDS, W. B., SCHNITZER, T. J., TROY, K. L. (2013) Torsional stiffness and strength of the proximal tibia are better predicted by finite element models than DXA or QCT. *Journal of Biomechanics*, **46**, pp. 1655–1662.

EDWARDS, W. B., TROY, K. L. (2012) A linear-actuated torsional device to replicate clinically relevant spiral fractures in long bones. *Proceedings of the Institution of Mechanical Engineers, Part H: Journal of Engineering in Medicine*, **226** (9), pp. 729-733

Encyclopædia Britannica Online – Photo Credit: Dr D Fawcett [Online] Available: www.britannica.com/EBchecked/media/101316/Longitudinal-section-of-the-humerus-showing-outer-compact-bone-and [2013, July 13]

ESER, P., FROTZLER, A., ZEHNDER, Y., WICK, L., KNECHT, H., DENOTH, J., SCHIESSL, H. (2004) Relationship between the duration of paralysis and bone structure: a pQCT study of spinal cord injured individuals. *Bone*, **34** (5), pp. 869-880.

FEWTRELL, M. S. (2003) Bone densitometry in children assessed by dual x ray absorptiometry: uses and pitfalls. *Archives of disease in childhood*, **88** (9), pp. 795-798.

FINDLAY, C. M. (2012) *Image analysis tool for the characterisation of bone turnover in the appendicular skeleton.* PhD thesis, University of Glasgow, Glasgow, UK.

GIBSON, L. J., ASHBY, M. F., (1988) *Cellular Solids Structure and Properties*, Pergamon Press, Oxford

GRIFFITH, J. F., GENANT, H. K. (2008) Bone mass and architecture determination: state of the art. *Best Practice & Research Clinical Endocrinology & Metabolism*, **22** (5), 737-764.

GUTEKUNST, D. J., PATEL, T. K., SMITH, K. E., COMMEAN, P. K., SILVA, M. J., SINACORE, D. R. (2013) Predicting *ex vivo* failure loads in human metatarsals using bone strength indices derived from volumetric quantitative computed tomography. *Journal of Biomechanics*. **46** (4), pp. 745–750

HABA, Y., LINDNER, T., FRITSCHE, A., SCHIEBENHÖFER, A. K., SOUFFRANT, R., KLUESS, D., SKRIPITZ, R., MITTELMEIER, W., BADER, R. (2012) Relationship Between Mechanical Properties and Bone Mineral Density of Human Femoral Bone Retrieved from Patients with Osteoarthritis. *The Open Orthopaedics Journal*, **6**, pp. 458-463.

HORWOOD, A., HOGAN, S. J., GODDARD, P., ROSSITER, J. (2001) Image normalization: a basic requirement for computer-based automatic diagnostic applications. Available: www.enm.bris.ac.uk/anm/preprints/2001r10.pdf

HOUSE OF LORDS: Select Committee on Public Service and Demographic Change (2013) *Ready for Ageing?* [Online] Available: www.publications.parliament.uk/pa/ld201213/ldselect/ldpublic/140/140.pdf

ILICH, J. Z., KERSTETTER, J. E. (2000) Nutrition in Bone Health Revisited: A Story Beyond Calcium. *Journal of the American College of Nutrition*, **19** (6), pp. 715–737.

JÄMSÄ, T., JALOVAARA, P. (1996) A cost-effective, accurate machine for testing the torsional strength of sheep long bones, *Med. Eng. Phys.*, **18**, pp. 433-435.

JAYALAKSHMI, M. K., PRABHU RAJ, N., SHANMUKHAPPA, N. J., SMILEE JOHNCY, S. (2011) Effect of sedentary life style on anthropometric and cardiovascular parameters. *International Journal of Biological & Medical Research*, **2** (4), pp. 846 – 851.

JEE, W. S. S. (2001) 'Integrate Bone Tissue Physiology: Anatomy and Physiology'. In: *Bone Mechanics Handbook*. Second Edition. Ed: COWIN, S. C. CRC Press LLC, Boca Raton.

KNOWELDEN, J., BUHR, A. J., DUNBAR, O. (1964) Incidence of Fractures in Persons over 35 Years of Age A Report to the MRC Working Party on Fractures in the Elderly. *British journal of preventive & social medicine*, **18** (3), pp. 130-141.

KONTULAINEN, S., LIU, D., MANSKE, S., JAMIESON, M., SIEVÄNEN, H., MCKAY, H. (2007) Analyzing cortical bone cross-sectional geometry by peripheral QCT: comparison with bone histomorphometry. *Journal of Clinical Densitometry*, **10** (1), pp. 86-92.

KRÖGER, H., KOTANIEMI, A., VAINIO, P., ALHAVA, E. (1992) Bone densitometry of the spine and femur in children by dual-energy x-ray absorptiometry. *Bone and Mineral*, **17** (1), pp. 75-85.

LANG, T., AUGAT, P., MAJUMDAR, S., OUYANG, X., GENANT, H. K. (1998) Noninvasive assessment of bone density and structure using computed tomography and magnetic resonance. *Bone*, **22** (5), 149S-153S.

LERNER, U. H. (2012) Osteoblasts, Osteoclasts, and Osteocytes: Unveiling Their Intimate-Associated Responses to Applied Orthodontic Forces. *Seminars in Orthodontics*, **18** (4), pp. 237-248.

LIND, P. M., LIND, L., LARSSON, S., ÖRBERG, J. (2001) Torsional testing and peripheral quantitative computed tomography in rat humerus. *Bone*, **29** (3), pp. 265-270.

LINK, T. M., VIETH, V., LANGENBERG, R., MEIER, N., LOTTER, A., NEWITT, D., MAJUMDAR, S. (2003). Structure analysis of high resolution magnetic resonance imaging of the proximal femur: in vitro correlation with biomechanical strength and BMD. *Calcified Tissue International*, **72** (2), pp. 156-165.

LLOYD, T., PETIT, M. A., LIN, H. M., BECK, T. J. (2004). Lifestyle factors and the development of bone mass and bone strength in young women. *The Journal of pediatrics*, **144** (6), pp. 776-782.

LOCHMÜLLER, E. M., GROLL, O., KUHN, V., ECKSTEIN, F. (2002) Mechanical strength of the proximal femur as predicted from geometric and densitometric bone properties at the lower limb versus the distal radius. *Bone*, **30** (1), pp. 207-216.

MACNEIL, J. A., BOYD, S. K. (2007) Accuracy of high-resolution peripheral quantitative computed tomography for measurement of bone quality. *Medical Engineering & Physics*, **29** (10), pp. 1096-1105.

MARIEB, E. N., HOEHN, K. (2007) *Human anatomy and physiology*. Seventh Edition. Pearson Education Inc, California, USA.

MARTIN, R. B. (1991) Determinants of the mechanical properties of bones. *Journal of Biomechanics*, **24**, pp. 79-88.

MARTINI, F. H., NATH, J. L., BARTHOLOMEW, E. F. (2012) *Fundamentals of anatomy and physiology*. Ninth Edition. Pearson Education Inc, California, USA.

MCGRAW-HILL CONCISE DICTIONARY OF MODERN MEDICINE. © 2002 by The McGraw-Hill Companies, Inc.

MedlinePlus - Broken bone (2009 – last update). [Online] Available: www.nlm.nih.gov/medlineplus/ency/article/000001.htm [2013, June 10]

MedlinePlus CT scan (2012 – last update). [Online] Available: www.nlm.nih.gov /medlineplus/ency/imagepages/1088.htm [2013, June 6]

MELLON, S. J., TANNER, K. E. (2012) Bone and its adaptation to mechanical loading: a review. *International Materials Reviews*, **57** (5) pp. 235–255.

MORGAN, E. F., BARNES, G. L., EINHORN, T. A. (2009) 'The Bone Organ System: Form and Function'. In: *Fundamentals of osteoporosis*. Eds: MARCUS, R., FELDMAN, D., NELSON, D., ROSEN, C. J. Academic Press, Elsevier, USA, pp. 1-24.

National Institute for Health and Care Excellence (NICE) - Osteoporosis: Assessing the risk of fragility fracture. (Short Clinical Guideline - CG146) (2012). [Online] Available: www.nice.org.uk/nicemedia/live/13857/60400/60400.pdf [2013, July 1]

National Institutes of Health - Bone Mass Measurement: What the Numbers Mean (2012, January – last update). [Online] Available: www.niams.nih.gov/Health_Info/Bone/Bone_Health/bone_mass_measure.asp [2013, June 28]

National Osteoporosis Society: Facts and figures (2008 – last update). [Online] Available: www.nos.org.uk/page.aspx?pid=328 [2013, July 1]

National Osteoporosis Society: Quantitative Computed Tomography (2010, May – last update). [Online] Available: www.nos.org.uk/document.doc?id=655 [2013, July 2]

NELSON, D. A., BARONDESS, D. A., HENDRIX, S. L., BECK, T. J. (2000) Cross-Sectional Geometry, Bone Strength, and Bone Mass in the Proximal Femur in Black and White Postmenopausal Women. *Journal of Bone and Mineral Research*, **15** (10), pp. 1992-1997.

NHS – Osteoarthritis (2012 – last update). [Online] Available: www.nhs.uk/ conditions/ osteoarthritis/Pages/Introduction.aspx [2013, June 21]

NHS Choices: Benefits of Exercise (2011a, July – last update). [Online] Available: www.nhs.uk/Livewell/fitness/Pages/Whybeactive.aspx2011 [2013, June 25]

NHS Choices: DEXA scan (2011b, December – last update). [Online] Available: www.nhs.uk/conditions/DEXA-scan/Pages/Introduction.aspx [2013, July 2]

Office for National Statistics: Population Ageing in the United Kingdom, its Constituent Countries and the European Union (2012, March – last update). [Online] Available: www.ons.gov.uk/ons/dcp171776_258607.pdf [2013, June 25]

ÖZKAYA, N., NORDIN, M., GOLDSHEYDER, D., LEGER, D. (2012a) 'Mechanical Properties of Biological Tissues' In: *Fundamentals of Biomechanics: Equilibrium, Motion, and Deformation*, Springer New York, pp. 221-236.

ÖZKAYA, N., NORDIN, M., GOLDSHEYDER, D., LEGER, D. (2012b) 'Multiaxial Deformations and Stress Analyses' In: *Fundamentals of Biomechanics*, Springer New York, pp. 189-219.

PACK, P. E., BASSETT, S. (2011) *CliffsNotes Anatomy and Physiology Quick Review*. Second Edition. Cliffs Notes, New Jersey, USA.

PLANELL, J. A., NAVARRO, M. (2009) 'Challenges of bone repair' In: *Bone repair biomaterials.* Eds: PLANELL, J. A., BEST, S. M., LACROIX, D., MEROLLI, A. CRC Press Woodhead Publishing Limited, Cambridge, England, pp. 3-24.

POOLE, K. E. S., WARBURTON, E. A., REEVE, J. (2005) Rapid long-term bone loss following stroke in a man with osteoporosis and atherosclerosis, *Osteoporosis International*, **6**, pp. 302–305.

Population Matters: Ageing populations (2011 – last update). [Online] Available: www.populationmatters.org/wp-content/uploads/D27Ageingpopulations.pdf [2013, June 25]

PSIHOGIOS, J. P., "Fracture Patterns of Human Cadaver Long Bones" (1995) *University of Tennessee Honors Thesis Projects.* Available: race.tennessee.edu/utk_chanhonoproj/132

RANTALAINEN, T., NIKANDER, R., HEINONEN, A., DALY, R. M., SIEVANEN, H. (2011) An open source approach for regional cortical bone mineral density analysis. *J Musculoskelet Neuronal Interact*, **11** (3), pp. 243-248.

ROLDÁN, E. J. A., CAPIGLIONI, R., COINTRY, G. R., CAPOZZA, R. F., FERRETTI, J. L. (2001) Postmenopausal changes in the distribution of the volumetric BMD of cortical bone. A pQCT study of the human leg. *JOURNAL OF MUSCULOSKELETAL AND NEURONAL INTERACTIONS*, **2** (2), pp. 157-162.

ROWNTREE, D. (2000) *Statistics without tears: An introduction for non-mathematicians*. Penguin Books, Engand.

SALMINEN, S. (2005) Femoral shaft fractures in adults: Epidemiology, fracture patterns, nonunions, and fatigue fractures. *Department of Orthopaedics and Traumatology, Department of Pediatric Surgery*.

SCHAFFLER, M. B., BURR, D. B. (1988) Stiffness of compact bone: effects of porosity and density. *Journal of Biomechanics*, **21** (1), pp. 13-16.

SCHMIDT, A. H., FINKEMEIER, C. G., TORNETTAIII, P. (2003) Treatment of closed tibial fractures. *The Journal of Bone & Joint Surgery*, **85** (2), pp. 352-368.

SCHNEIDER, C. A., RASBAND, W. S., ELICEIRI, K. W. (2012) NIH Image to ImageJ: 25 years of image analysis. *Nature Methods*, **9**, pp. 671-675.

SCHWARTZ, J. H. (2007) *Skeleton Keys: An Introduction to Human Skeletal Morphology, Development, and Analysis*. Second Edition. Oxford University Press, Oxford.

Science Photo Library – Photo Credit: Dr F Hossler [Online] Available: www.sciencephoto.com/media/121882/view [2012, March 8]

Scottish Intercollegiate Guidelines Network (SIGN) (2003) Guidelines 71. Management of osteoporosis. A national clinical guideline. SIGN, Edinburgh, www.sign.ac.uk

SEEMAN, E., DELMAS, P. D. (2006) Bone quality - the material and structural basis of bone strength and fragility. *New England Journal of Medicine.* **354** (21), pp. 2250-2261.

SHARIR, A., BARAK, M. M., SHAHAR, R. (2008) Whole bone mechanics and mechanical testing. *The Veterinary Journal*, **177** (1), pp. 8-17.

SIMS, N., BARON, R. (2002) 'Bone: Structure, Function, Growth, and Remodeling' In: *Orthopaedics.* Eds: FITZGERALD, R. H., KAUFER, H., MALKANI, A. L. Elsevier Health Sciences, USA, pp 147-159.

SINGER, B. R., McLAUCHLAN, G. J., ROBINSON, C. M., CHRISTIE, J. (1998). Epidemiology of fractures in 15 000 adults the influence of age and gender. *Journal of Bone & Joint Surgery, British Volume*, **80** (2), pp. 243-248.

SOUTH-PAUL, J. E. (2001) Osteoporosis: part I. Evaluation and assessment. *American Family Physician*, **63** (5), pp. 897-904.

STARK, Z., SAVARIRAYAN, R. (2009) Osteopetrosis: Review. *Orphanet Journal of Rare Diseases*, **4** (5), pp. 1-12.

STENSTRÖM, M., OLANDER, B., LEHTO-AXTELIUS, D., ERIK MADSEN, J., NORDSLETTEN, L., ALM CARLSSON, G. (2000) Bone mineral density and bone structure parameters as predictors of bone strength: an analysis using computerized microtomography and gastrectomy-induced osteopenia in the rat. *Journal of biomechanics*, **33** (3), pp. 289-297.

STEPAN, J. J. (2002) Techniques for measuring bone mineral density. In: *International Congress Series* (Vol. 1229, pp. 63-68). Elsevier

TASCAU, M. T., DREUCEAN, M., RUSU, L. (2009) Biomechanical behavior of canine tibia based on bending tests and numerical analysis. *Applied Computational Intelligence and Informatics, 5th International Symposium on*, pp. 129-132.

TURNER, C. H, BURR, D. B. (2001) 'Experimental Techniques for Bone Mechanics'. In: *Bone Mechanics Handbook*. Second Edition. Ed: COWIN, S. C. CRC Press LLC, Boca Raton.

TURNER, C. H. (2002) Biomechanics of bone: determinants of skeletal fragility and bone quality. *Osteoporosis International*, **13** (2), pp. 97-104.

U.S. Department of Health and Human Services (2004) Bone Health and Osteoporosis: A Report of the Surgeon General. U.S. Department of Health and

Human Services, Office of the Surgeon General. Rockville, MD. Available: www.surgeongeneral.gov/library/reports/bonehealth/full_report.pdf

VAN DER MEULEN, M. C. H., JEPSEN, K. J., MIKIĆ, B. (2001) Understanding bone strength: size isn't everything. *Bone*, **29** (2), pp. 101-104.

VAN RIETBERGEN, B., MAJUMDAR, S., PISTOIA, W., NEWITT, D. C., KOTHARI, M., LAIB, A., RÜEGSEGGER, P. (1998) Assessment of cancellous bone mechanical properties from micro-FE models based on micro-CT, pQCT and MR images. *Technology and Health Care*, **6** (5), pp. 413-420.

VAN WYNSBERGHE, D., NOBACK, C. R., CAROLA, R. (1995) *Human Anatomy and Physiology*. Third Edition. McGraw-Hill, New York.

VARGHESE, B. A. (2011) *Quantitative computed-tomography based bone-strength indicators for the identification of lowbone-strength individuals in a clinical environment.* PhD thesis, Wright State University, Ohio, USA.

VIJAY, A., SHANKAR, N., LIGESH, C. A. S., ANBURAJAN, M. (2011) Evaluation of osteoporosis using CT image of proximal femur compared with dual energy x-ray absorptiometry (DXA) as the standard. In: *Electronics Computer Technology (ICECT), 2011 3rd International Conference on* (Vol. 3, pp. 334-338). IEEE

WACHTER, N. J., KRISCHAK, G. D., MENTZEL, M., SARKAR, M. R., EBINGER, T., KINZL, L., CLAES, L., AUGAT, P. (2002) Correlation of bone mineral density with strength and microstructural parameters of cortical bone in vitro. *Bone*, **31** (1), pp. 90-95.

WÄHNERT, D., HOFFMEIER, K. L., KLOS, K., STOLARCZYK, Y., FRÖBER, R., HOFMANN, G. O., MÜCKLEY, T. (2012) Biomechanical characterization of an osteoporotic artificial bone model for the distal femur. *Journal of Biomaterials Applications*, **26** (5), 565-579.

WALSH, W. R., YU, Y., YANG, L. Y., HOCKING, R., CHAPMAN-SHEATH, P., BRUCE, W (2002) 'Biology and Biomechanics of Fracture Healing' In: *Internal fixation in osteoporotic bone*. Ed: AN, Y. Thieme, New York.

WARMING, L., HASSAGER, C., CHRISTIANSEN, C. (2002) Changes in bone mineral density with age in men and women: a longitudinal study. *Osteoporosis International*, **13** (2), pp. 105-112.

WEHRLI, F. W. (2010) Role of Cortical and Trabecular Bone Architecture in Osteoporosis. Department of Radiology University of Pennsylvania School of Medicine Philadelphia

WOOLF, A. D., PFLEGER, B. (2003) Burden of major musculoskeletal conditions. *Bulletin of the World Health Organization*, **81**(9), pp. 646-656.

World Health Organisation: Physical inactivity a leading cause of disease and disability, warns WHO (2002, April – last update). [Online] Available: www.who.int/mediacentre/news/releases/release23/en/ [2013, June 25]

World Health Organization. (2004) WHO scientific group on the assessment of osteoporosis at primary health care level.

ZIOUPOS, P., COOK, R. B., HUTCHINSON, J. R. (2008) Some basic relationships between density values in cancellous and cortical bone, *Journal of Biomechanics*, **41**, pp. 1961–1968.

Appendix A

ETHICAL AND SPONSORSHIP APPROVAL
UEC13/23 Coupaud/Newe/Riches/Gislason/Fogg: Biomechanical Characterisation of Osteoporotic Bone Mechanical Testing

Dear Applicants

I can confirm that the University Ethics Committee (UEC) has approved this protocol and appropriate insurance cover and sponsorship have now also been confirmed.

I would remind you that the UEC must be informed of any changes you plan to make to the research project, so that it has the opportunity to consider them. Any change of staffing within the research team should be reported to UEC.

The UEC would also expect you to report back on the progress and outcome of your project, with an account of anything which may prompt ethical questions for any similar future project and with anything else that you feel the Committee should know.

Any adverse event that occurs during an investigation must be reported as quickly as possible to UEC and, within the required time frame, to any appropriate external agency.

The University agrees to act as sponsor of the above mentioned project subject to the following conditions:

1. That the project obtains/has and continues to have University/Departmental Ethics Committee approval.

2. That the project is carried out according to the project protocol.

3. That the project continues to be covered by the University's insurance cover.

4. That the Director of Research and Knowledge Exchange Services is immediately notified of any change to the project protocol or circumstances which may affect the University's risk assessment of the project.

5. That the project starts within 12 months of the date of this letter.

As sponsor of the project the University has responsibilities under the Scottish Executive's Research Governance Framework for Health and Community Care. You should ensure you are aware of those responsibilities and that the project is carried out according to the Research Governance Framework.

On behalf of the Committee, I wish you success with this project.

Kind regards

Helen Baigrie
Contracts Manager
Research & Knowledge Exchange Services
University of Strathclyde
Graham Hills Building
50 George Street
Glasgow
G1 1QE

Direct Line +44 (0) 141 548 4539
Fax +44 (0) 141 552 4409

http://www.strath.ac.uk/ri/

Information for university staff can be found on the R & KE Portal: www.strath.ac.uk/rkeportal

The Internationalisation Information Portal for staff is available at https://moss.strath.ac.uk/internationalisation

11th July 2013

To Whom it May Concern,

As the lead Licensed Teacher of Anatomy at the University of Glasgow I grant permission, under the terms of the Anatomy Act and its 2006 Amendments , for anatomical specimens to utilised for this project. These specimens were donated with the express purpose of use in anatomical research and education, and I am satisfied that the proposed uses are appropriate and are allowed under the terms of the Act.

I therefore authorise project team members, under the supervision of Dr Sylvie Coupaud to use these specimens for the proposed study only. The specimens must be stored and transported in accordance with Laboratory of Human Anatomy (LHA) policies. When in use, the area used for the investigations/scanning must be controlled such that only members of the project team are able to observe or come into contact with the cadaveric material. All areas used must be cleaned in accordance with LHA policies.

Should there be any issues with the tissue or its use, storage or transportation, please don't hesitate to contact me using the details below.

Sincerely,

Dr Quentin A Fogg
BSc (Hons), PhD (Adel)
William Hunter Senior Lecturer in Anatomy
Facilities Manager, Laboratory of Human Anatomy

Thomson Building, University of Glasgow, University Avenue,
Glasgow, UK G12 8QQ Phone:+44 (0) 141 330 5860 Fax: +44 (0) 141 330 4299
Email: quentin.fogg@glasgow.ac.uk